

INTERIM REPORT

Accession No. _____

Report No. EGG-CDAP-5166

Contract Program or Project Title: Containment Analysis Development

Subject of this Document: BEACON/MOD3 Assessment/Adjustment

Type of Document: Informal Report

Author(s): Richard J. Doyle, Walter J. Mings, Judith A. Ramsthaler,
Brian L. Gries, James F. Lime

Date of Document: May 1980

Responsible NRC Individual and NRC Office or Division: S. Fabric, Reactor Safety Research

This document was prepared primarily for preliminary or internal use. It has not received full review and approval. Since there may be substantive changes, this document should not be considered final.

EG&G Idaho, Inc.
Idaho Falls, Idaho 83415

Prepared for the
U.S. Nuclear Regulatory Commission
Washington, D.C.
Under DOE Contract No. DE-AC07-76ID01570
NRC FIN No. A6042

THIS DOCUMENT CONTAINS
POOR QUALITY PAGES

INTERIM REPORT

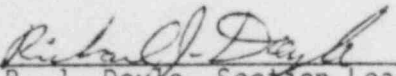
NRC Research and Technical
Assistance Report

8009190768

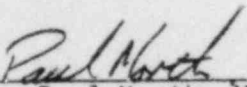
MAY 1980

BEACON/MOD3 ASSESSMENT/ADJUSTMENT

Approved



R. J. Doyle, Section Leader
BEACON/CONTEMPT



Paul North, Manager
Code Development and
Analysis Program

CONTENTS

INTRODUCTION	1
OVERVIEW	2
MODEL ASSESSMENT/ADJUSTMENT	3
"Best-Estimate" Models	3
Form Loss	4
Out-of-Plane Coupling	6
CONCLUSIONS	7
REFERENCES	8
Appendix A - Jet Impingement Analysis	9
Appendix B - Pipe Flow Nodalization Study	39
Appendix C - Drexel Entrainment/Deentrainment Analysis	52
Appendix D - Battelle-Frankfurt C-9 Experiment	62
Appendix E - Battelle-Frankfurt D-3 Matrix	89

BEACON/MOD3 ASSESSMENT/ADJUSTMENT REPORT

INTRODUCTION

BEACON/MOD3 is the latest version of the BEACON Code. Several major additions were made to the previous version (MOD2A) to produce MOD3. These include:

- o "Best-estimate" calculations for:
 - Interphase drag
 - Interphase mass transfer
 - Wall film formation
- o Form loss input option
- o Out-of-plane coupling option.

The optional "best-estimate" package was checked and adjusted, using separate-effects problems. The addition of the form loss and out-of-plane coupling models required that several assessment problems be run to allow judgement of the performance of the code. This report documents the BEACON/MOD3 assessment/adjustment task which was completed before the code was released to the National Energy Software Center.

OVERVIEW

The problems presented in this report were run in order to check and adjust the "best-estimate" models and to assess the overall performance of the code.

The overall technique used was to adjust the "best-estimate" variables for interphase drag, evaporation/condensation, and flashing, based on two separate effects experiments, and then to evaluate their validity in modeling two containment tests and an entrainment/deentrainment experiment. Additionally, a nodalization study was performed to assess BEACON form losses in junctions with respect to an analytical solution of the same type of junction. The sensitivity of this calculation to nodalization was then determined. The calculations performed were:

<u>Separate Effects Calculations</u>	<u>Containment Calculations</u>
o KWU Jet Test 6	o Battelle-Frankfurt C-9 Experiment
o Battelle-Frankfurt C-12 Jet	
o Pipe Flow Nodalization Study	
o Drexel Entrainment/Deentrainment Analysis	o Battelle-Frankfurt D-3 Matrix

The main text of this report summarizes the findings of these studies and describes any problems encountered. For details of each individual study, see Appendices A through E.

MODEL ASSESSMENT/ADJUSTMENT

"Best-Estimate" Models

Interphase Drag

Interphase momentum exchange is calculated in BEACON as a function of the velocity difference between the liquid and vapor phases multiplied by the drag coefficient KDRAG. This coefficient has dimensions of $N \cdot s/m^4$. For the "best-estimate" option, KDRAG is recalculated each computational time-step as a function of density, void fraction, velocity, and viscosity. It was determined from the jet problems that a minimum value for absolute stability presently is $KDRAG = 1 \times 10^7$. This is the current minimum value used in the code. The Drexel Test runs were made using KDRAG calculated without this constraint, and results indicate that the computed values give quite good experimental agreement. However, as a result of these same runs, it was determined that the KFIX equations used in the code are unstable using these values for KDRAG (between 1×10^{-3} and 1) and eventually diverge. Presently, work is being done to improve the KFIX equations to allow the use of the best-estimate drag coefficient values which, for those regimes in which the code was able to run, appeared to give excellent agreement with experimental data.

Interphase Mass Transfer

In addition to studying KDRAG, the jet problems were run to evaluate the evaporation and condensation rate multipliers, RLAME and RLAMC, and the flashing criterion, FLCRIT.

Values of 0.1 for the evaporation and condensation rate multipliers gave the closest agreement with the jet experimental data.

At calculated values of liquid superheat above the flashing criterion, FLCRIT, the BEACON "best-estimate" model uses the Rivard-Torrey flashing

model.¹ Between saturation and FLCRIT a diffusion limited evaporation model is used.² During the Battelle-Frankfurt C-9 and D-3 test runs it was discovered that the discontinuities of switching between evaporation models in liquid superheat regimes caused instabilities in the wall film model. Therefore, the present value of FLCRIT is 0.0, thereby using the flashing model for all liquid-superheat evaporation rates. This gave good overall results in the containment problems.

Wall Film Formation

The Battelle-Frankfurt C-9 and D-3 test runs both used the wall film model. In addition, the D-3 cases included a matrix to assess the effect of the film model on the overall results.

The results show fairly good data agreement, but the present difficulty with interphase drag complicates the evaluation. The present high drag value has the effect of transporting too much liquid to locations throughout the containment in simulations such as these. This promotes excessive wall film build up in the code, inhibiting heat transfer to the walls.

Form Loss

The KFIX numerical scheme used in BEACON calculates entrance and exit losses for junctions with two-dimensional meshes. The accuracy of the loss is dependent on the degree of nodalization. A Pipe Flow nodalization study (Appendix B) was executed to determine the effect of nodalization on the accuracy of the calculated form losses. The Battelle-Frankfurt D-3 test matrix also contained a nodalization study which investigated this effect.

Sufficient nodalization for the code to exhibit this effect occurs when the Eulerian region of greater flow area is wider by at least two cells on each side of the junction. This conclusion is reached as a result of both nodalization studies.

The Pipe Flow study showed that the magnitude of the effective form loss for incompressible flow agrees with the analytical solution for flow through a thin orifice but is about double the analytical result for entrance or exit losses for any single abrupt area change. This error in effective loss, however, had a relatively minor effect on flow rates with respect to the analytical solution.

BEACON/MOD3 now contains an optional input for junction form loss. This is primarily intended for one-dimensional to lumped-parameter junctions, as the numerical scheme will not calculate any loss at this type of interface. This feature improves stability for lumped-parameter calculations, and was used in the calculation of the Drexel and the Battelle-Frankfurt C-9 and D-3 tests. Results of these cases indicate that this model works as intended, improving results and eliminating the previous instabilities.

Out-of-Plane Coupling

The out-of-plane coupling option was used in modeling the Battelle-Frankfurt C-9 Test and exhibited proper performance with no apparent problems. This feature improves the flexibility of the BEACON code in modeling complex containment problems. The option provides a quasi-third-dimensional capability in the flow model.

CONCLUSIONS

The check and adjustment task has been completed. Several problems involving interaction among models were encountered and solved. The one significant problem remaining is the interphase drag calculational scheme, which is presently being investigated. The BEACON code is now capable of modeling quite complex PWR geometries, with a high degree of detail. Several future assessment tasks will be performed, without further adjustment of the models, in order to evaluate the performance of the code in its present configuration.

REFERENCES

1. W. C. Rivard and M. D. Torrey, Numerical Calculation of Flashing From Long Pipes Using a Two-Field Model, LA-6104-ms, 1977.
2. Charles R. Broadus et al., BEACON/MOD3: A Computer Program for Thermal-Hydraulic Analysis of Nuclear Reactor Containments-User's Manual, NUREG/CR-1148, EGG-2008, April 1980.

APPENDIX A

JET IMPINGEMENT ANALYSIS

INTRODUCTION

Two interphasic mass transfer formulations are used in the BEACON best-estimate computational mode. For flashing flow or flow regimes where high mass transfer rates are present, the Rivard-Torrey bulk-boiling model is used. For other flow regimes, the Sahota diffusion-limited, dispersed-flow formulations are used. The basis for determining which model to use is by means of a simple flashing parameter defined as

$$FLCRIT = (T_l - T_s) C_{pl} / h_{fg}$$

where

T_l = liquid temperature (K)

T_s = saturation temperature (K)

C_{pl} = specific heat at constant pressure (J/kg·K)

h_{fg} = heat of vaporization (J/kg).

This parameter is a measure of the degree of superheat in the liquid. If, in a given cell, FLCRIT is computed to be greater than an internally specified value, the Rivard-Torrey model is used; otherwise, the Sahota formulations are used. The computation of FLCRIT and selection of the appropriate model is done automatically on a cell-by-cell basis.

The purpose of the jet impingement analysis was to adjust the interphasic exchange rate in the flashing mode and to determine the FLCRIT value at which to switch flashing models. Adjustment of the Sahota dispersed-flow formulation had been previously accomplished.

The interphasic mass transfer rate is adjusted by λ , a multiplier on the computed mass transfer rate. For this study, the multiplier was varied from 0.001 to 0.1 (a range selected on the basis of previous experiences), typically giving mass transfer rates on the order of 1000 to 40000 kg/(s·m³). The interphasic momentum and heat transfer rates, K and R, were set to high values, locking the phases together in velocity and temperature. The flashing parameter FLCRIT was varied from 0.0 to 0.2, representing approximately 0 to 100 K liquid superheat before using the Rivard-Torrey model.

SYSTEM DESCRIPTION

Facilities

Two jet impingement tests were analyzed to adjust the interphasic exchange rates for a best-estimate prediction of high-speed, two-phase, flashing flow. The jet tests were selected from a series of jet impingement experiments conducted by Kraftwerk Union (KWU) and from the C-series of containment blowdown experiments conducted by Battelle-Frankfurt, both of Germany.

In the jet tests selected, the discharging jet flow was directed perpendicularly to a circular baffle plate. The pressure measurements taken along the plate at steady-state conditions were compared to model predictions and used as a basis for adjusting the interphasic exchange parameters.

Events

The KWU jet test modeled was Test 6 of the series reported in Reference A-1. The discharge diameter of the jet was 10 mm, the baffle plate diameter was 260 mm, and the separation distance between jet and plate was 5 mm, providing an (L/D) ratio of 0.5. The discharge flow was a high pressure two-phase water mixture at saturated conditions.

The second jet modeled was taken from the Battelle-Frankfurt containment blowdown test C12 which is reported in References A-2 and A-3. This jet was larger than the KWU jet, with a jet discharge diameter of 100 mm, a baffle plate diameter of 600 mm, and a separation distance from plate to exit of 240 mm, for an (L/D) ratio of 2.4. The discharge flow was high pressure saturated liquid water.

MODEL DESCRIPTION

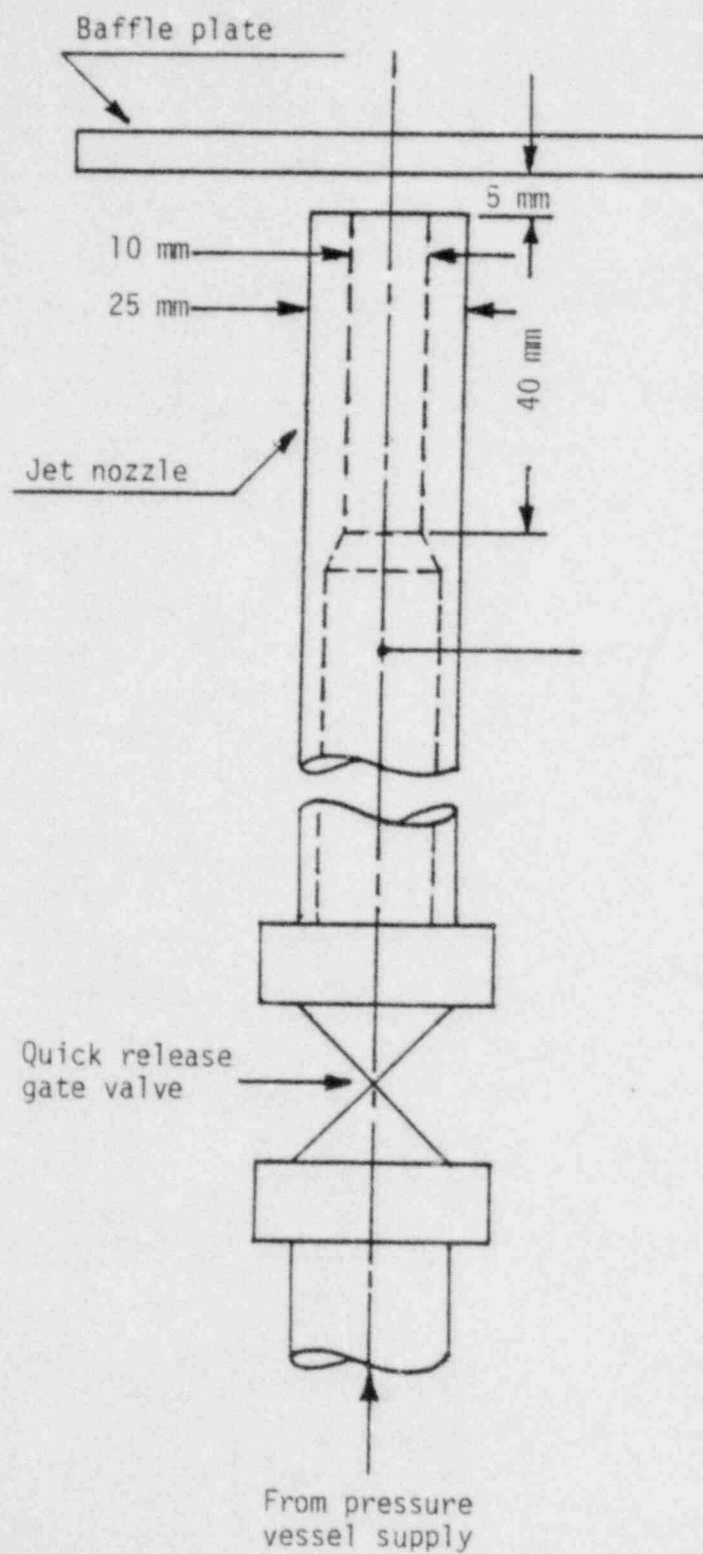
Both jet geometries were modeled in two-dimensional axisymmetric coordinates with the flow field assumed symmetric about the centerline of the issuing jet. The left boundary of the two-dimensional computing mesh was the centerline of symmetry and the top boundary of the mesh was the baffle plate surface. A bottom inflow boundary was used to model the jet exit flow. The nozzle exit velocities and state conditions were computed from upstream measurements of state conditions and mass flow rates.

The remaining bottom boundary of the computing mesh was treated as a rigid, free-slip surface. The right boundary was specified as a constant pressure boundary. Both of these boundaries were removed as far away as practical from the vicinity of the jet core by using several coupled meshes. Variable mesh spacing was used to minimize the number of computational cells.

Analysis of the KWU Jet

The test geometry for the KWU jet is shown in Figure A-1. The critical mass flow rate (\dot{m}), pressure, temperature, and quality as measured upstream of the nozzle exit (X_v) are also noted in Figure A-1. The conditions out the nozzle exit, which served as inflow boundary conditions for the computer model, were determined to be:

Pressure 2.75 MPa



$$P = 3.4 \text{ MPa}$$

$$T = 510.9 \text{ K}$$

$$X_V = 0.34$$

$$\dot{m} = 30.55 \times 10^3 \frac{\text{kg}}{\text{m}^3 \cdot \text{s}}$$

Figure A-1. Test geometry of KWU Jet Test 6.

Temperature 502.2 K

Void fraction 0.728

Velocity 134 m/s.

These conditions were computed from a momentum-force balance between the nozzle exit and the baffle plate, taking into account the actual loads measured on the plate, and assuming that homogeneous, equilibrium flow existed between the nozzle exit and the point of measurement.

The computing mesh setup is shown in Figure A-2. Two additional mesh regions were used to extend the right and bottom boundaries away from the jet core vicinity in order to minimize the influence of boundary conditions. A listing of the input card images for this model is given in Figure A-3.

Analysis of the C12 Jet

The test geometry of the C12 jet is shown in Figure A-4. The upstream mass flow conditions are also noted. The nonalization of this problem is shown in Figure A-5. As in the KWU jet modeling, additional meshes were used to move the bottom and right boundaries away from the flow field of interest. The nozzle lip protruding above the jet exit plane was modeled with rectangular obstacle cells. The jet inflow velocity was determined from continuity calculations with the assumption that homogeneous, equilibrium flow existed between the measurement station and the nozzle exit. A force balance check of the jet exit momentum against the measured loads on the plate indicated that this was valid. A listing of the input data cards for this model is given in Figure A-6.

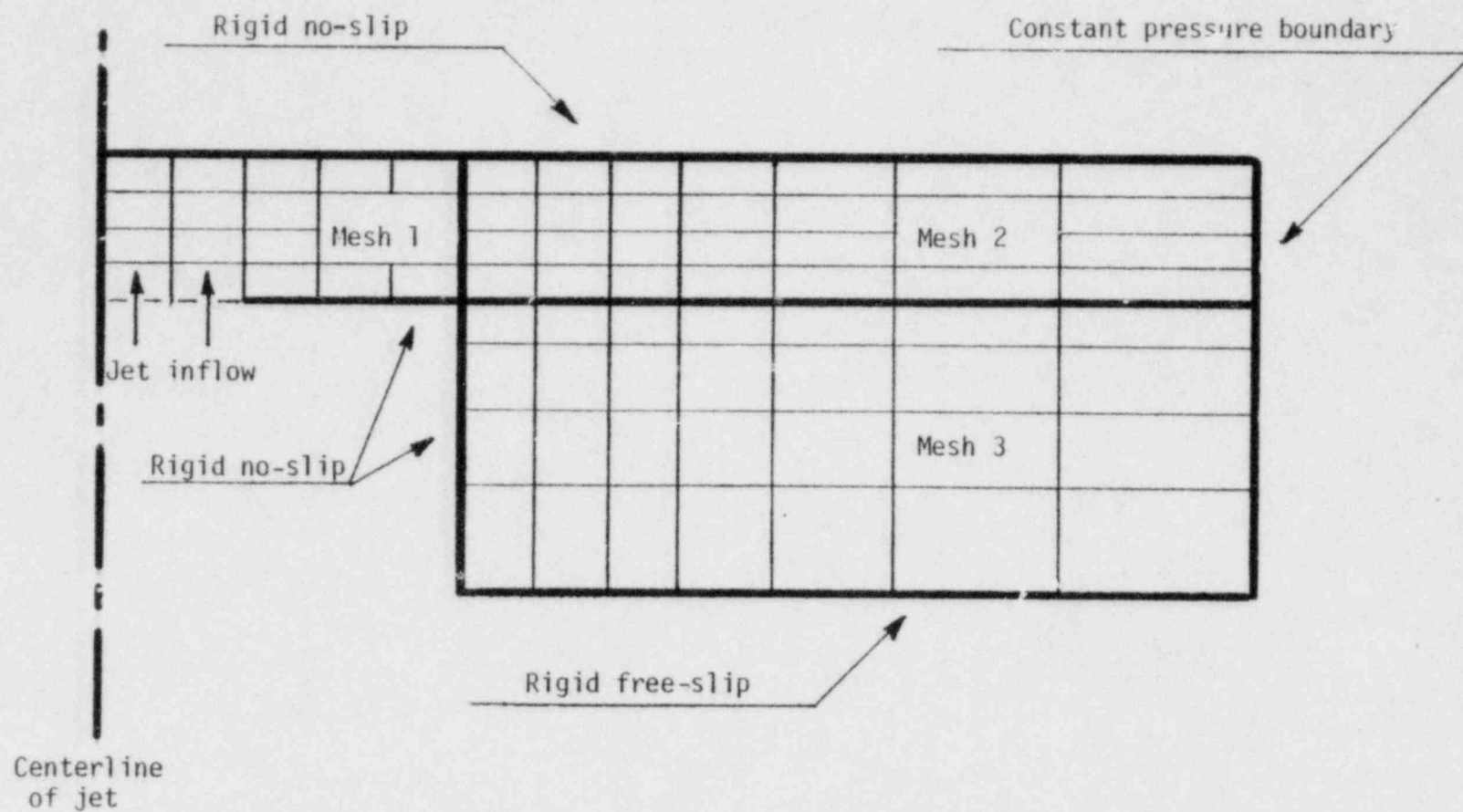


Figure A-2. Mesh setup for the KWU jet analysis.

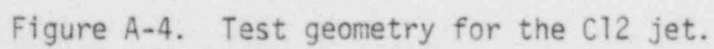
POOR ORIGINAL

```

0C100 'KWUJET, MCD3G, BEST'
0C110 0.0, 0.0005, 0.00000001, SEC, 5.0, 10, XEQ BEST
0C120 0.00001, 0.1
0C130 AUTOUT, 0, 0.1, 1.5
00140 PRINT, NOPRINT, PRINT, NOPRINT, NOPRINT
0C150 PLOTS, 0.6, 1 1 0 0 0 0 1 0 0 0 0
0C190
0C200 1.0, 0.00001, 0.00001, 100, 5, 5
*0C220 1, 2.0E08, 1.0, 0.001, 2.366E5
*00230 1, 0.01, 0.01, 1.0E20
00240 LASL, PT, BAR, DEGC, M, SEC-1
* MESH DIMENSIONS
11000 AXISYM, 8, 4, 0.0025, 0.00125, 0.0, M, 0.0, 0.0
21000 AXISYM, 4, 4, 0.0025, 0.00125, 0.02, M, 0.0, 0.0
31000 AXISYM, 7, 4, 0.0025, 0.00125, 0.0125, M, 0.0, 0.0
* VARIABLE MESH SPACING
21020 .0032, .0042, .0055, .0071
31020 .0025, .0025, .0025, .0032, .0042, .0055, .0071
31030 .00357, .00275, .00211, .00163
* SLIP/NOSLIP BOUNDARIES
11010 SLIP, SLIP, SLIP, SLIP, NOSLIP
21010 SLIP, SLIP, SLIP, SLIP, NOSLIP
31010 SLIP, SLIP, SLIP, SLIP, NOSLIP
* INITIAL STATE CONDITIONS
11101 AIR 2, 2, 9, 5, 0, 1.00, 20.0
21101 AIR 2, 2, 5, 5, 0, 1.00, 20.0
31101 AIR 2, 2, 8, 5, 0, 1.00, 20.0
* SPECIFIED FLOW BOUNDARIES
11501 INFLCW, 2, 1, 3, 1
11601 MIXTLRE, 27.5, 229.1, 229.1, 0.728, 0.0
11701 0.0, 134.0, 0.0, 134.0
21501 CONSTP, 6, 2, 6, 5
31501 CONSTP, 9, 2, 9, 5
21601 AIR 1.00, 20.0
31601 AIR 1.00, 20.0
* MESH COUPLING INPUT
6C01 RIGHT 1 9 2 4 2 2 2 4
6C02 BOTTOM 1 7 2 3 3 2 5 3
6C03 BOTTOM 2 2 2 4 3 5 5 4

```

Figure A-3. Input data listing for the KWU jet model.



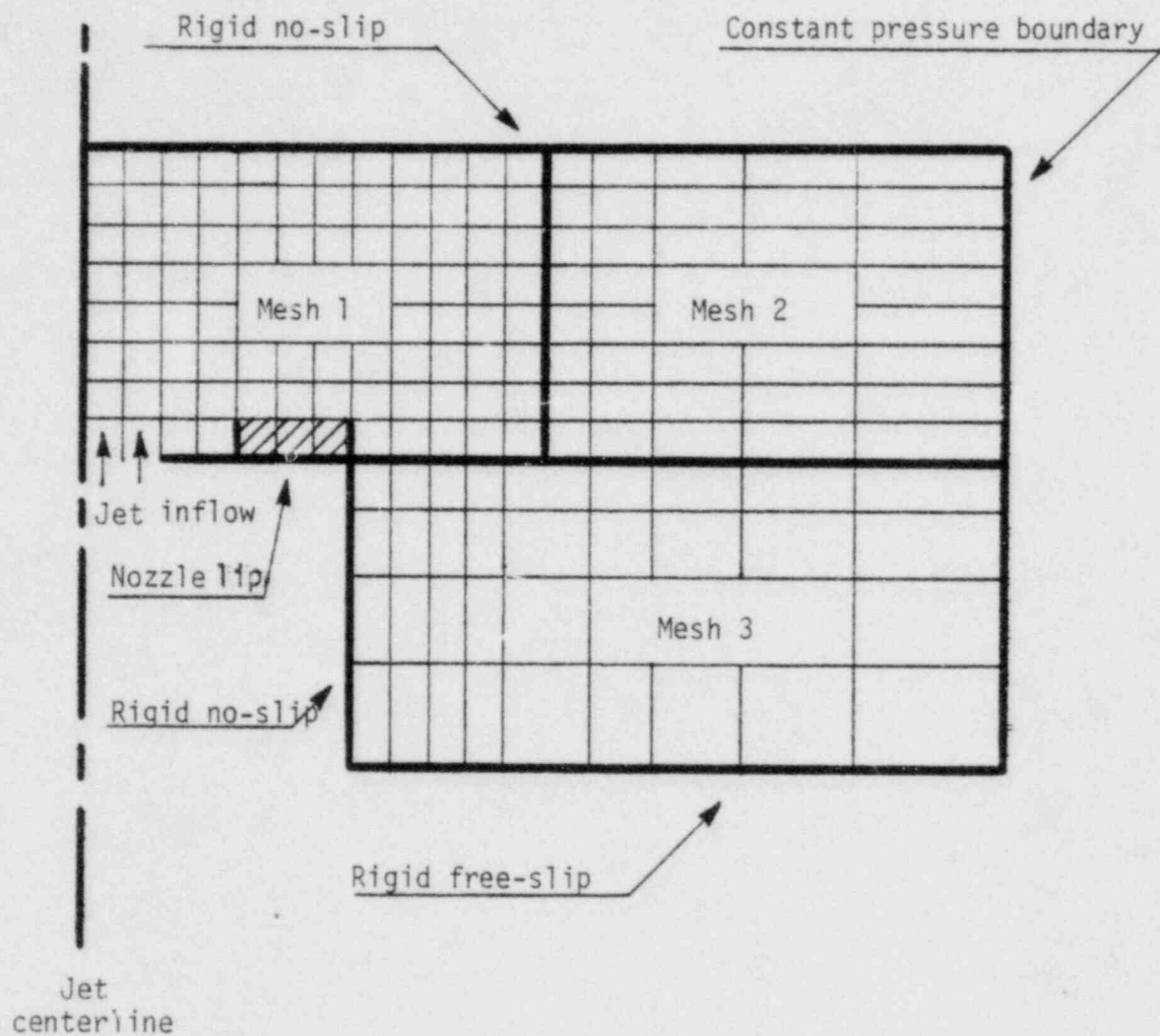


Figure A-5. Mesh setup for the C12 jet analysis.

POOR ORIGINAL

```

100      'REV. C12JET, K=1E07 BOTH, L=.03, FLCRIT=.03'
* REVISD JET INFLOW CONDITIONS
105      NUREAD, C, NWRITE, 1
110      0.0, 0.005, 0.000001, SEC, 5.0, 1, XEQ BEST
120      0.001, 0.1
130      AUTOCT, C, 0.1, 1.5
140      PRINT, NOPRINT, PRINT, PRINT, NOPRINT
150      NOPLUTS, 0.6, 1 1 0 0 0 0 0 0 0 0 0 0
160      3
200      1.0, 0.00001, 0.00001, 100, 5, 5
*220      1, 2.2E08, 1.C, 0.001, 100.C
*230      1, 0.015, 0.015, 1.0E20
240      LASL, PT, BAR, DEGC, M, SEC-1
* MESH DIMENSIONS
11000    AXISYM, 12, 8, 0.025, 0.030, 0.0, M, C.C, 0.0
21000    AXISYM, 5, 8, 0.025, 0.030, 0.3, M, C.C, 0.0
31000    AXISYM, 10, 4, 0.025, 0.030, 0.175, M, C.C, 0.0
* VARIABLE MESH SPACING
21020    .032, .042, .055, .071, .093
31020    .025, .025, .025, .025, .025, .032, .042, .055, .071, .093
* SLIP/NOSLIP BOUNDARIES
11010    SLIP, SLIP, SLIP, NOSLIP
21010    SLIP, SLIP, SLIP, NOSLIP
31010    SLIP, SLIP, SLIP, NOSLIP
* INITIAL STATE CONDITIONS
11101    AIR, 2, 2, 13, 9, C, 1.00, 20.C
21101    AIR, 2, 2, 6, 9, C, 1.00, 20.C
31101    AIR, 2, 2, 11, 5, C, 1.00, 20.C
* OBSTACLE CELLS FOR NOZZLE LIP
11401    NOSLIP, 6, 2, 8, 2
* SPECIFIED FLOW BOUNDARIES
11501    INFLOW, 2, 1, 3, 1
11601    LIQUID, 70.0, 265.0
11701    0.0, 56.0, 0.0, 56.0
21501    CONSTP, 7, 2, 7, 9
31501    CONSTP, 12, 2, 12, 5
21601    AIR, 1.00, 20.0
31601    AIR, 1.00, 20.0
* MESH COUPLING INPUT
6001    RIGHT, 1, 13, 2, 8, 2, 2, 2, 8
6002    BOTTOM, 1, 9, 2, 5, 3, 2, 5, 5
6003    BOTTOM, 2, 2, 2, 5, 3, 7, 5, 5

```

Figure A-6. Input card listing for the C12 jet model.

TABLE A-1. COMPUTED PRESSURES IN MPa ALONG BAFFLE PLATE, KWU JET

A-1.1 Effect of λ ($K = 1.0 \times 10^7$, $R = 1.0 \times 10^{10}$, FLCRIT = 0.05)

Cell (I,J)	(FLCRIT = 0.03)			
	$\lambda = 0.001$	$\lambda = 0.01$	$\lambda = 0.03$	$\lambda = 0.1$
2,5	3.579	3.597	3.627	3.735
3,5	2.734	2.756	2.793	2.887
4,5	1.426	1.457	1.512	1.638
5,5	0.832	0.863	0.920	1.050
6,5	0.507	0.535	0.582	0.676
7,5	0.318	0.340	0.374	0.439
8,5	0.207	0.222	0.247	0.291
9,5	0.140	0.151	0.167	0.197

A-1.2 Effect of K ($\lambda = 0.01$, $R = 1.0 \times 10^{10}$, FLCRIT = 0.1)

Cell (I,J)	$K = 1.0 \times 10^6$	$K = 1.0 \times 10^7$	$K = 1.0 \times 10^8$
2,5	2.695	3.602	4.198
3,5	1.967	2.745	3.217
4,5	0.869	1.446	1.608
5,5	0.574	0.857	0.891
6,5	0.406	0.534	0.520
7,5	0.294	0.339	0.314
8,5	0.222	0.223	0.202
9,5	0.172	0.151	0.136

TABLE A-1. (Continued)

A-1.3 Effect of R ($\lambda = 0.025$, $K = 1.0 \times 10^7$, $FLCRIT = 0.03$)

<u>Cell (I,J)</u>	<u>$R = 1.0 \times 10^8$</u>	<u>$R = 1.0 \times 10^{10}$</u>	<u>$R = 1.0 \times 10^{15}$</u>
2,5	3.593	3.643	3.645
3,5	2.746	2.771	2.769
4,5	1.476	1.496	1.496
5,5	0.857	0.907	0.911
6,5	0.530	0.573	0.575
7,5	0.341	0.367	0.369
8,5	0.230	0.242	0.243
9,5	0.161	0.164	0.165

A-1.4 Effect of $FLCRIT$ ($\lambda = 0.01$, $K = 2.0 \times 10^7$, $R = 1.0 \times 10^{10}$)^a

<u>Cell (I,J)</u>	<u>$FLCRIT = 0.05$</u>	<u>$FLCRIT = 0.1$</u>	<u>$FLCRIT = 0.2$</u>
2,5	3.707	3.696	3.603
3,5	2.797	2.821	2.732
4,5	1.410	1.447	1.371
5,5	0.830	0.831	0.711
6,5	0.499	0.493	0.409
7,5	0.313	0.307	0.359
8,5	0.205	0.201	0.228
9,5	0.139	0.127	0.148

a. The cases shown reflect slightly different inflow velocities which since have been changed.

RESULTS

KWU Jet

A problem transient time of 0.0005 second was sufficient to attain steady-state conditions.

Computer analyses were obtained for parametric variations of λ , K, R, and FLCRIT. These parameters were varied individually. The computational cell pressures along the baffle plate are presented in Table A-1 as follows:

<u>Table Section</u>	<u>Parameter</u>	<u>Parameter Function</u>	<u>Parameter Variation</u>
A-1.1	λ	Mass transfer	0.001, 0.01, 0.03, 0.1
A-1.2	K	Momentum transfer	1.0×10^6 , 1.0×10^7 , 1.0×10^8
A-1.3	R	Heat transfer	1.0×10^8 , 1.0×10^{10} , 1.0×10^{15}
A-1.4	FLCRIT	Flashing switch	0.05, 0.1, 0.2

From Table A-1, it can be seen that K has a strong effect on pressure while λ , R, and FLCRIT have negligible effects. The pressure profiles for K are compared to measured data in Figure A-7. Based on this comparison the best-estimate value for K is 1.0×10^7 .

The flow field of the jet, with established best-estimate parameter values, is shown by the velocity vector plot of Figure A-8. Expansion of the jet flow is suppressed by the width of the nozzle lip and the close proximity of the nozzle lip to the baffle plate. Beyond the nozzle lip, the flow expands and plumes considerably, with the result that there are no flow vortices or recirculation near the nozzle lip, as might be expected from entrainment effects [see the velocity vector plot for the C12 jet (Figure A-13), for example.]

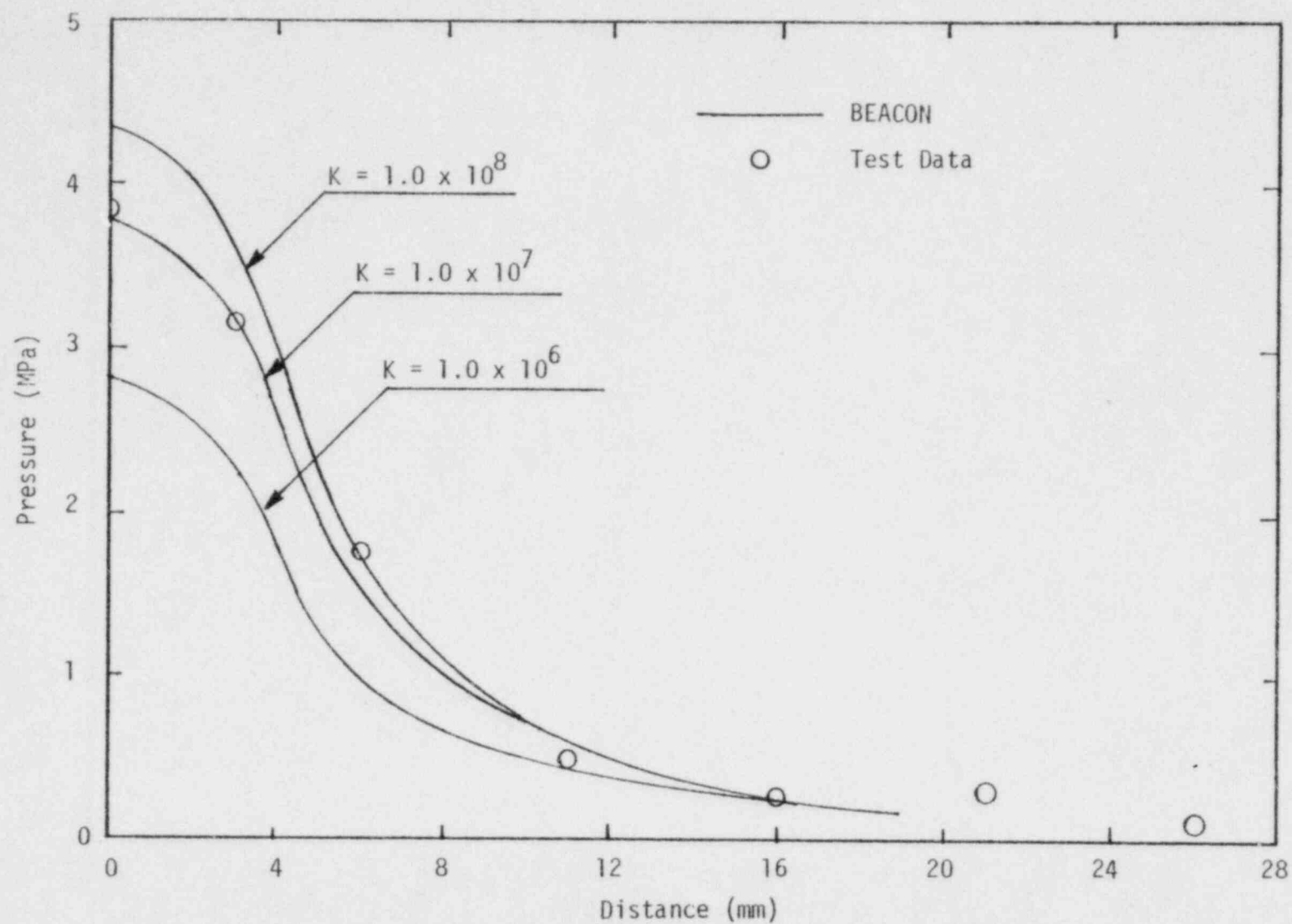
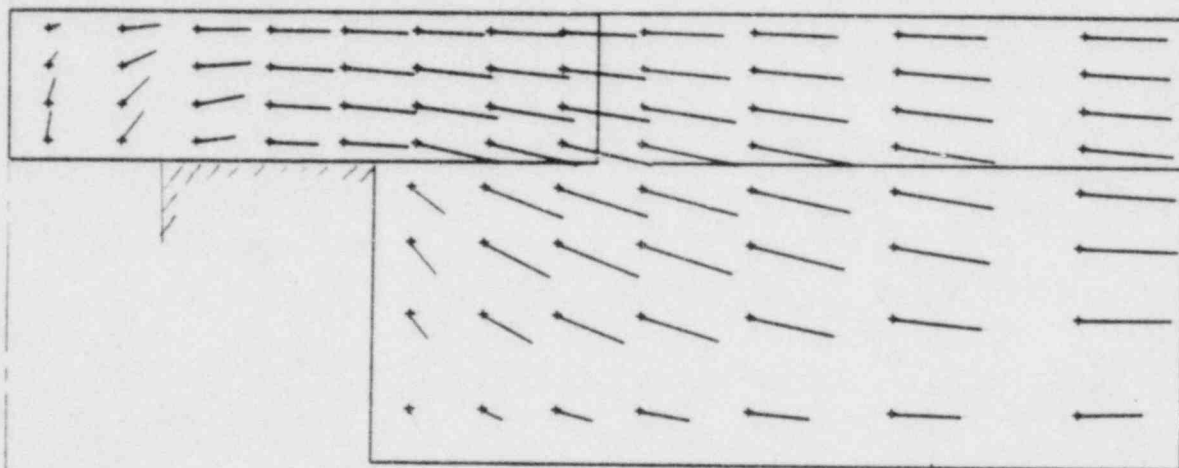


Figure A-7. KWU jet pressure distribution showing the effects of momentum transfer.



Jet
Centerline

Figure A-8. BEACON velocity vector plot from the KWU jet analysis.

Contour patterns for pressure, void fraction, and net mass transfer rate are shown in Figure A-9 for the jet core vicinity (mesh region 1). The pressure contours show that the pressure is highest at the center of the plate and rapidly diminishes radially outward. The void fraction contours show that the liquid phase of the two-phase inflow mixture tends to accumulate in the jet core. Even though the inflowing void fraction is 0.728, the void fraction of the jet core at the baffle plate is 0.436. The net mass transfer rate contours show that interphasic mass transfer is inhibited until the flow has a chance to expand further. The highest mass transfer rate occurs along the plate away from the jet core and not in the nozzle exit or near the nozzle lip, as might be expected.

The analysis of the KWU jet serves to tentatively select a best-estimate value for the interphasic momentum transfer rate. The KWU jet was insensitive to the other interphasic exchange parameters and these needed to be determined by analysis of the C12 jet.

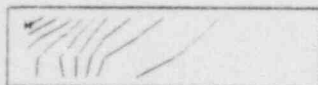
C12 Jet

A problem transient time of 0.005 second was sufficient to reach steady-state flow conditions.

Parametric variations of λ , K , R , and FLCRIT were also obtained for the C12 jet. The computed pressures along the baffle plate for the following variations are tabulated in Table A-2:

<u>Table</u> <u>Section</u>	<u>Parameter</u>	<u>Parameter</u> <u>Function</u>	<u>Parameter</u> <u>Variation</u>
A-2.1	λ	Mass transfer	0.001, 0.005, 0.01, 0.03
A-2.2	K	Momentum transfer	1.0×10^6 , 1.0×10^7 , 1.0×10^8
A-2.3	R	Heat transfer	1.0×10^8 , 1.0×10^{10} , 1.0×10^{15}
A-2.4	FLCRIT	Flashing switch	0.025, 0.05, 0.1, 0.2

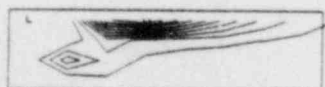
POOR ORIGINAL



PRESSURE
TIME= 5.000-04 CYCLE= 595 MESH= 1 GEOM= AXISYM JMM= BEST= BEST
MIN= 3.080+04 MAX= 3.052+00 L= 3.080+04 H= 3.290+08 DQ= 3.621+05



VOID FRACT
TIME= 5.000-04 CYCLE= 595 MESH= 1 GEOM= AXISYM JMM= BEST= BEST
MIN= 4.355-01 MAX= 9.978-01 L= 4.355-01 H= 9.716-01 DQ= 5.623+08



NET MASS TRANSFER RATE
TIME= 5.000-04 CYCLE= 595 MESH= 1 GEOM= AXISYM JMM= BEST= BEST
MIN= 1.974-01 MAX= 2.565+04 L= 1.974-01 H= 2.308+04 DQ= 2.565+03

Figure A-9. BEACON contour plots of pressure, void fraction, and net mass transfer rate from the KWU jet analysis.

From Table A-2, it can be seen that λ has the strongest effect on pressure. The effect of varying K and R is negligible on pressure, as is FLCRIT, with various values of λ . The pressure variation due to λ is plotted in Figure A-10 and is compared to measured data. The shapes of the computed pressure profiles are the same as the curve fit given for the test data in Reference A-3, and is lower in magnitude than the measured data. Increasing λ above 0.03 did not appreciably increase the pressure level.

Numerical instabilities occurred for cases where $R \leq 1.0 \times 10^8$. Numerical instability also occurred for $K \leq 1.0 \times 10^6$, but the lower limit of K was 1.0×10^7 based upon the KWU jet analysis. Certain combinations of λ and FLCRIT also affected numerical stability. Table A-3 presents the combination of λ and FLCRIT values investigated and their effect on numerical stability. Based on this comparison, it appears that FLCRIT must be less than 0.05 in order to achieve numerical stability for the range of λ investigated.

The C12 jet geometry had a nozzle lip flange extending 40 mm above the nozzle exit plane (see Figure A-4). Further analysis revealed that the nozzle lip height had a strong effect on the pressures computed on the baffle plate. As previously mentioned, the nozzle lip flange was modeled with rectangular obstacle cells. The cell dimensions used in the computing mesh modeled the lip height as 30 mm instead of 40 mm. This approximation of the nozzle lip was felt to be sufficiently accurate for the analysis.

In an attempt to more closely match the test data, the correct lip height of 40 mm was modeled. The axial cell dimensions were progressively changed so that the nozzle lip height of 40 mm could be modeled without changing the number of computational cells. The required input cards to change the axial cell dimensions are:

```
11030 .040, .037, .034, .031, .028, .025, .023, .022
21030 (Same as card 11030)
31030 .086, .066, .051, .040.
```

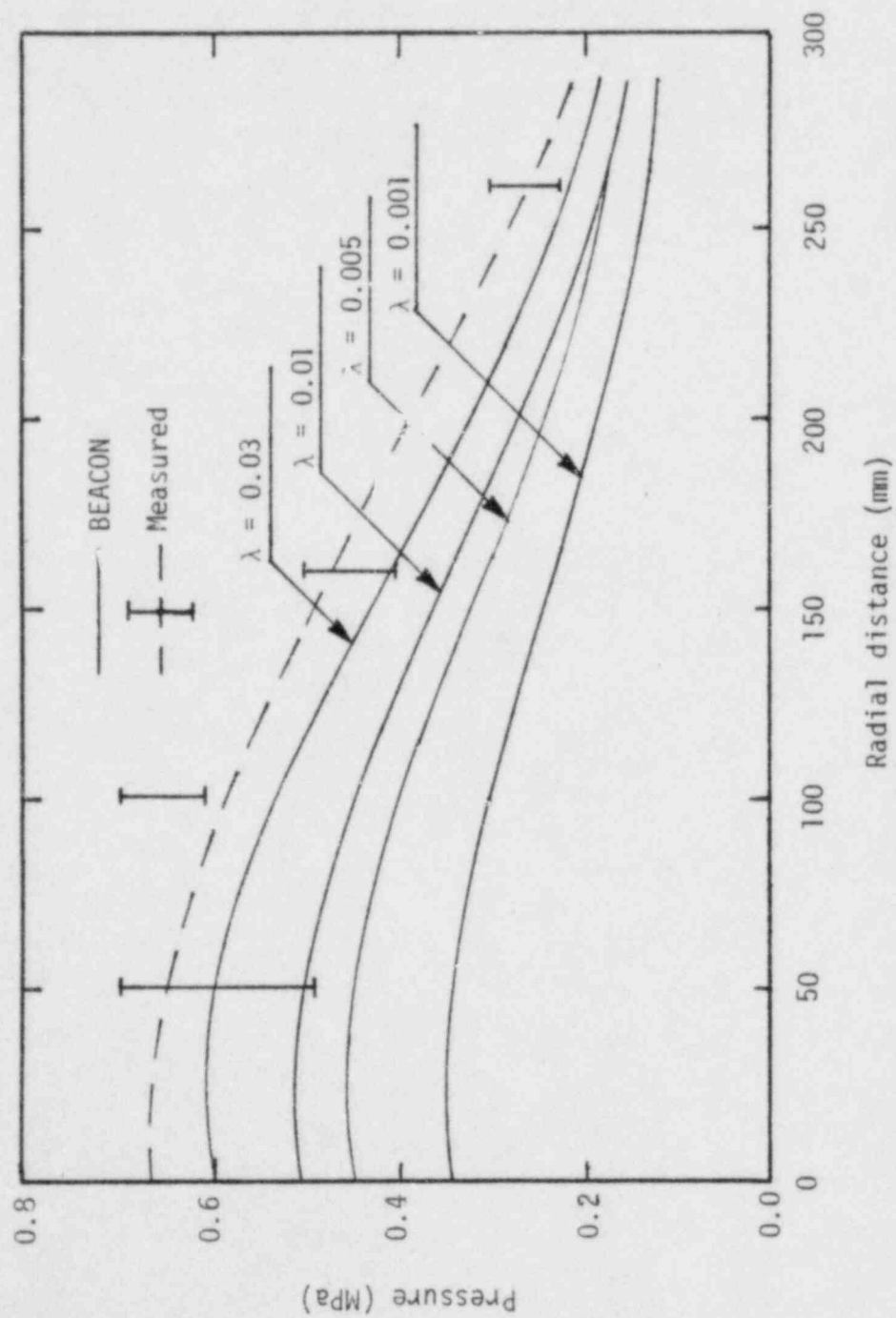


Figure A-10. C12 jet pressure distribution showing the effects of mass transfer.

TABLE A-2. COMPUTED PRESSURES IN MPa ALONG BAFFLE PLATE, C12 JET

A-2.1 Effect of λ ($K = 1.0 \times 10^7$, $R = 1.0 \times 10^{10}$, $FLCRIT = 0.03$)

Cell (I,J)	$\lambda = 0.001$	$\lambda = 0.005$	$\lambda = 0.01$	$\lambda = 0.03$
2,9	0.399	0.458	0.513	0.602
3,9	0.352	0.460	0.515	0.605
4,9	0.340	0.446	0.501	0.591
5,9	0.317	0.418	0.471	0.558
6,9	0.286	0.381	0.430	0.512
7,9	0.254	0.339	0.383	0.458
8,9	0.223	0.297	0.334	0.401
9,9	0.197	0.259	0.288	0.346
10,9	0.174	0.226	0.247	0.296
11,9	0.154	0.199	0.212	0.252
12,9	0.138	0.177	0.182	0.215
13,9	0.123	0.159	0.157	0.182

A-2.2 Effect of K ($\lambda = 0.03$, $R = 1.0 \times 10^{10}$, $FLCRIT = 0.03$)

Cell (I,J)	$K = 1.0 \times 10^6$	$K = 1.0 \times 10^7$	$K = 1.0 \times 10^8$
2,9	0.591	0.602	0.604
3,9	0.595	0.605	0.607
4,9	0.581	0.591	0.592
5,9	0.550	0.558	0.559
6,9	0.506	0.512	0.512
7,9	0.454	0.458	0.458
8,9	0.399	0.401	0.401
9,9	0.345	0.346	0.346
10,9	0.296	0.296	0.296
11,9	0.253	0.252	0.252
12,9	0.215	0.215	0.215
13,9	0.182	0.182	0.182

TABLE A-2. (Continued)

A-2.3 Effect of R ($\lambda = 0.03$, $K = 1.0 \times 10^7$, FLCRIT = 0.03)

Cell (I,J)	$R = 1.0 \times 10^8$	$R = 1.0 \times 10^{10}$	$R = 1.0 \times 10^{13}$
2,9	Unstable	0.602	0.602
3,9	Unstable	0.605	0.605
4,9	Unstable	0.590	0.590
5,9	Unstable	0.558	0.558
6,9	Unstable	0.512	0.512
7,9	Unstable	0.458	0.458
8,9	Unstable	0.401	0.401
9,9	Unstable	0.346	0.346
10,9	Unstable	0.296	0.296
11,9	Unstable	0.252	0.252
12,9	Unstable	0.215	0.215
13,9	Unstable	0.182	0.182

A-2.4 Effect of FLCRIT ($K = 1.0 \times 10^7$, $R = 1.0 \times 10^{10}$)

Cell (I,J)	at $\lambda = 0.007$			at $\lambda = 0.025$	
	FLCRIT = 0.05	0.1	0.2	0.025	0.05
2,9	0.476	0.472	0.360	0.588	Same
3,9	0.479	0.475	0.364	0.591	Same
4,9	0.466	0.462	0.352	0.571	Same
5,9	0.438	0.434	0.327	0.544	Same
6,9	0.399	0.397	0.296	0.499	Same
7,9	0.356	0.354	0.262	0.446	Same
8,9	0.312	0.310	0.230	0.390	Same

TABLE A-2. (Continued)

Cell (I,J)	at $\lambda = 0.007$			at $\lambda = 0.025$	
	FLCRIT = 0.05	0.1	0.2	0.025	0.05
9,9	0.270	0.269	0.201	0.337	Same
10,9	0.234	0.234	0.177	0.288	Same
11,9	0.204	0.204	0.158	0.246	Same
12,9	0.180	0.179	0.142	0.209	Same
13,9	0.159	0.158	0.129	0.177	Same

TABLE A-3. EFFECT OF λ AND FLCRIT ON NUMERICAL STABILITY

<u>λ</u>	<u>FLCRIT</u>				
	<u>0.025</u>	<u>0.03</u>	<u>0.05</u>	<u>0.1</u>	<u>0.2</u>
0.03	s	s	u	--	--
0.025	s	s	s	u	--
0.02	s	s	s	u	--
0.01	s	s	s	u	u
0.007	s	s	s	s	s

s = stable

u = unstable

The revised nodalization was investigated for λ 's of 0.01, 0.02, 0.03, and 0.1. The pressure profiles are shown in Figure A-11 and compared to measured data. The change in nozzle lip height resulted in significantly higher pressures in the jet core vicinity and a more favorable comparison to test data. At distances greater than 150 mm from the jet centerline, closest agreement with the data was obtained with $\lambda = 0.1$.

The revised nodalization was also investigated for FLCRIT = 0.0 and 0.03 where $\lambda = 0.03$. The results were nearly identical, substantiating the earlier conclusions that FLCRIT had negligible effects on calculated pressures.

The effect of nozzle lip height is more evident in Figure A-12 which shows the pressure profiles obtained for nozzle lip heights of 40 mm, 30 mm (the original model), and 0 mm (no lip). The jet flashing and flow expansion is so strong and immediate that any relief in terms of increased flow area between the jet exit and plate results in significant pressure differences on the baffle plate.

A velocity vector plot of the C12 jet flow field, with the correct lip height and interphasic values of $\lambda = 0.02$, $K = 1.0 \times 10^7$, $R = 1.0 \times 10^{10}$, and FLCRIT = 0.03, is presented in Figure A-13. In contrast to the KWU jet flow field (Figure A-5), there is no pluming effect beyond the nozzle lip. Furthermore, flow entrainment and recirculation are evident in the surrounding flow field which is not present in the KWU jet flow field.

Contour plots of pressure, void fraction, and net mass transfer rate are presented in Figure A-14 for the jet core vicinity. These contour patterns show that flashing occurs immediately after the jet flow exits and that most of the interphasic mass transfer takes place in the area surrounded by the nozzle lip flange.

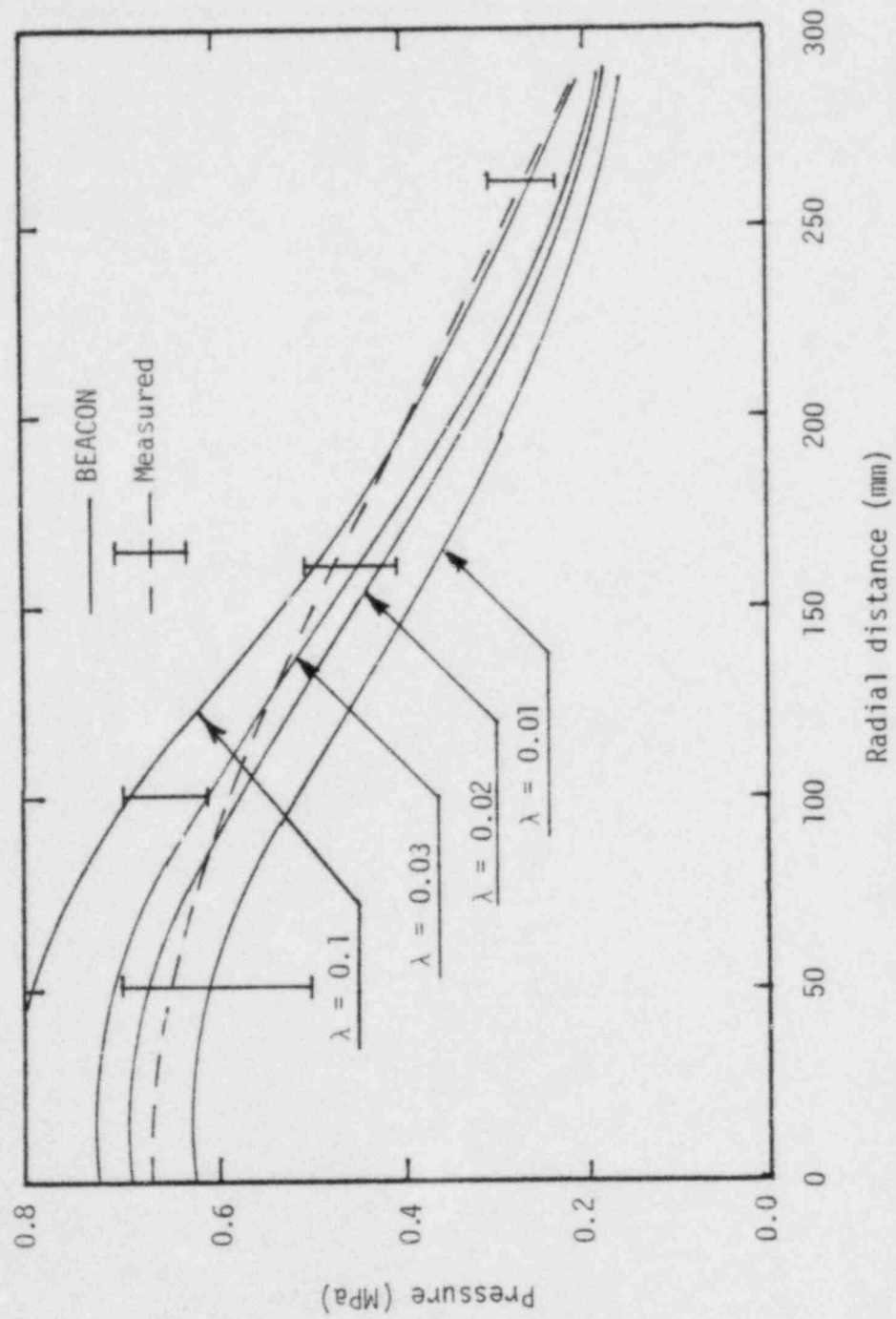


Figure A-11. C12 jet pressure distribution using correct lip height and showing the effects of mass transfer.

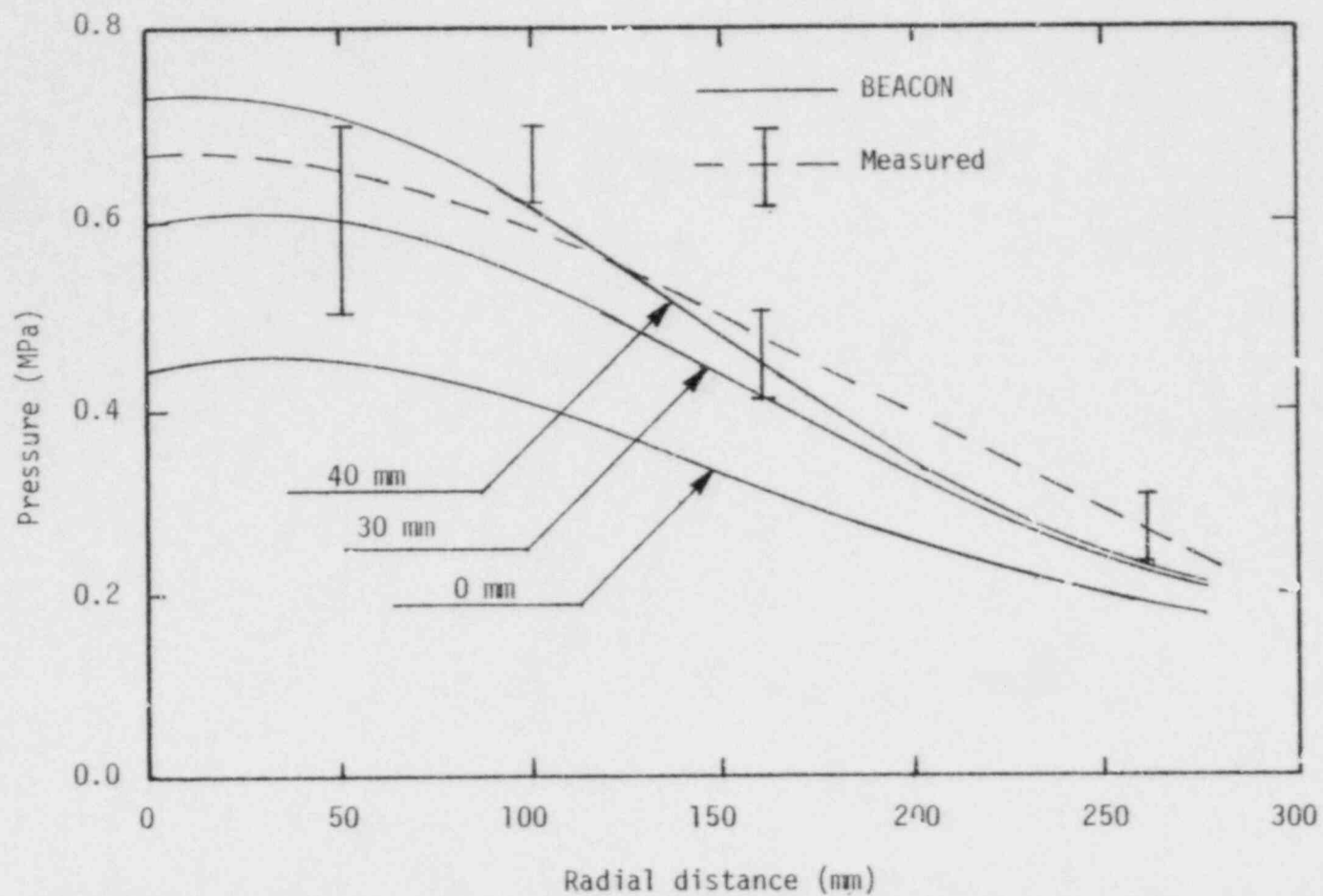


Figure A-12. C12 jet pressure distribution showing the effect of nozzle lip height.

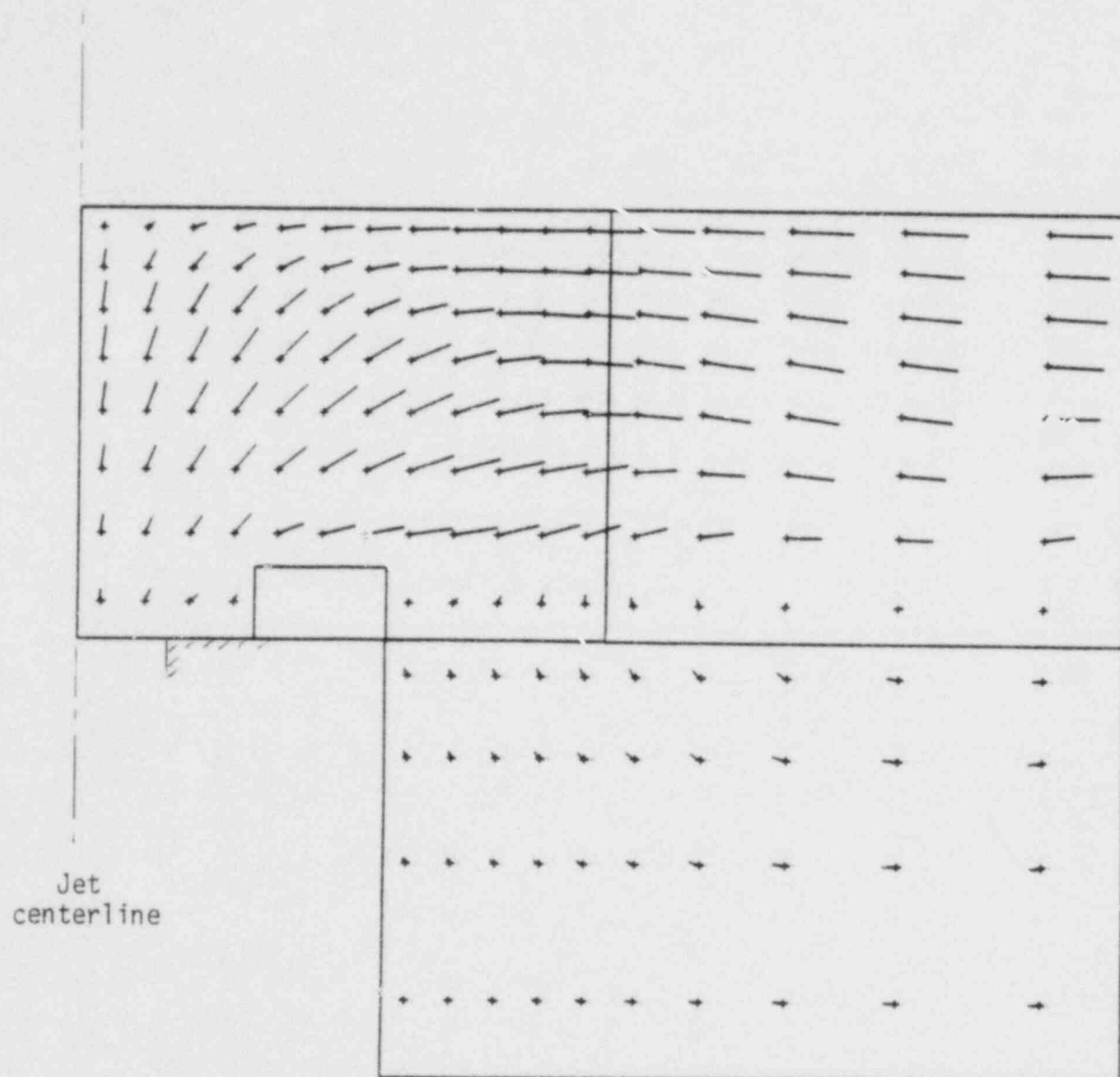
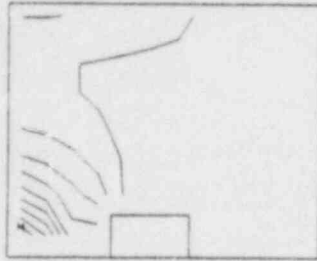
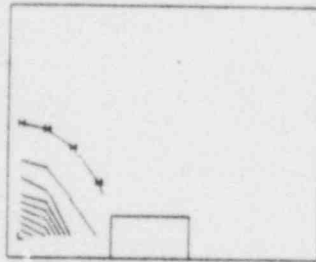


Figure A-13. BEACON velocity vector plot from the C12 jet analysis.

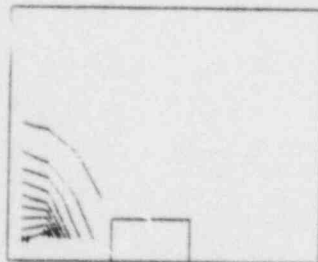
POOR ORIGINAL



PRESSURE
TIME= 5.000-03 CYCLE= 478 MESH= 1 DEGR= AXISY JWR= BEST= BEST
MIN= 5.810-04 MAX= 3.133-06 L= 5.810-04 H= 2.825-06 DG= 3.075-05



VOID FRACT
TIME= 5.000-03 CYCLE= 478 MESH= 1 DEGR= AXISY JWR= BEST= BEST
MIN= 5.935-01 MAX= 1.000-00 L= 5.935-01 H= 9.993-01 DG= 4.000-02



NET MASS TRANSFER RATE
TIME= 5.000-03 CYCLE= 478 MESH= 1 DEGR= AXISY JWR= BEST= BEST
MIN= 9.727-04 MAX= 2.034-04 L= 9.727-04 H= 2.041-04 DG= 2.034-03

Figure A-14. BEACON contour plots of pressure, void fraction, and net mass transfer rate from the C12 jet analysis.

CONCLUSIONS AND RECOMMENDATIONS

Two jet impingement tests have been modeled and analyzed. Parametric variations of the interphasic exchange parameters have been obtained. Best-estimate values for these parameters have been selected based on comparisons with test data. The best-estimate values selected are:

<u>Parameter</u>	<u>Function</u>	<u>Value</u>
λ	Mass transfer multiplier	0.1
K	Momentum transfer rate	1.0×10^7
R	Heat transfer rate	1.0×10^{10}
FLCRIT	Flashing switch	0.0

The value of $\lambda = 0.1$ was selected for two reasons. First, using this value and the correct nozzle lip height gave very good results at distances greater than 150 mm from the C12 jet centerline. Since BEACON containment analyses normally involve distances much greater than this, the greatest accuracy would probably result from using $\lambda = 0.1$. Second, previous flashing model studies by Rivard and Torrey using the KACHINA code^{A-4} also indicated that the best value for λ was 0.1. The best-estimate values of $K = 1.0 \times 10^7$, $R = 1.0 \times 10^{10}$, and $FLCRIT = 0.0$ were selected based on code stability criteria and data agreement considerations.

The analysis has also shown that the nozzle lip geometry has a strong effect on the jet flow field. Future analyses of other two-phase jet experiments should use an accurate modeling of the nozzle lip geometry.

REFERENCES

- A-1 Sicherheitstechnisches Forschungsprogramm Auf Dem Gebiet Der Leichtwasserreaktoren Abschlußbericht, Kraftwerk Union, Reaktortechnik, October 1975 (in German only).
- A-2 Untersuchung der Vorgänge in einem mehrfach unterteilten Containment beim Bruch einer Kühltelleitung wassergekühlter Reaktoren Technischer, Bericht BF RS 50-32-C12-1, Battelle-Institute, Frankfurt, September 1976 (in German only).
- A-3 Experimental Investigation of the Jet Force and its Local Distribution in Case of Rupture of a Primary Circuit Pipe, Bericht BF-RS 50-62-7, Battelle-Institute, Frankfurt, January 1979.
- A-4 W. C. Rivard and M. D. Torrey, Numerical Calculation of Flashing from Long Pipes Using a Two-Field Model, LA-6104-MS, 1977.

APPENDIX B

PIPE FLOW NODALIZATION STUDY

INTRODUCTION

Pressure losses in a flowing fluid caused by variations in the configuration of the flow channel are calculated by the BEACON code when it is used for the hydraulic analysis of a fluid flow system.

This study was made to determine the accuracy of the pressure loss values computed by BEACON and also to determine if the results were dependent upon the degree of flow channel nodalization used. The study was made using practical rates of incompressible flow through various geometries in varying sizes of pipe. The selected combinations of geometries and pipe sizes resulted in an array of nine basic cases. For each case, the nodalization was adjusted to determine the effect of mesh fineness on pressure loss calculations. In most cases, the results were reasonable but higher than the analytical solution and independent of nodalization.

SYSTEM DESCRIPTION

The flow system used for this study consisted of an inlet line connected to an outlet line in a manner which allowed representation of an abrupt contraction, an abrupt expansion, or a thin plate orifice. Pipe sizes of 2-, 3-, 4- and 6-in. diameter were used to obtain flow area ratios of 2.25:1, 4:1, and 9:1. Incompressible fluid flow through the system was maintained by imposing a driving force of 4 psi at the system inlet. Pipe lengths were selected in order to maintain a minimum length/diameter ratio of 20:1.

Figure B-1 shows the array of nine basic cases which resulted from the combination of three flow geometries with three flow area ratios. The

Flow
area
ratio

2.25:1

4:1

9:1

Geometry

Contraction

Orifice

Expansion

Case 110	Case 140	Case 170
Case 120 Gross mesh ↓ Typically varied to study mesh effect ↓ Fine mesh	Case 150	Case 180 Gross mesh ↓ Typically varied to study mesh effect ↓ Fine mesh
Case 130	Case 160	Case 190

Figure B-1. Pipe flow study cases.

figure also indicates how the problem nodalization was varied from gross mesh to fine mesh for each case.

Each case was analyzed to a real time value at which steady-state conditions were achieved. Steady-state conditions were verified by substituting code calculated values in the one-dimensional steady-state continuity equation until these values satisfied the equation.

MODEL DESCRIPTION

The piping system for each pipe flow study case was represented for code analysis with an axisymmetric mesh using obstacle cells to obtain the desired geometric configuration. Figure B-2 depicts the actual flow system and the corresponding code representation used for the case of an abrupt contraction with an area flow ratio of 4:1.

To simplify the evaluation of results, the pipe flow cases were analyzed using the input option of zero gravity. A test case specifying full gravity effects verified that this approach did not invalidate results. The no-slip input option was specified to simulate friction at the outer boundary of the mesh which represented the pipe wall.

A driving force of 4 psi was maintained across the system by using a constant velocity input boundary and a constant pressure outflow boundary. Incompressible fluid conditions at the system inlet were maintained at approximately 50 psi and 100°F. Inlet flow velocities for each case were based on suggested flow rates through various pipe sizes taken from a handbook of fluid flow.^{B-1}

With these initial conditions specified, each case was analyzed to obtain values of pressure, temperature, density, and velocity at steady state. These values were used to determine the pressure losses for each case and the effect of mesh size on the calculated values.

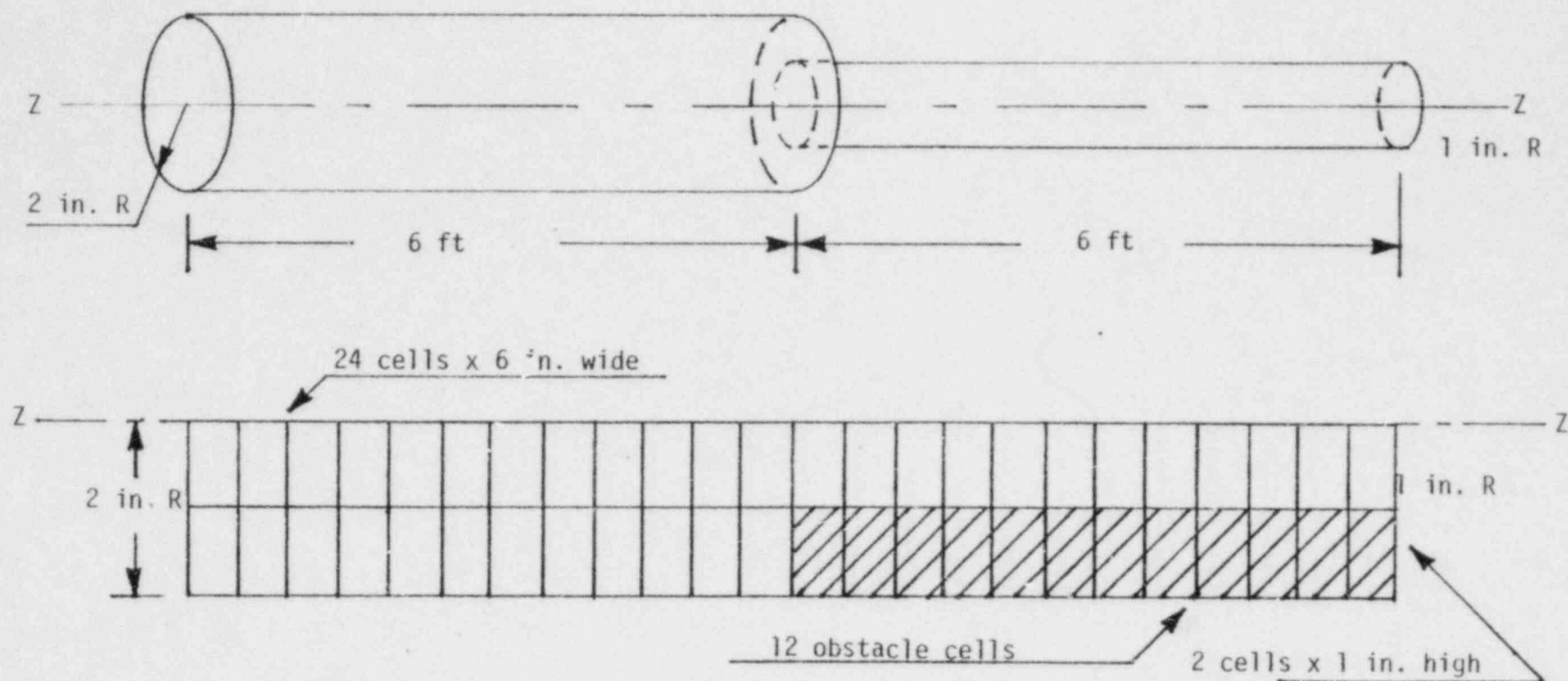


Figure B-2. Pipe flow mesh for the area flow ratio 4:1 abrupt contraction case.

RESULTS

For each case, a comparison was made of code calculated form loss versus reference or experimental form loss. This was done by using the code calculated hydraulic parameters to compute a form resistance coefficient for each flow case. This analytic coefficient was then compared to a reference coefficient taken from a flow resistance coefficient handbook (see Reference B-2). A complete tabulation of form loss coefficients versus reference values is shown in Table B-1. The table shows that the analytically determined form loss coefficients were generally larger than the experimental values taken from the reference handbook. It also shows that the values did not vary appreciably as the mesh fineness was increased. This is shown graphically in Figure B-3.

Following is a typical calculation which demonstrates the evaluation procedure used for each flow case. Figures B-4 and B-5 show BEACON code input and one page of code output for this typical case.

Case 120:

Abrupt Contraction
Flow Area Ratio 4:1
Gross Mesh.

Output Values at 4 Seconds:

	<u>Inlet</u>	<u>Outlet</u>
P = pressure (N/m^2)	316368.	296476.
ρ = density (kg/m^3)	988.986	988.920
V = velocity (m/sec)	1.21926	4.88201
A = area (m^2)	0.00811	0.00203

TABLE B-1. FORM LOSS COEFFICIENTS

Flow Area Ratio	Mesh Fineness (Inlet Node Cells)	Flow Geometry		
		Contraction	Expansion	Orifice
2.25:1	Experimental value	0.278	0.309	1.22
	1 (Gross mesh)	----	0.74	----
	2	0.58	0.74	1.37
	4 (Fine mesh)	0.58	----	1.37
4:1	Experimental value	0.375	0.563	1.85
	1	----	0.94	----
	2	0.81	0.94	1.69
	4	0.75	0.94	1.72
	6	0.75	0.94	1.72
	8	0.75	----	1.79
9:1	Experimental value	0.444	0.790	2.53
	1	----	0.99	----
	2	1.42	0.99	1.87
	4	1.42	----	1.87

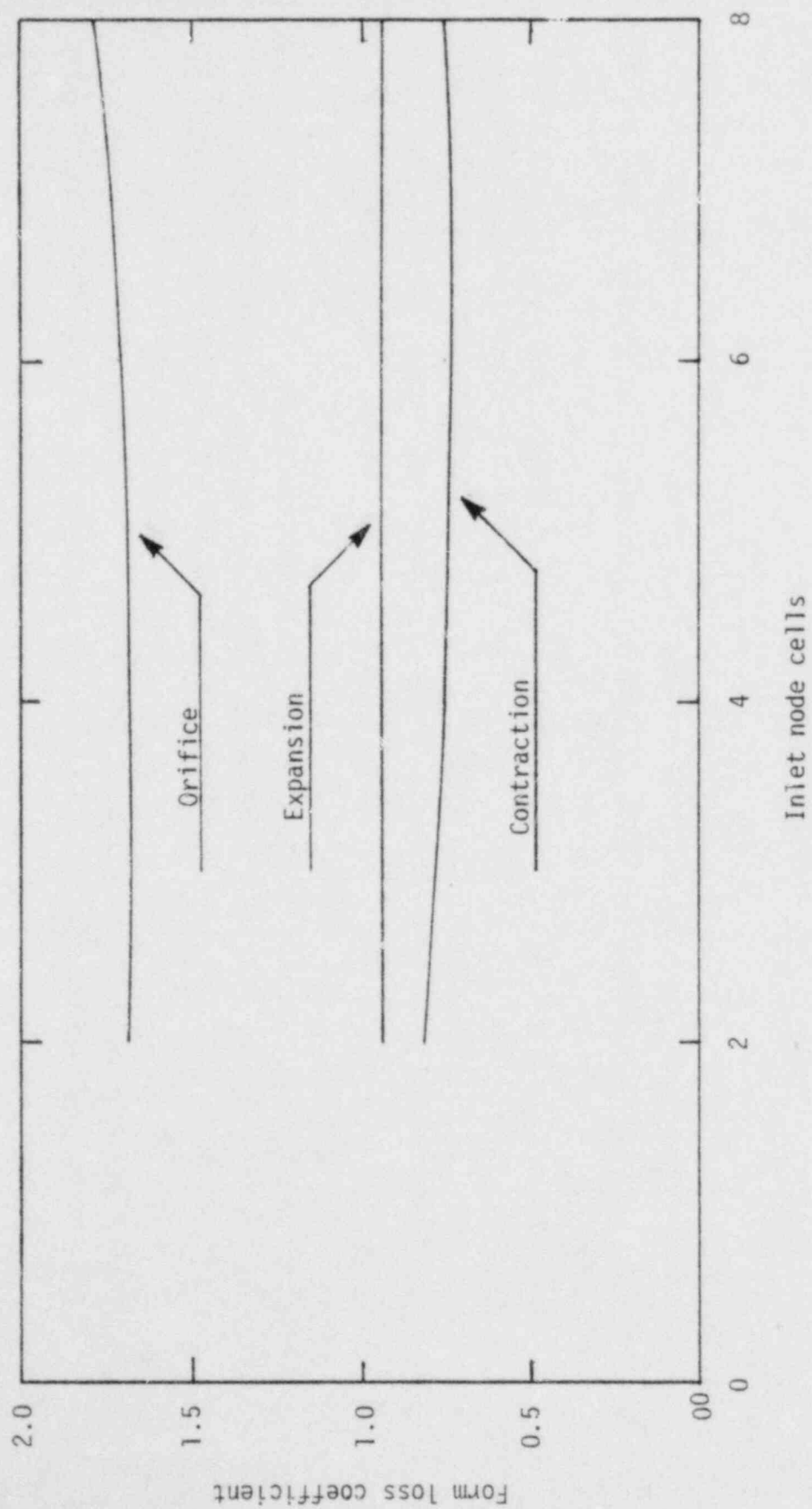


Figure B-3. Node study results showing how calculated form loss coefficients vary with increased mesh fineness.

LISTING OF INPUT DATA FOR CASE 1

```

00100 *NODE STUDY--CONTRACTION--CASE 120F1
00101 *PROB1--ALPHA2 CONTRN OF 4.1--MESH--FINAL
00102 *STEADY STATE--LIQUID--AXISYMMETRIC--NO GRAV
00103 *SMALL SCALE--SMALL EPS--GORE VISC--4 DELTA V--16FPS2
00104 *****
00105 *BASIC BOOLEAN INPUT
00106 *NOREAD, 0, WRITE, 20, NOCOPY
00107 *0.0, 1.0, 0.00010, 1.0, 0.0, 10, XEQ, USERDEF
00108 *0.001, 0.02, 0.002, 0.5, 0.05, 25.0
00109 *
00110 *PRINT, NOPRINT, NOPRINT, NOPRINT, NOPRINT, NOPRINT
00111 *PLOTS, 0.00, 0.1 0.0 0.0 0.0 0.0 0.0 0.0 0.0
00112 *
00113 *1.0, 0.00000, 0.00000, 0.0, 1.0, 1
00114 *0.0, 0.0, 0.0, 500000.0
00115 *0.0, 0.0, 0.0, 1.0
00116 *ASL, 1, 1.0/IN2, DEGR, FT, SEC-1
00117 *
00118 *AXISYP, 2, 2, 1.0, 0.0, 0.0, IN, 0.0, 0.0
00119 *SLIP, NO SLIP, 1, 1, 1
00120 *MIXTURE, 2, 2, 3, 25, 0, 45.0, 650.0, 650.0, 0.001, 1.0
00121 *
00122 *SMALL SCALE REGION INPUT
00123 *
00124 *DECIRED BOUNDARY INPUT
00125 *INFLOW, 2, 1, 3, 1
00126 *INLET, 0.0, 0.0, 650.0, 650.0, 0.001, 1.0
00127 *0.0, 4.0, 0.0, 4.0
00128 *CENTIP, 2, 2, 3, 26
00129 *MIXTURE, 43.0, 650.0, 650.0, 0.001, 1.0

```

Figure B-4. BEACON input for the air flow ratio 4.1 abrupt contraction case.

POOR ORIGINAL

TIME	4.000E+00	CYCLE	1259	MCOE STUDY--CONTRACTION--CASE	120F	GEOM-AXIS	15	EOSOPT-LASL	BEST-USERDEF	RGP	RIP	KDRAG	12/22
RESHNO	1	1	1	1	1	1	1	1	1	1	1	1	1
1	1	1	1	1	1	1	1	1	1	1	1	1	1
2	1	1	1	1	1	1	1	1	1	1	1	1	1
3	1	1	1	1	1	1	1	1	1	1	1	1	1
4	1	1	1	1	1	1	1	1	1	1	1	1	1
5	1	1	1	1	1	1	1	1	1	1	1	1	1
6	1	1	1	1	1	1	1	1	1	1	1	1	1
7	1	1	1	1	1	1	1	1	1	1	1	1	1
8	1	1	1	1	1	1	1	1	1	1	1	1	1
9	1	1	1	1	1	1	1	1	1	1	1	1	1
10	1	1	1	1	1	1	1	1	1	1	1	1	1
11	1	1	1	1	1	1	1	1	1	1	1	1	1
12	1	1	1	1	1	1	1	1	1	1	1	1	1
13	1	1	1	1	1	1	1	1	1	1	1	1	1
14	1	1	1	1	1	1	1	1	1	1	1	1	1
15	1	1	1	1	1	1	1	1	1	1	1	1	1
16	1	1	1	1	1	1	1	1	1	1	1	1	1
17	1	1	1	1	1	1	1	1	1	1	1	1	1
18	1	1	1	1	1	1	1	1	1	1	1	1	1
19	1	1	1	1	1	1	1	1	1	1	1	1	1
20	1	1	1	1	1	1	1	1	1	1	1	1	1
21	1	1	1	1	1	1	1	1	1	1	1	1	1
22	1	1	1	1	1	1	1	1	1	1	1	1	1
23	1	1	1	1	1	1	1	1	1	1	1	1	1
24	1	1	1	1	1	1	1	1	1	1	1	1	1
25	1	1	1	1	1	1	1	1	1	1	1	1	1
26	1	1	1	1	1	1	1	1	1	1	1	1	1
27	1	1	1	1	1	1	1	1	1	1	1	1	1
28	1	1	1	1	1	1	1	1	1	1	1	1	1
29	1	1	1	1	1	1	1	1	1	1	1	1	1
30	1	1	1	1	1	1	1	1	1	1	1	1	1
31	1	1	1	1	1	1	1	1	1	1	1	1	1
32	1	1	1	1	1	1	1	1	1	1	1	1	1
33	1	1	1	1	1	1	1	1	1	1	1	1	1
34	1	1	1	1	1	1	1	1	1	1	1	1	1
35	1	1	1	1	1	1	1	1	1	1	1	1	1
36	1	1	1	1	1	1	1	1	1	1	1	1	1
37	1	1	1	1	1	1	1	1	1	1	1	1	1
38	1	1	1	1	1	1	1	1	1	1	1	1	1
39	1	1	1	1	1	1	1	1	1	1	1	1	1
40	1	1	1	1	1	1	1	1	1	1	1	1	1
41	1	1	1	1	1	1	1	1	1	1	1	1	1
42	1	1	1	1	1	1	1	1	1	1	1	1	1
43	1	1	1	1	1	1	1	1	1	1	1	1	1
44	1	1	1	1	1	1	1	1	1	1	1	1	1
45	1	1	1	1	1	1	1	1	1	1	1	1	1
46	1	1	1	1	1	1	1	1	1	1	1	1	1
47	1	1	1	1	1	1	1	1	1	1	1	1	1
48	1	1	1	1	1	1	1	1	1	1	1	1	1
49	1	1	1	1	1	1	1	1	1	1	1	1	1
50	1	1	1	1	1	1	1	1	1	1	1	1	1
51	1	1	1	1	1	1	1	1	1	1	1	1	1
52	1	1	1	1	1	1	1	1	1	1	1	1	1
53	1	1	1	1	1	1	1	1	1	1	1	1	1
54	1	1	1	1	1	1	1	1	1	1	1	1	1
55	1	1	1	1	1	1	1	1	1	1	1	1	1
56	1	1	1	1	1	1	1	1	1	1	1	1	1
57	1	1	1	1	1	1	1	1	1	1	1	1	1
58	1	1	1	1	1	1	1	1	1	1	1	1	1
59	1	1	1	1	1	1	1	1	1	1	1	1	1
60	1	1	1	1	1	1	1	1	1	1	1	1	1
61	1	1	1	1	1	1	1	1	1	1	1	1	1
62	1	1	1	1	1	1	1	1	1	1	1	1	1
63	1	1	1	1	1	1	1	1	1	1	1	1	1
64	1	1	1	1	1	1	1	1	1	1	1	1	1
65	1	1	1	1	1	1	1	1	1	1	1	1	1
66	1	1	1	1	1	1	1	1	1	1	1	1	1
67	1	1	1	1	1	1	1	1	1	1	1	1	1
68	1	1	1	1	1	1	1	1	1	1	1	1	1
69	1	1	1	1	1	1	1	1	1	1	1	1	1
70	1	1	1	1	1	1	1	1	1	1	1	1	1
71	1	1	1	1	1	1	1	1	1	1	1	1	1
72	1	1	1	1	1	1	1	1	1	1	1	1	1
73	1	1	1	1	1	1	1	1	1	1	1	1	1
74	1	1	1	1	1	1	1	1	1	1	1	1	1
75	1	1	1	1	1	1	1	1	1	1	1	1	1
76	1	1	1	1	1	1	1	1	1	1	1	1	1
77	1	1	1	1	1	1	1	1	1	1	1	1	1
78	1	1	1	1	1	1	1	1	1	1	1	1	1
79	1	1	1	1	1	1	1	1	1	1	1	1	1
80	1	1	1	1	1	1	1	1	1	1	1	1	1
81	1	1	1	1	1	1	1	1	1	1	1	1	1
82	1	1	1	1	1	1	1	1	1	1	1	1	1
83	1	1	1	1	1	1	1	1	1	1	1	1	1
84	1	1	1	1	1	1	1	1	1	1	1	1	1
85	1	1	1	1	1	1	1	1	1	1	1	1	1
86	1	1	1	1	1	1	1	1	1	1	1	1	1
87	1	1	1	1	1	1	1	1	1	1	1	1	1
88	1	1	1	1	1	1	1	1	1	1	1	1	1
89	1	1	1	1	1	1	1	1	1	1	1	1	1
90	1	1	1	1	1	1	1	1	1	1	1	1	1
91	1	1	1	1	1	1	1	1	1	1	1	1	1
92	1	1	1	1	1	1	1	1	1	1	1	1	1
93	1	1	1	1	1	1	1	1	1	1	1	1	1
94	1	1	1	1	1	1	1	1	1	1	1	1	1
95	1	1	1	1	1	1	1	1	1	1	1	1	1
96	1	1	1	1	1	1	1	1	1	1	1	1	1
97	1	1	1	1	1	1	1	1	1	1	1	1	1
98	1	1	1	1	1	1	1	1	1	1	1	1	1
99	1	1	1	1	1	1	1	1	1	1	1	1	1
100	1	1	1	1	1	1	1	1	1	1	1	1	1

Figure B-5. BEACON output for the area flow ratio 4:1 abrupt contraction case.

Steady-State Check:

$$(\rho VA)_{in} = (\rho VA)_{out}$$

$$(988.986)(1.21926)(0.00811) = (988.920)(4.88201)(0.00203)$$

$$9.77929 \sim 9.78860$$

$$\text{Error} = \frac{0.00931}{9.77929} \times 100 = 0.09\%$$

This indicates values are steady-state.

Analytical Form Loss:

$$P_{in} + \left(\frac{\rho V^2}{2}\right)_{in} = P_{out} + \left(\frac{\rho V^2}{2}\right)_{out} + F_v$$

$$316368 + \frac{(988.986)(1.21926)^2}{2} = 296476 + \frac{(988.970)(4.88201)^2}{2} + F_v$$

$$F_v = 316368 + 735 - 296476 - 11785$$

$$F_v = \text{form loss} = 8842 \text{ N/m}^2 \text{ (analytical).}$$

Experimental Form Loss:

$$\text{Re} = \text{Reynold's No.} = \frac{w_o D_H}{\gamma}$$

$$w_o = \text{flow velocity (m/sec)}$$

$$D_{t1} = \text{hydraulic diameter (m)}$$

$$\gamma = \text{kinematic viscosity (m}^2/\text{sec)}$$

$$Re = \frac{(4.88)(2)}{(1.5 \times 10^{-5})} = 6.5 \times 10^5.$$

This indicates that appropriate form loss coefficients should be taken from Section III, Diagram 3-9 of Reference B-2. For expansion cases, the values were taken from Section IV, Diagram 4-1. For orifice cases the coefficients were taken from Section IV, Diagram 4-13.

$$F/V = K \left(\frac{\rho V^3}{2} \right)$$

$$K = \text{form loss coefficient} = 0.375$$

$$F/V = (0.375) \frac{(988.920)(4.88201)^2}{2}$$

$$F/V = (0.375)(11785)$$

$$F/V = \text{form loss} = 4419 \text{ N/m}^2 \text{ (experimental).}$$

Result:

The code calculated form loss is about twice the experimental value for this case. In terms of the form loss coefficient, the reference form loss is 0.375 while the analytical form loss is 0.75.

CONCLUSIONS AND RECOMMENDATIONS

The study showed that the BEACON code predicted form related pressure losses which were reasonable, but which were generally higher than expected based upon experimental results taken from a handbook of hydraulic resistance coefficients (see Reference B-2). The study also showed that the BEACON calculated form losses were relatively independent of the degree of nodalization used for each problem.

Specifically, for incompressible flow in pipe sizes of 6-in. diameter and smaller, the BEACON code calculates pressure losses associated with abrupt area changes which are larger than experimentally determined values. The closest agreement was obtained for the orifice geometry while the expansion and contraction cases resulted in coefficients which were about double the predicted values. For the typical case reported in the results section, a doubled value for the resistance coefficient actually amounted to an error of less than 1 psid in the predicted pressure loss across the system. The degree of nodalization had little effect on predicted values.

The BEACON numerical technique yields pressure loss values which are reasonable but high for liquid flow through abrupt area changes in small pipes. This conforms with conclusions based upon results obtained with a smaller transient analysis code.^{B-3} For this type of a problem, a form loss value should not be specified in BEACON input values. Neither should a fine mesh be specified in defining nodalization for this type of analysis.

The form loss calculational technique in the BEACON code should be modified to permit the input option of a negative form loss. This would permit the downward adjustment of form related pressure losses for cases where it is known that the analytical values are too high. Presently, a negative form loss is identified as a fatal input error. A companion analysis using incompressible flow in large ducts would be of value as further code evaluation. This should be done following the addition of the negative form loss capability to the code.

REFERENCES

- B-1. Flow of Fluids, Crane Company, Technical Paper 410, 1976.
- B-2. I. E. Idel'chik, Handbook of Hydraulic Resistance, AEC-TR-6630, 1966.
- B-3. Transient Reactor Analysis Code, User's Manual Draft, Los Alamos Scientific Laboratory.

APPENDIX C

DREXEL ENTRAINMENT/DEENTRAINMENT ANALYSIS

INTRODUCTION

The purpose of this analysis was to examine the ability of BEACON to correctly calculate entrainment and deentrainment of liquid water in subcompartments subjected to LOCA conditions. This task was accomplished by using BEACON to model an experiment which was carried out at Drexel University to determine entrainment rates.^{C-1} Although evaluating deentrainment rates was not a specific objective of the Drexel experiments, deentrainment data was included in the report as part of the time-history plots for entrainment.

SYSTEM DESCRIPTION

Figure C-1 is a schematic of the Drexel experimental setup. A premixed air-water mixture was sprayed through a nozzle into a square steel duct. The ratio of air to water was held constant throughout the test which lasted for approximately 40 minutes. As the mixture flowed through the test section, the portion of interest for the BEACON analysis, part of the water settled in the test section and part flowed out the orifice at the end of this section. In order to measure the amount of water settling in the test section, the collected water was weighted at selected time intervals until steady-state was achieved. The water volume history from this experiment was used in the BEACON comparison.

MODEL DESCRIPTION

Figure C-2 is a schematic of the BEACON model of the Drexel experiment. The BEACON model consisted of three Eulerian meshes and one lumped parameter compartment. The first mesh consisted of one cell which had air and liquid sources with mass flow rates matching those used in the

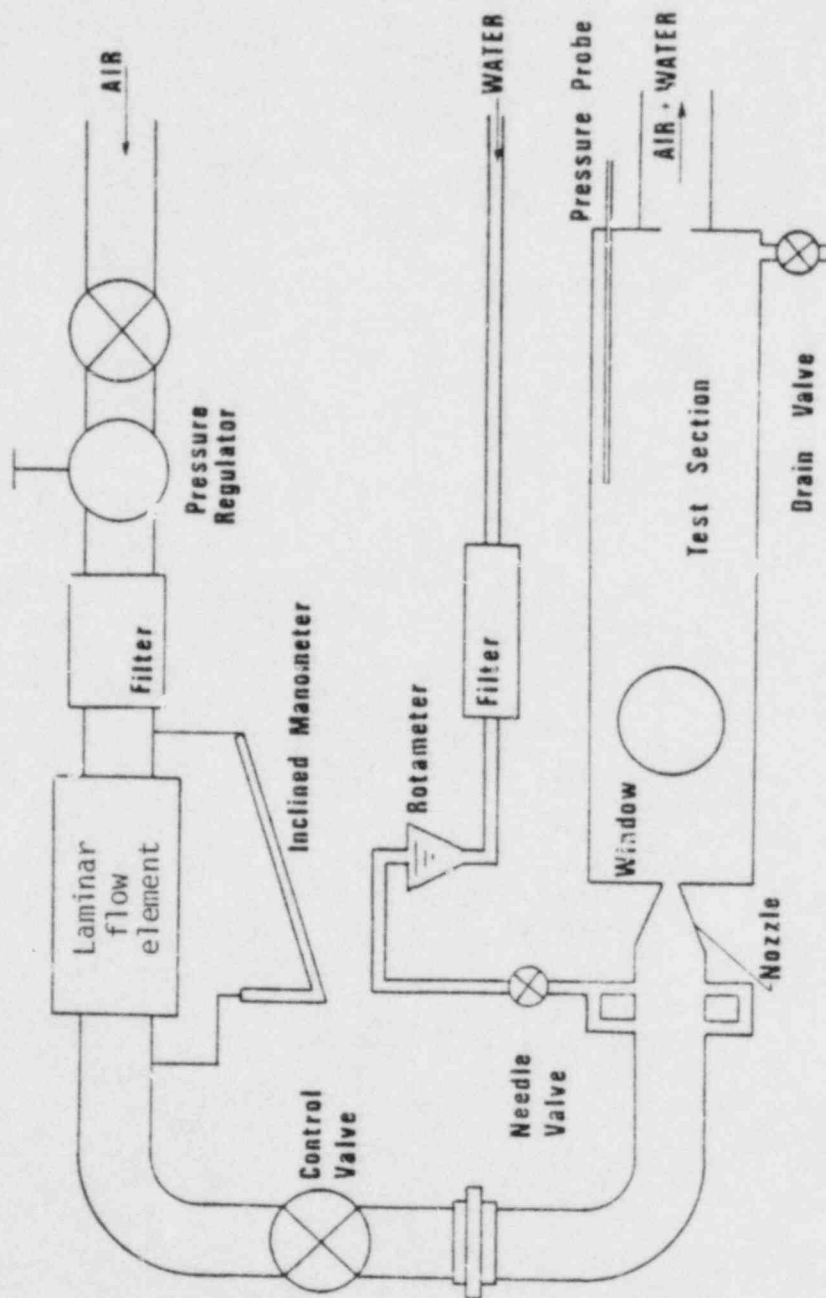


Figure C-1. Schematic arrangement of the Drexel experimental setup.

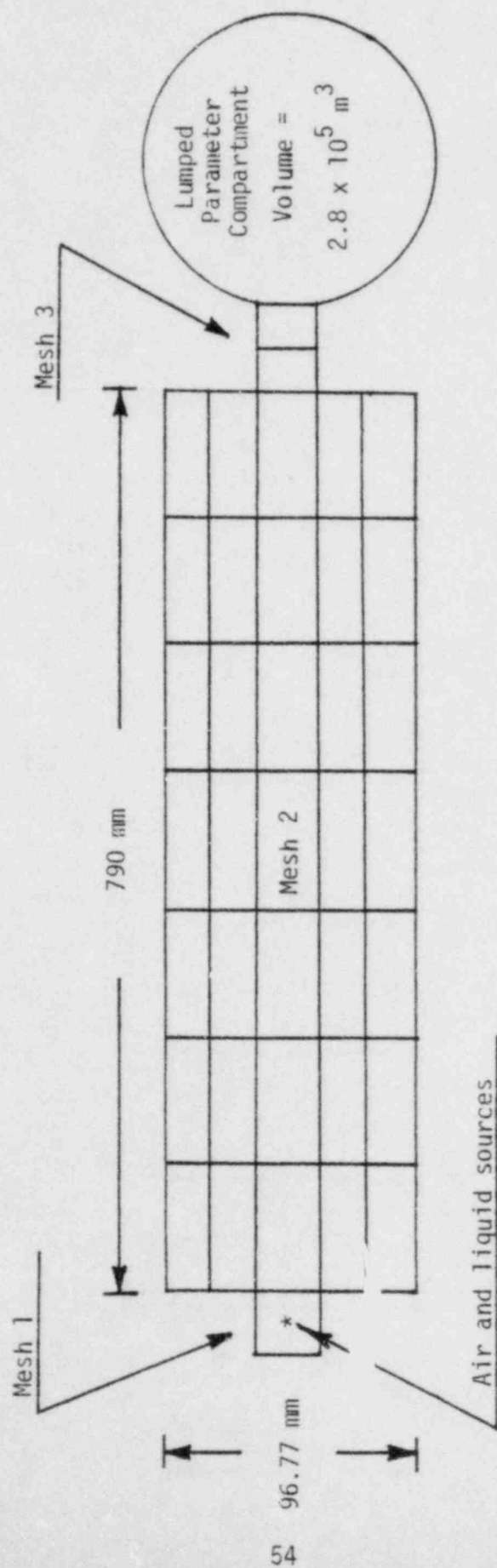


Figure C-2. Schematic of the BEACoN model of the Drexel experiment.

Drexel experiment. This cell was coupled to the left end of mesh 2, which was a two-dimensional (two-D) mesh, simulating the test section of the experiment. The right end of mesh 2 was then coupled to another one-dimensional (one-D) mesh which was used to model the outlet orifice of the test section. Finally, this one-D mesh was coupled to a very large lumped parameter compartment which functioned as a receiver for the outflow. The inlet nozzle to the test section was not considered to be of great importance in relation to the objectives of the problem and was thus not modeled. The BEACON input data is shown in Figure C-3.

The comparison to be made with the data at a given time is the total amount of liquid water mass in mesh 2. This is done by the summation

$$\text{Total liquid mass} = \sum_{i=1}^N (\rho_{L_i}') (V_i)$$

where

ρ_{L_i}' = microscopic liquid density in cell i ; mass of liquid in cell i per unit volume of cell i (printed out in BEACON major edits as RLP)

V_i = volume of cell i

N = total number of fluid cells in mesh 2.

It was not practical to run the code for the full 40 minutes of the test. Instead, BEACON was used to model the first few seconds of the test to compare deentrainment rates. Then, the code was run for a few seconds under conditions which existed in the Drexel test section at steady-state to evaluate entrainment calculations.


```

00100 DREXEL ENTRAINMENT TEST - COARSE NODALIZATION
00105 NOREAD 1 NOCOPY
00110 0.0 2.0 .0001 SEC 5.0 1 XEQ BEST
00120 .01 0.2 .1 10.0
00130 AUTJOT 20 .1 1.2
00140 PRINT NOPI INT PRINT NOPI NOPI NOPI NOPI
00150 PLOTS .9 1 1 0 0 1 0 0 0 0 0 0 0
00160 3 .01
00200 1.5 .0001 .0001 100 5 G
00240 LASL PT LBF/IN2 CLCF FT SEC-1
011000 CARTSN 1 1 30. 25.4 25.4 MM 0. 1.
021000 CARTSN 7 5 15. 25.4 25.4 MM 0. 1.
021020 70. 100. 150. 150. 100. 70.
021030 17.64 17.64 25.4 17.64 17.64
031000 CARTSN 2 1 40. 25.4 25.4 MM 0. 1.
004001 3 3 2 2 2 2 2 2 2 2 2 2 2
011101 AIR 2 2 2 2 2 2 2 2 2 2 2 2 2
021101 AIR 2 2 2 2 2 2 2 2 2 2 2 2 2
031101 AIR 2 2 2 2 2 2 2 2 2 2 2 2 2
012000 2.800 1.6 FT3
012010 AIR 14.7 6.4
003010 LAQU 10 1 2 2 003011
003060 AIR 1 2 2 003061
003011 SEC KG/SEC C J/KG FT SEC-1
003061 SEC KG/SEC C J/KG FT SEC-1
003012 .0 .000602 84000 0. 0.
003013 10. .000602 84000 0. 0.
003062 .0 .00768 2.945E5 0. 0.
003063 10. .00768 2.945E5 0. 0.
006001 RIGHT 1 2 2 1 2 2 4 1
006002 RIGHT 2 2 4 1 3 2 2 1
007001 RIGHT 3 3 2 1 1.

```

Figure C-3. BEACON input data for the Drexel entrainment test.

RESULTS

When the first BEACON deentrainment run was completed, it was quite evident that not enough water was being deentrained (see Figure C-4). The reason for this was that the interphasic drag coefficient, KDRAG, was limited in the code to a minimum value of 10^7 . Since the best-estimate calculations for KDRAG generally range between 10^{-3} and 10, the best-estimate drag calculations were effectively disabled and the two-phase velocities were locked together, thus preventing correct liquid deentrainment. It was therefore decided to rerun the problem with the code modified to lower the minimum KDRAG value from 10^7 to 10^{-3} . This allowed the code to use the internally calculated values for KDRAG. The results of this run were very close to the Drexel deentrainment data for 0.0 to 2.0 seconds (see Figure C-4).

The first entrainment run was made with KDRAG limited to values above 10^7 . In this case, too much water was entrained and BEACON did not achieve a steady-state condition as in the experiment (see Figure C-5). When the lower limit on KDRAG was set to 10^{-3} , as in the deentrainment run, the numerical scheme became unstable and the code was unable to run.

Entrainment/deentrainment in BEACON is also influenced by the film model, which models liquid films on the walls of compartments. In order to see how the film option might affect the Drexel problem, both the entrainment and deentrainment runs were repeated using the film option. Minimum values for KDRAG were set to 10^7 and then to 10^{-3} . The effect of the film was so small that the runs with film showed almost identical results as those without film.

CONCLUSIONS AND RECOMMENDATIONS

At the present time, BEACON cannot use realistic values for an interphasic drag coefficient due to instabilities which exist in the numerical scheme. If, however, unrealistically high values are used, the

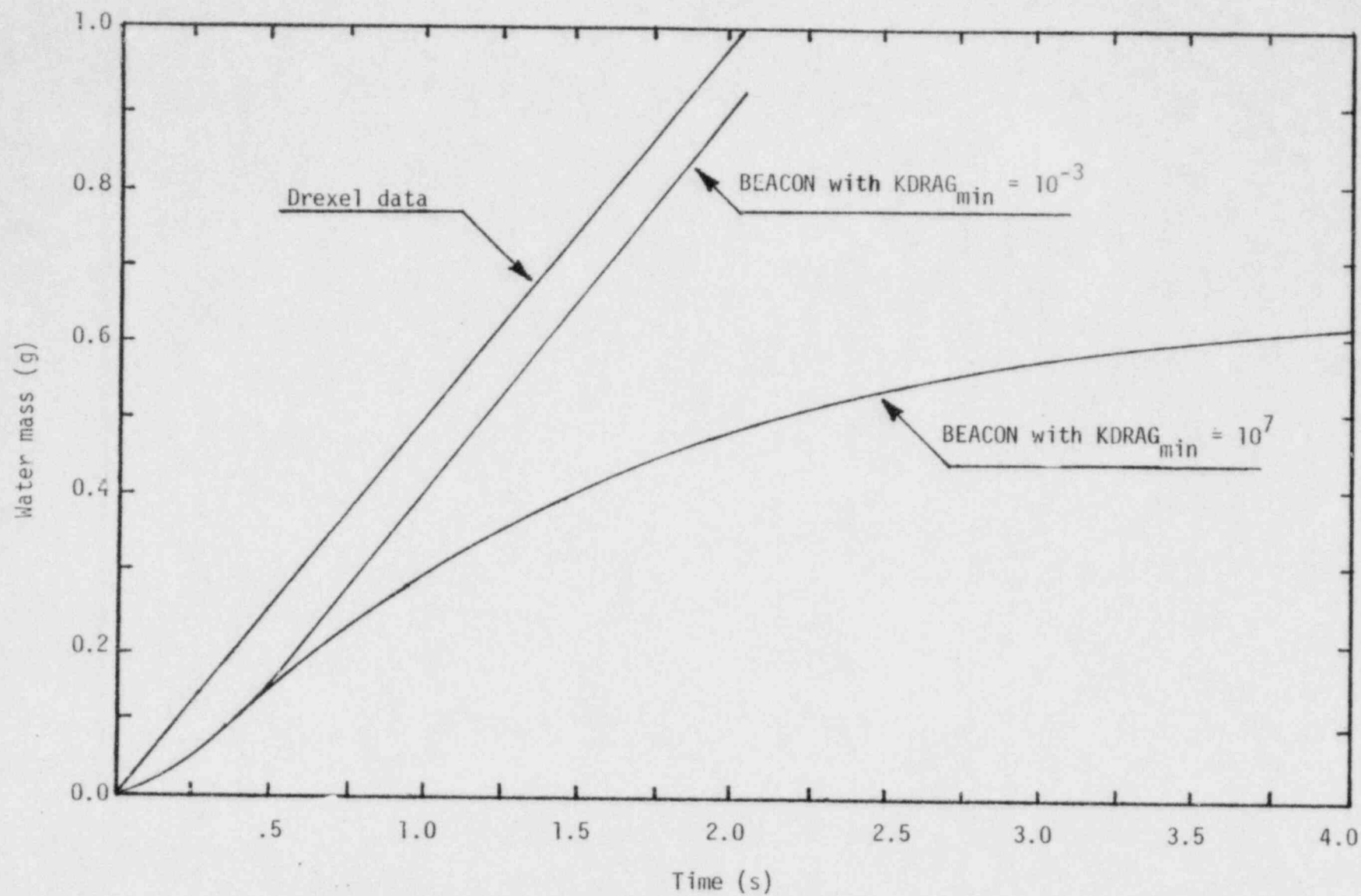


Figure C-4. Comparison of Drexel and BEACON deentrainment.

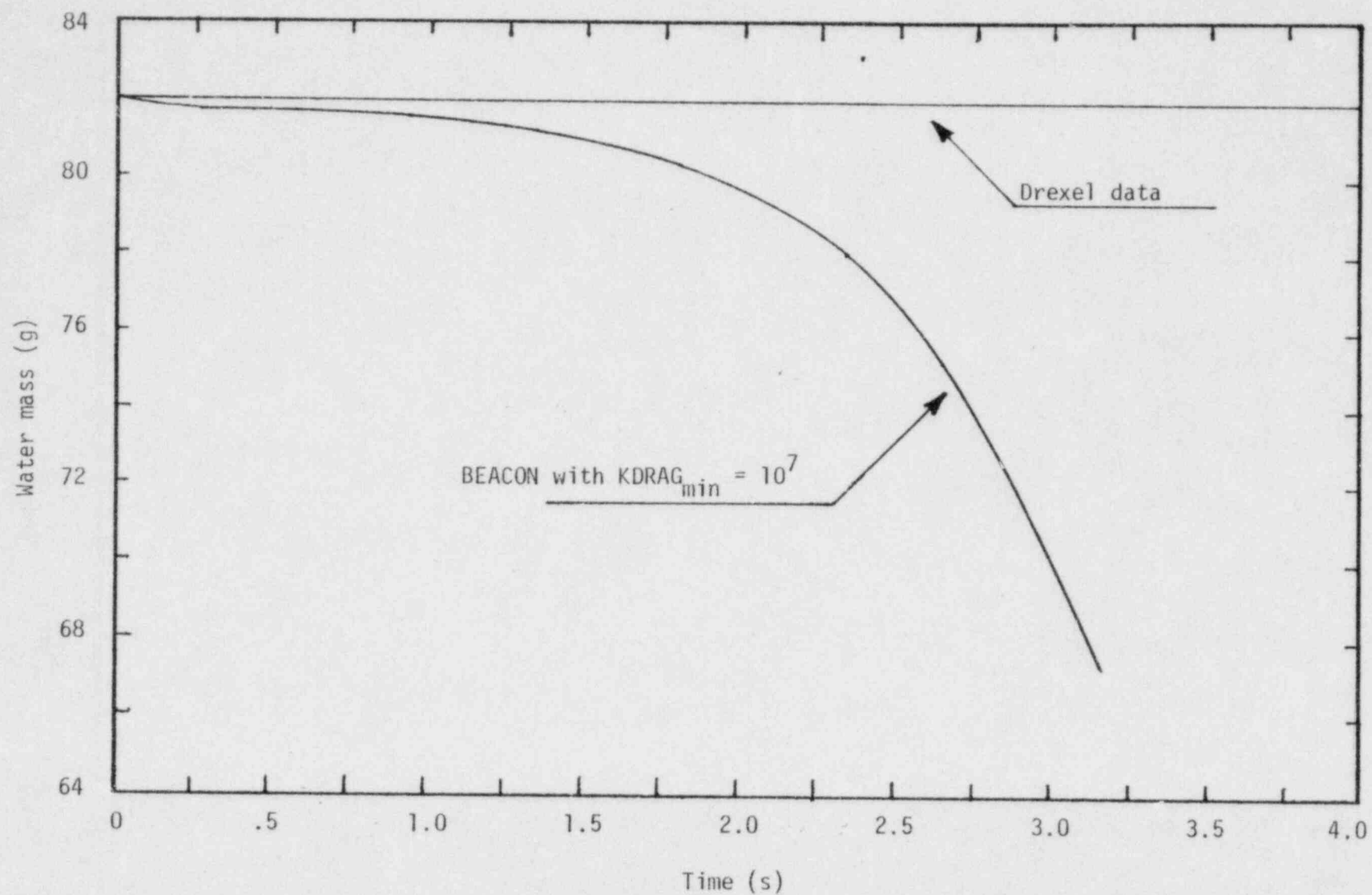


Figure C-5. Comparison Drexel and BEACON entrainment.

code will run but is very inaccurate in predicting entrainment/deentrainment rates. Investigation of this phenomenon indicates that this occurs because some of the K-FIX equations are unstable at extreme void fractions with reasonable values of KDRAG. It also appears that it may be possible to "tune" the equations so that realistic values of KDRAG could be used for the interphasic drag coefficient, resulting in realistic entrainment/deentrainment calculations. The new equations would then be unstable for very high values of KDRAG, and would not allow a user to lock the phases together artificially. Since the emphasis in BEACON development has been on best-estimate calculations, it is recommended that this "tuning" of the equations be done.

REFERENCES

- C-1. Drexel University, Water Entrainment in Intercompartmental Flow, EPRI
NP-648 Project 275-1, February 1978.

APPENDIX D

BATTELLE-FRANKFURT C-9 EXPERIMENT

INTRODUCTION

The C-9 experiment was one in a series of tests performed at the Battelle-Frankfurt facility in Germany simulating the rupture of a primary coolant pipe in a dry PWR containment. This series of experiments was conducted to investigate pressure and temperature phenomena occurring during postulated LOCA conditions. Data obtained from these tests were then used in the development and verification of containment computer codes such as BEACON.

This analysis of the C-9 experiment represents the first time a containment water-line break has been modeled with BEACON/MOD3. The purpose of this study is to evaluate the best-estimate correlations in the new MOD3 version of the code, to identify any areas where further development would be advantageous, and to establish guidelines for future use. The ultimate goal in the development of the code is to obtain results that accurately predict pressure and temperature response during a loss-of-coolant accident.

The Battelle-Frankfurt C-9 experiment was modeled using heat structures, wall film, and best-estimate correlations options. Only the first 2 seconds of the test were analyzed since BEACON is primarily a short-term analysis code. Comparisons were made between the calculated pressures and temperatures and those observed during the simulated LOCA.

SYSTEM DESCRIPTION

The Battelle-Frankfurt test facility is a 1:64 volumetric-scale version of the 1200 MW Biblis, Block A nuclear power plant containment.^{D-1} Experiments utilize up to nine rooms, interconnected by

orifices, nozzles, and circular wall apertures. The interior of the facility is constructed of reinforced concrete coated with several layers of fillers and sealers to prevent water infiltration. Steel and aluminum plates and instrument shields are present in various locations throughout the compartments. The tests are initiated by puncturing a rupture disc to permit pressurized water or steam from an external pressure vessel to enter one of the compartments. A view of the containment test system is given in Figure D-1.

The configuration used for the C-9 experiment consisted of nine compartments concentrically arranged around a central buffer tank. The compartments were interconnected by sharp-edged steel orifices and circular wall openings. A schematic of the test, showing room volumes and aperture flow areas, is given in Figure D-2. Initial conditions were reported (only for Room 9) as:

Pressure	=	0.1 MPa
Temperature	=	290 K. ^{D-2}

Initial conditions were assumed to be the same throughout the containment.

For the C-9 test, the coolant pipe rupture was simulated by introducing water from the pressure vessel (11.85 MPa, 564.4 K) into Room 4 through a 100 mm diameter orifice in the rupture device. The blowdown was directed onto a 600 mm diameter baffle plate 240 mm from the orifice.

During the experiment, the blowdown mass flow rate, temperature, pressure, and density data were measured as well as selected temperatures, pressures, and differential pressures in the various compartments. Blowdown enthalpies were determined from the temperatures recorded in the high pressure system.

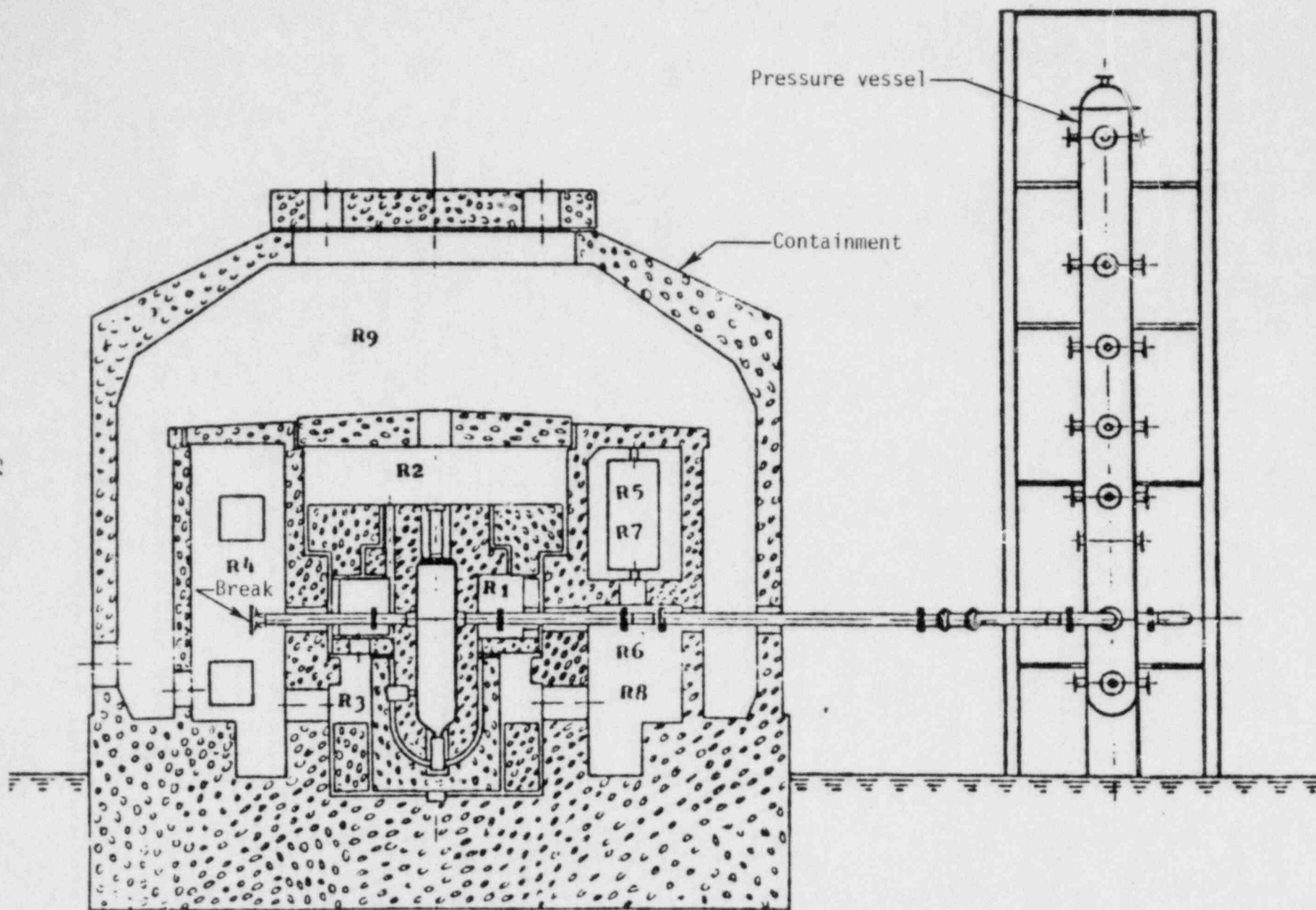


Figure D-1. Rattelle-Frankfurt containment test system.

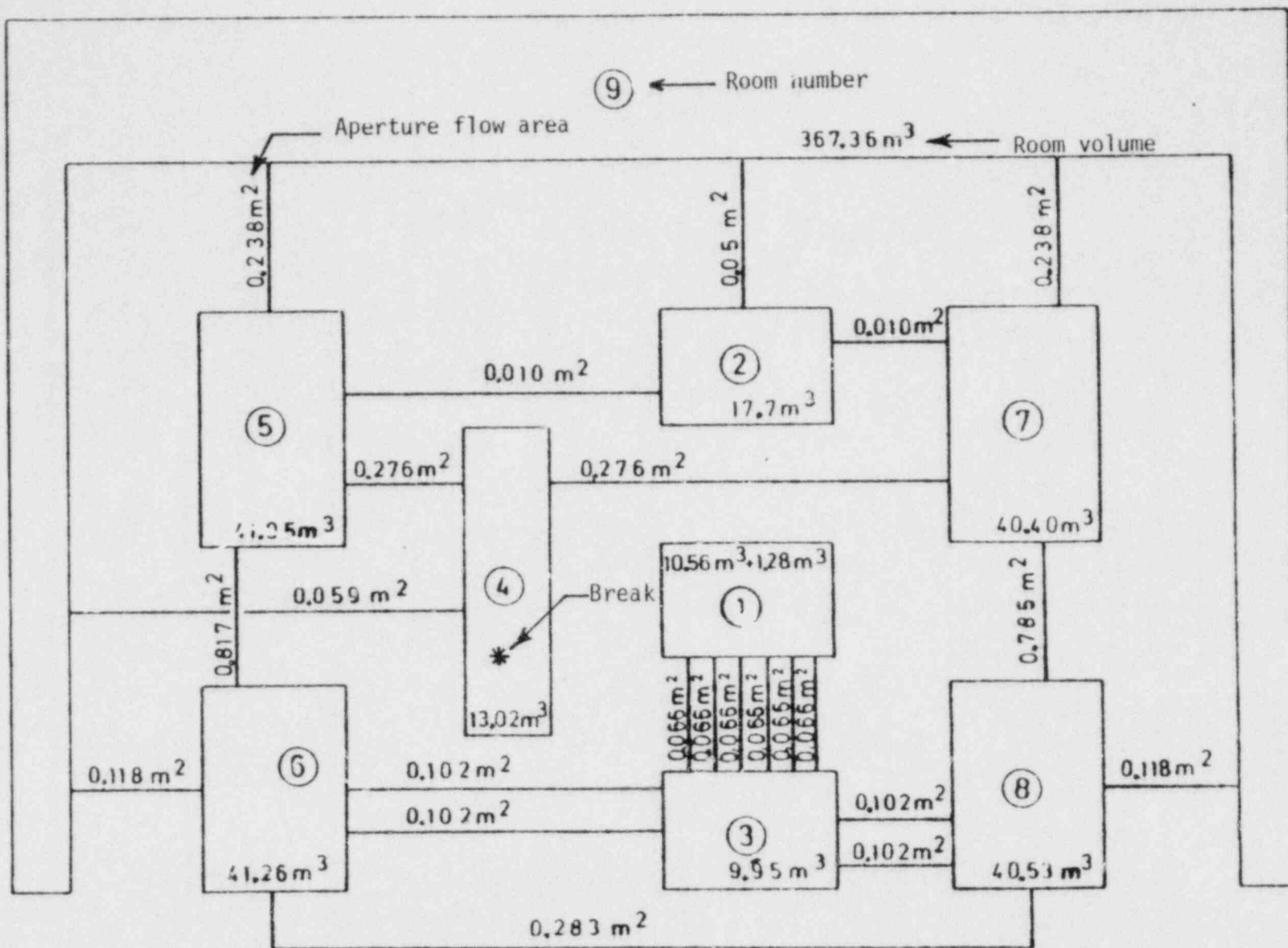


Figure D-2. C-9 test configuration, room volumes, and aperture flow areas.

MODEL DESCRIPTION

The C-9 test facility was modeled using a combination of one-dimensional (1-D) and two-dimensional (2-D) Cartesian meshes and one lumped parameter region (LPR), as shown in Figure D-3. The total number of volumes used in the BEACON calculation was:

1. 200 cells in five 2-D meshes
2. Ten one-dimensional meshes
3. One lumped parameter region.

Rooms 4, 5, 6, 7, and 8 were modeled using BEACON two-dimensional Cartesian meshes with the variable spacing option. The actual lengths and depths of the compartments were utilized with small adjustments in room heights made to achieve correct volumes. The sumps in the floors of Rooms 4, 6, and 8 were simulated by using the restricted flow option in the lower row of cells. This option allowed the reduced volumes and flow areas in the lower part of these rooms to be modeled.

Fine nodalization was used in the break compartment (Room 4) in order to adequately describe the source and to model the rapidly changing conditions. Coarser nodalization was utilized in the other rooms where conditions did not change as significantly. In all rooms, however, restrictions were placed on the cell dimensions such that (a) the lengths of neighboring cells did not differ by over a factor of two, and (b) the flow areas of neighboring cells did not differ by over a factor of four. This was done to avoid abrupt differences in adjacent cell sizes.

The apertures between the rooms were modeled using one-dimensional meshes of equivalent flow area. In Rooms 6 and 8 there were several openings leading to Rooms 3 and 9. These were combined and modeled as one aperture from each room to reduce the total number of meshes for the

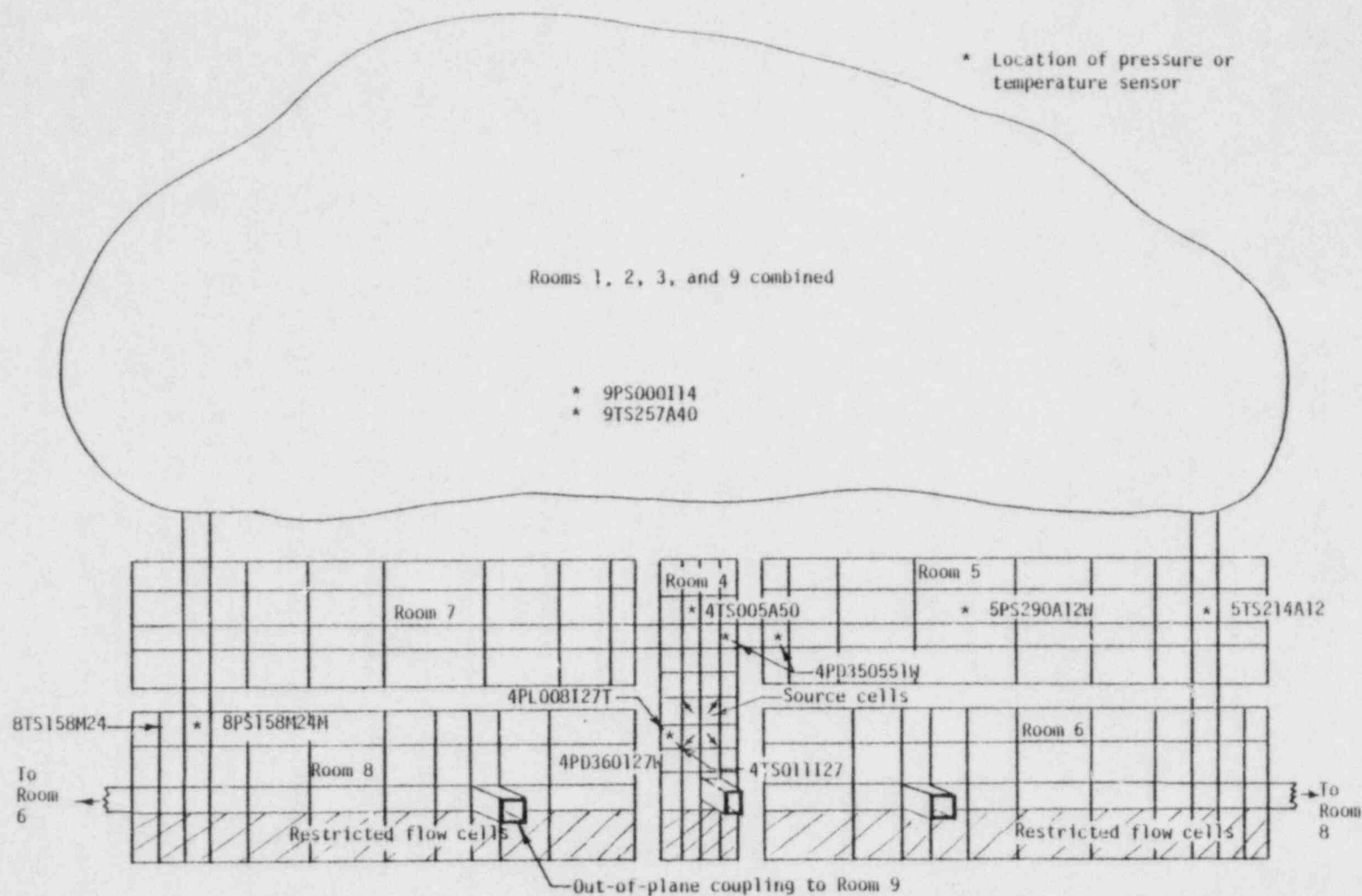


Figure D-3. BEACON modeling diagram of the Battelle-Frankfurt C-9 experiment showing the data sensor locations.

problem. Where needed, the out-of-plane coupling option was used to connect the 1-D meshes to the Cartesian meshes.

Rooms 1, 2, 3, and 9 were combined into one lumped parameter region because of the complexity of the problem and because of computer time limitations. The combined volumes of these rooms was 406.85 m^3 . The lumped parameter model is generally used for large rooms where velocity effects are negligible and homogeneous conditions are assumed.

Junction form losses were input only where the 1-D meshes connected to the lumped parameter region. Estimated values for these losses were obtained from a handbook of hydraulic resistance coefficients.^{D-3} Previous experience with the code has shown that the use of form losses are necessary into the LPR to eliminate pressure oscillations in the results. Form losses were not used in the 2-D regions because they are implicitly calculated within BEACON.

The no-slip option was specified for all meshes to simulate friction along the walls, while Fanning friction factors of 0.005 were input to simulate frictional pressure losses due to fluid motion.

The wall film model was specified for all 2-D meshes. This option is used to track liquid film accumulation on walls and other structures. Film was not used in the 1-D regions as previous experience has shown that it does not affect the results discernibly in these regions. There is no film model for lumped parameter regions.

The concrete, steel, and aluminum surfaces in the 2-D and LPR rooms were modeled using 22 heat structures of equivalent surface area and thickness. These models simulate the effects of heat transfer to the compartment walls and other surfaces from the fluid regions. Where possible, several objects of the same material were combined into one common heat structure to save computing time. No heat structures were used for the 1-D regions because of their small surface areas. A single layer

of coating on the concrete was simulated by summing the thicknesses and averaging the thermal conductivities and volumetric heat capacities of the various fillers and sealers.^{D-4} The BEACON best-estimate correlations were used to calculate heat transfer coefficients between the heat structures and the adjacent vapor, liquid, or film. Locations of the various heat structures are depicted in Figure D-4.

Initial conditions for the C-9 test were assumed to be the same for all of the rooms. The values used were:

Pressure	=	0.1 MPa
Temperature	=	290 K
Mass Fraction for Air	=	0.9925
Void Fraction	=	1.0.

* The BEACON time-dependent mass and energy source option was used to model the high pressure water-line break in Room 4. Four source cells were chosen in order to provide a means of simulating the dispersion of the flow upon impact with the baffle plate and to center the break location within the framework of the selected nodalization. The source was directed radially from the centers of each of the break cells as shown in Figure D-3. Source velocities were estimated by relating results of a previous jet test analysis (C-12) to the C-9 mass flow rates. The blowdown specific enthalpies were then corrected for velocity effects.

The BEACON auto-timestep option was selected for use throughout the mesh regions. BEACON calculates this timestep based upon fluid velocities and cell sizes in the Eulerian regions. In the initial C-9 run, the calculated timestep was reduced by a Courant multiplier of 0.5 and limited by a maximum timestep of 0.001 second. These limitations were not sufficiently restrictive, however, and had to be progressively reduced to 0.2 and 0.00015 second, respectively, to overcome code instabilities.

A constant timestep of 0.001 second was used for both the lumped parameter region and heat structure calculations.

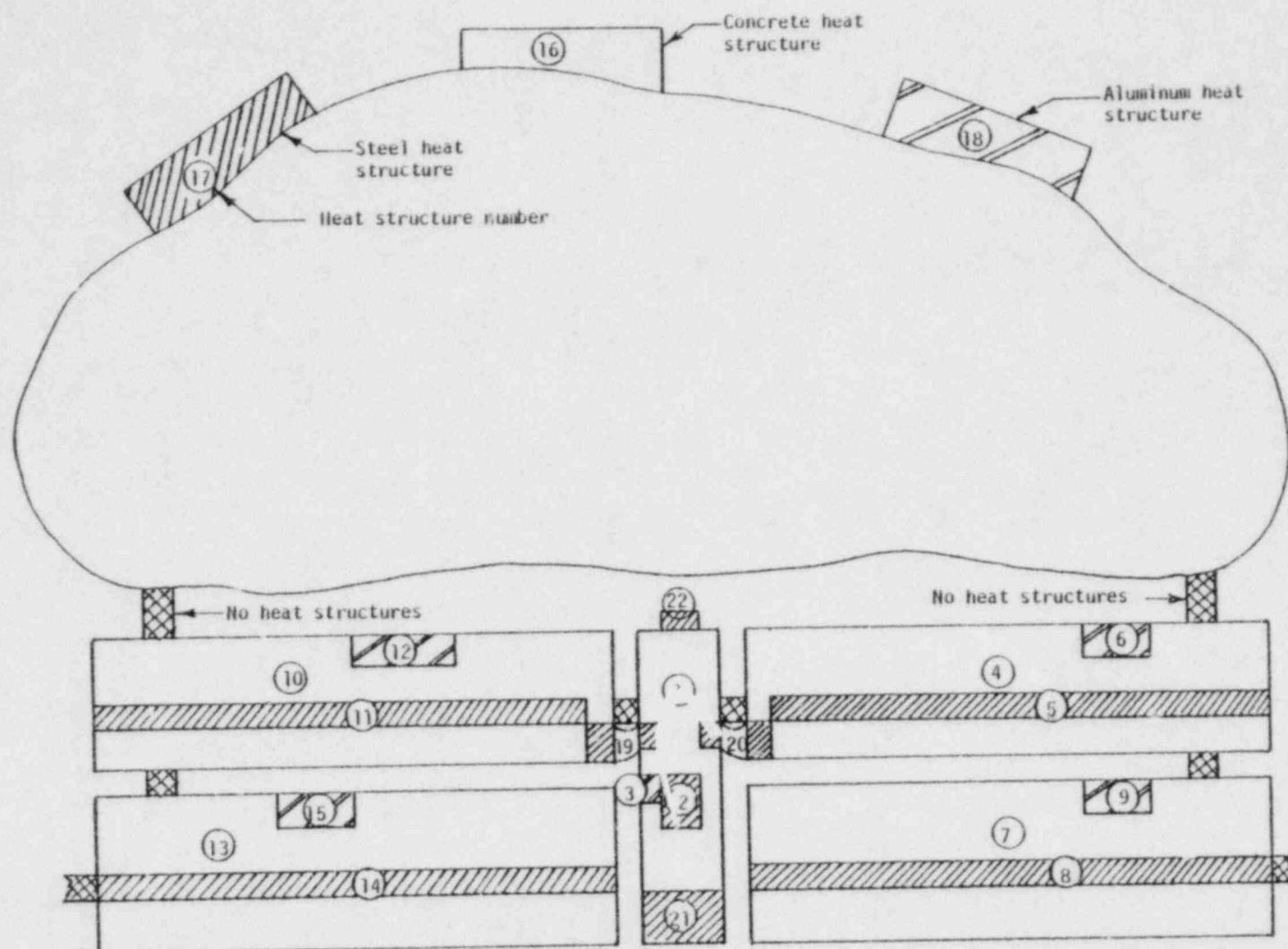


Figure D-4. BEACON heat structures used in modeling the C-9 experiment.

Iteration parameters used for the C-9 calculations were $\text{OMEGA} = 1.0$ and $\text{EP SG} = \text{EP SL} = 0.00001$. Recent studies have shown that, for most problems, significant CPU time savings (up to 50%) can be realized by running with a low value for the relaxation parameter (OMEGA). Also, preliminary runs for C-9 indicated that allowing the maximum relative errors in the gas and liquid density calculations (EP SG and EP SL) to exceed 0.00001 resulted in discrepancies in the conservation of mass.

The BEACON best-estimate correlations were used to calculate the interphasic exchange parameters. The flashing criteria parameter (FLCRIT) was specified as 0.0 because preliminary attempts to run with higher values were unsuccessful. This parameter dictates the amount of superheat allowed before flashing takes place. The flashing and condensation rate multipliers (RLAME and RLAMC) were set to 0.1 based on previous results using the KACHINA code.^{D-5}

A listing of the BEACON input for the C-9 experiment is given in Figure D-5.

RESULTS

In this section, comparisons are made between the BEACON calculated pressures and temperatures and those obtained experimentally from the C-9 test. This study was made to establish a basis for evaluating results obtained using the BEACON/MOD3 best-estimate correlations. The BEACON cells used for the comparisons were selected to be equivalent to the actual sensor locations as nearly as possible. It should be noted, however, that some of the differences between calculated results and data may be attributed to imperfect correspondence between the BEACON cell and the sensor location. Identification numbers on the graphs and in Figure D-3 correspond to the sensor locations used in the test.

72

POOR ORIGINAL

```

*
10000001 HEAT SLAB INPUT
10000002 M, BTU/HR, DEGC
10000003 -1 2.294E6 0.001
*
10000004 WATT/M-DEGC, J/M3-DEGC, WATT/M2-DEGC
10000005 CONCRETE STEEL ALUMINUM
10000006 COATING STAINLESS MGO2
10001001 1.73 2.294E6 32.00 3.69E6 205.957 2.33E6
+ 274 2.294E6 17.307 3.919E6 .554 7.431E5
10100000 ROOM 4 CONCRETE
20100001 6 1 0.0 0.0 100 0.01 0.
10100002 MULTI 7 2 2 11 DUMMY 0 0 0 0 0
10100003 M2, 39.42, FACES NONE
10100009 11 11 0 0
10102000 0 2
10102001 .0095 2 .00 5
10103001 4 1 1 5
10104001 0.0 2
10106001 16.9 3
10200000 ROOM 4 STEEL NEAR SOURCE
10200001 3 1 0.0 0.0 100 0.01 0.
10200002 MULTI 7 3 5 4 5 DUMMY 0 0 0 0 0
10200003 M2, 0.500, NONE, NONE
10200009 11 11 0 0
10202000 0 2
10202001 .017 2
10203001 2 2
10204001 0.0 2
10206001 16.9 3
10300000 ROOM 4 ALUMINUM
10300001 3 1 0.0 0.0 100 0.01 0.
10300002 SINGLE 7 2 0 2 5 DUMMY 0 0 0 0 0
10300003 M2, 0.630, NONE, NONE
10300009 11 11 0 0
10302000 0 2
10302001 .008 2
10303001 3 2
10304001 0.0 2
10306001 16.9 3
10400000 ROOM 5 CONCRETE
10400001 6 1 0.0 0.0 100 0.01 0.
10400002 MULTI 9 2 2 10 5 DUMMY 0 0 0 0 0
10400003 M2, 76.078, FACES NONE
10400009 11 11 0 0
10402000 0 2
10402001 .0095 2 .00 5
10403001 4 1 1 5
10404001 0.0 2
10406001 16.9 3
10500000 ROOM 5 STEEL
10500001 3 1 0.0 0.0 100 0.01 0.
10500002 MULTI 9 3 3 10 3 DUMMY 0 0 0 0 0
10500003 M2, 39.44, NONE, NONE
10500009 11 11 0 0
10502000 0 2
10502001 .003 2
10503001 2 2
10504001 0.0 2
10506001 16.9 3
10600000 ROOM 5 ALUMINUM
10600001 3 1 0.0 0.0 100 0.01 0.
10600002 SINGLE 9 7 5 7 5 DUMMY 0 0 0 0 0
10600003 M2, 1.200, NONE, NONE
10600009 11 11 0 0
10602000 0 2
10602001 .008 2
10603001 3 2
10604001 0.0 2
10606001 16.9 3

```

Figure D-5. (continued)

POOR ORIGINAL

```

10700000 'ROOM 5 CONCRETE'
10700001 6 1 0.0 0.0 100 0.01 0.
10700002 MULTI 1 2 2 12 5 DUMMY 0 0 0 0 0
10700003 M2, 90.123, FACES, NONE
10700009 11 11 0 0
10702000 0 2
10702001 .0095 2 .05 5
10703001 4 1 1 5
10704001 0.0 5
10706001 16.9 6
10800000 'ROOM 6 STEEL'
10800001 3 1 0.0 0.0 100 0.01 0.
10800002 MULTI 1 2 3 12 3 DUMMY 0 0 0 0 0
10800003 M2, 15.639, NONE, NONE
10800009 11 11 0 0
10802000 0 2
10802001 .005 2
10803001 2 2
10804001 0.0 2
10806001 16.9 3
10900000 'ROOM 5 ALUMINUM'
10900001 3 1 0.0 0.0 100 0.01 0.
10900002 SINGLE 1 8 5 8 5 DUMMY 0 0 0 0 0
10900003 M2, 1.148, NONE, NONE
10900009 11 11 0 0
10902000 0 2
10902001 .008 2
10903001 3 2
10904001 0.0 2
10906001 16.9 3
11000000 'ROOM 7 CONCRETE'
11000001 6 1 0.0 0.0 100 0.01 0.
11000002 MULTI 1 2 2 12 5 DUMMY 0 0 0 0 0
11000003 M2, 76.626, FACES NONE
11000009 11 11 0 0
11002000 0 2
11002001 .0095 2 .05 5
11003001 4 1 1 5
11004001 0.0 5
11006001 16.9 6
11100000 'ROOM 7 STEEL'
11100001 3 1 0.0 0.0 100 0.01 0.
11100002 MULTI 1 2 3 9 3 DUMMY 0 0 0 0 0
11100003 M2, 11.886, NONE, NONE
11100009 11 11 0 0
11102000 0 2
11102001 .005 2
11103001 2 2
11104001 0.0 2
11106001 16.9 3
11200000 'ROOM 7 ALUMINUM'
11200001 3 1 0.0 0.0 100 0.01 0.
11200002 SINGLE 5 7 5 7 5 DUMMY 0 0 0 0 0
11200003 M2, 1.200, NONE, NONE
11200009 11 11 0 0
11202000 0 2
11202001 .008 2
11203001 3 2
11204001 0.0 2
11206001 16.9 3
11300000 'ROOM 3 CONCRETE'
11300001 6 1 0.0 0.0 100 0.01 0.
11300002 MULTI 1 2 2 12 5 DUMMY 0 0 0 0 0
11300003 M2, 91.996, FACES, NONE
11300009 11 11 0 0
11302000 0 2
11302001 .0095 2 .05 5
11303001 4 1 1 5
11304001 0.0 5
11306001 16.9 6

```

Figure D-5. (continued).

POOR ORIGINAL

```

1140000 'ROOM 3 STEEL'
1140001 3 1 0.0 0.0 100 0.01 0.
1140002 MULT 1 3 2 3 12 3 DUMMY 0 0 0 0
1140003 M2, 8.373, NONE, NONE
1140009 11 11 0 0
1140200 0 2
1140201 .008 2
1140301 2 2
1140401 .0 2
1140601 16.9 3
1150000 'ROOM 3 ALUMINUM'
1150001 3 1 0.0 0.0 100 0.01 0.
1150002 SINGLE 3 7 5 7 5 DUMMY 0 0 0 0
1150003 M2, 1.200, NONE, NONE
1150009 11 11 0 0
1150200 0 2
1150201 .008 2
1150301 3 2
1150401 .0 2
1150601 16.9 3
1160000 'ROOM 3 CONCRETE'
1160001 6 1 0.0 0.0 100 0.01 0.
1160002 LUMPED 1 0 0 0 0 DUMMY 0 0 0 0
1160003 M2, 812.131, NONE, NONE
1160009 11 11 0 0
1160200 0 2
1160201 .00095 2 .05 5
1160301 4 1 1 5
1160401 .0 2
1160601 16.9 3
1170000 'ROOM 4 STEEL'
1170001 3 1 0.0 0.0 100 0.01 0.
1170002 LUMPED 1 0 0 0 0 DUMMY 0 0 0 0
1170003 M2, 61.095, NONE, NONE
1170009 11 11 0 0
1170200 0 2
1170201 .008 2
1170301 2 2
1170401 .0 2
1170601 16.9 3
1180000 'ROOM 9 ALUMINUM'
1180001 3 1 0.0 0.0 100 0.01 0.
1180002 LUMPED 1 0 0 0 0 DUMMY 0 0 0 0
1180003 M2, 5.438, NONE, NONE
1180009 11 11 0 0
1180200 0 2
1180201 .008 2
1180301 3 2
1180401 .0 2
1180601 16.9 3
1190000 'ROOM 4 STEEL NEAR R7 OUTLET'
1190001 3 1 0.0 0.0 100 0.01 0.
1190002 SINGLE 7 2 9 5 13 3 0 0
1190003 M2, 0.384, NONE, NONE
1190009 11 11 11 11
1190200 0 2
1190201 .005 2
1190301 2 2
1190401 .0 2
1190601 16.9 3
1200000 'ROOM 4 STEEL NEAR R5 OUTLET'
1200001 3 1 0.0 0.0 100 0.01 0.
1200002 SINGLE 7 2 9 5 13 3 0 0
1200003 M2, 0.384, NONE, NONE
1200009 11 11 11 11
1200200 0 2
1200201 .005 2
1200301 2 2
1200401 .0 2
1200601 16.9 3

```

Figure D-5. (continued).

POOR ORIGINAL

```

1210000 'ROOM 4 STEEL BOTTOM OF ROOM'
1210001 3 1 0.0 0.0 100 0.01 0.
1210002 MULTI 7 2 2 2 2 DUMMY 0 0 0 0 0
1210003 M2, 1.0 3, NONE, NONE
1210009 11 11 0 0
1210200 0 2
1210201 .005 2
1210301 2 2
1210401 0.0 2
1210501 16.9 3
1220000 'ROOM 4 STEEL TOP OF ROOM'
1220001 3 1 0.0 0.0 100 0.01 0.
1220002 MULTI 7 3 11 4 11 DUMMY 0 0 0 0 0
1220003 M2, .234, TOP, NONE
1220009 11 11 0 0
1220200 0 2
1220201 .012 2
1220301 2 2
1220401 0.0 2
1220501 16.9 3

```

Figure D-5. (continued).

Pressure Comparisons

Pressure comparisons for Rooms 4, 5, 8, and 9 are given in Figures D-6 through D-9. Those for Rooms 6 and 7 are not presented, since the results are similar to those of Rooms 8 and 5, because of near-symmetry. In general, pressure agreement is quite good, especially in Rooms 5, 8, and 9. The pressures near the break in Room 4 overpredict the data by about 18% at 2 seconds. However, effects in this room are magnified because of its small volume (13.02 m^3). Calculated pressures in Rooms 5 and 8 underpredict the data slightly (about 2%) while pressures for Room 9 show very good agreement with data.

The results suggest that overly large pressure losses are being calculated by BEACON through the apertures from Room 4 to Rooms 5, 7, and 9. A comparison between calculated and measured pressure differences between Rooms 4 and 5, shown in Figure D-10, support this theory. Although data for this sensor were available only to 0.5 second, similar results are also observed between Rooms 4 and 9 out to 2 seconds, as shown in Figure D-11. Prior investigations using incompressible flows have shown that, when abrupt changes in flow area are modeled, BEACON calculates pressure losses larger than those derived experimentally. These losses are believed to be inherent in the K-FIX numerical scheme, upon which BEACON is based. Although similar investigations have not been made with compressible flows, the C-9 results seem to substantiate these observations.

The high pressures predicted for Room 4 may be attributed to the incorrect calculation of pressure losses across the flow apertures. The high resistance to flow limited the transfer of fluid out of the room resulting in the overprediction of room pressure. To verify this theory, a comparison was made of the totals (for all rooms) of the measured and calculated $\frac{PV}{T}$ terms. These totals were nearly identical, indicating that the

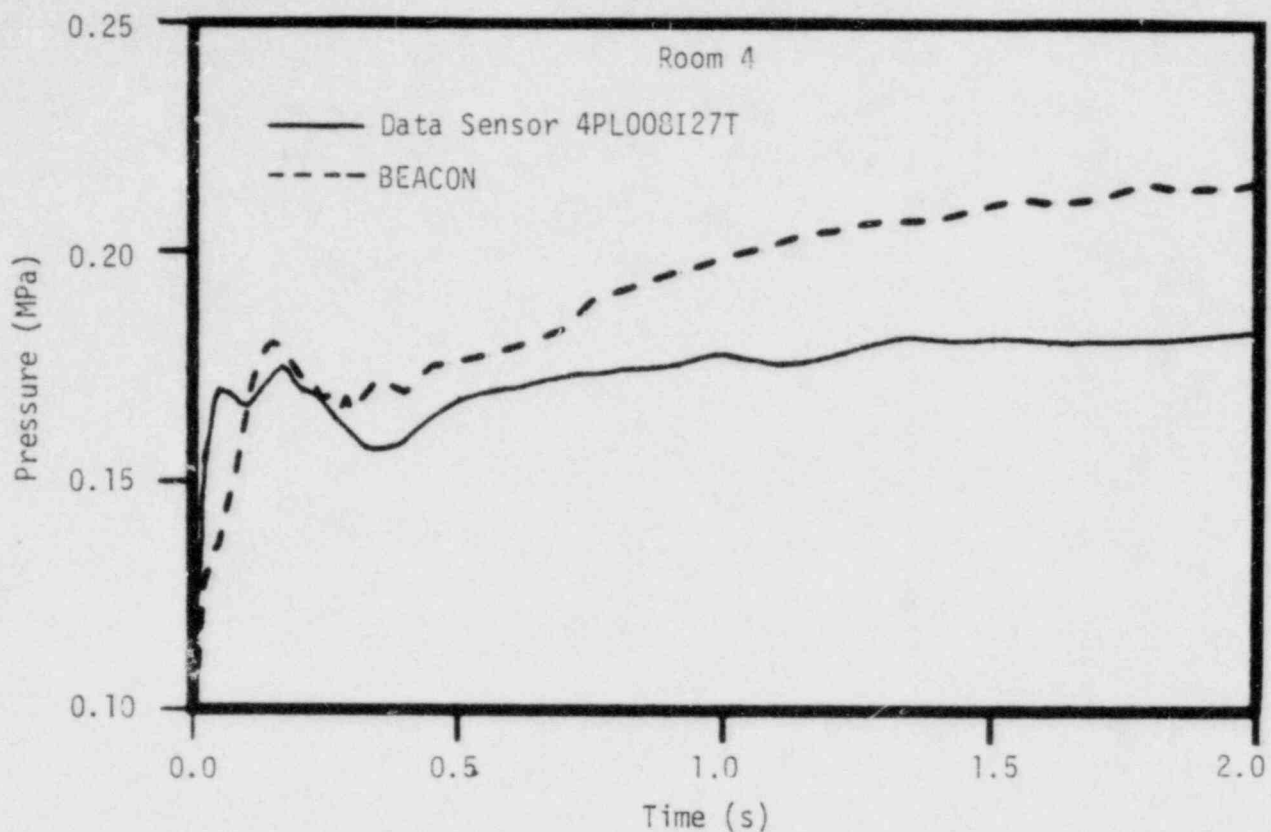


Figure D-6. Comparison of calculated and measured pressures near the break in Room 4.

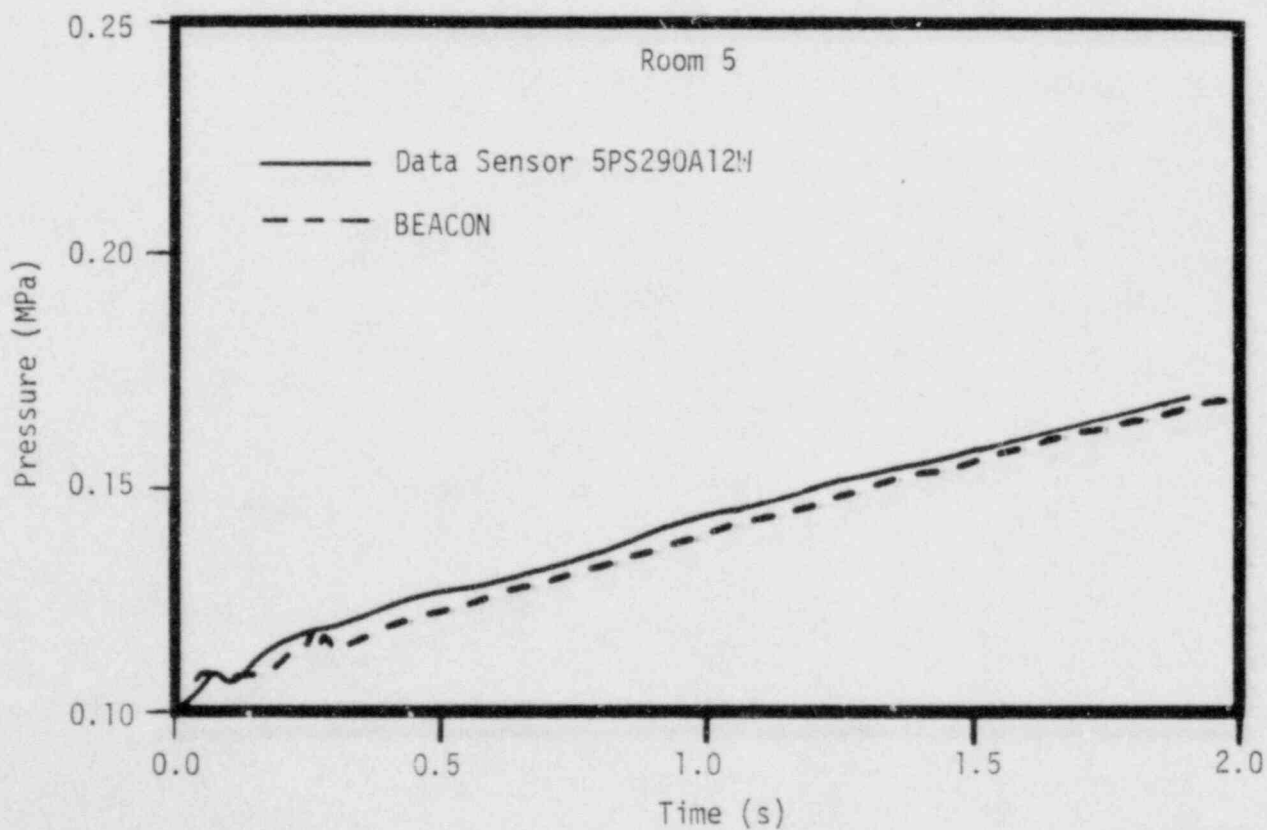


Figure D-7. Comparison of calculated and measured pressures in Room 5.

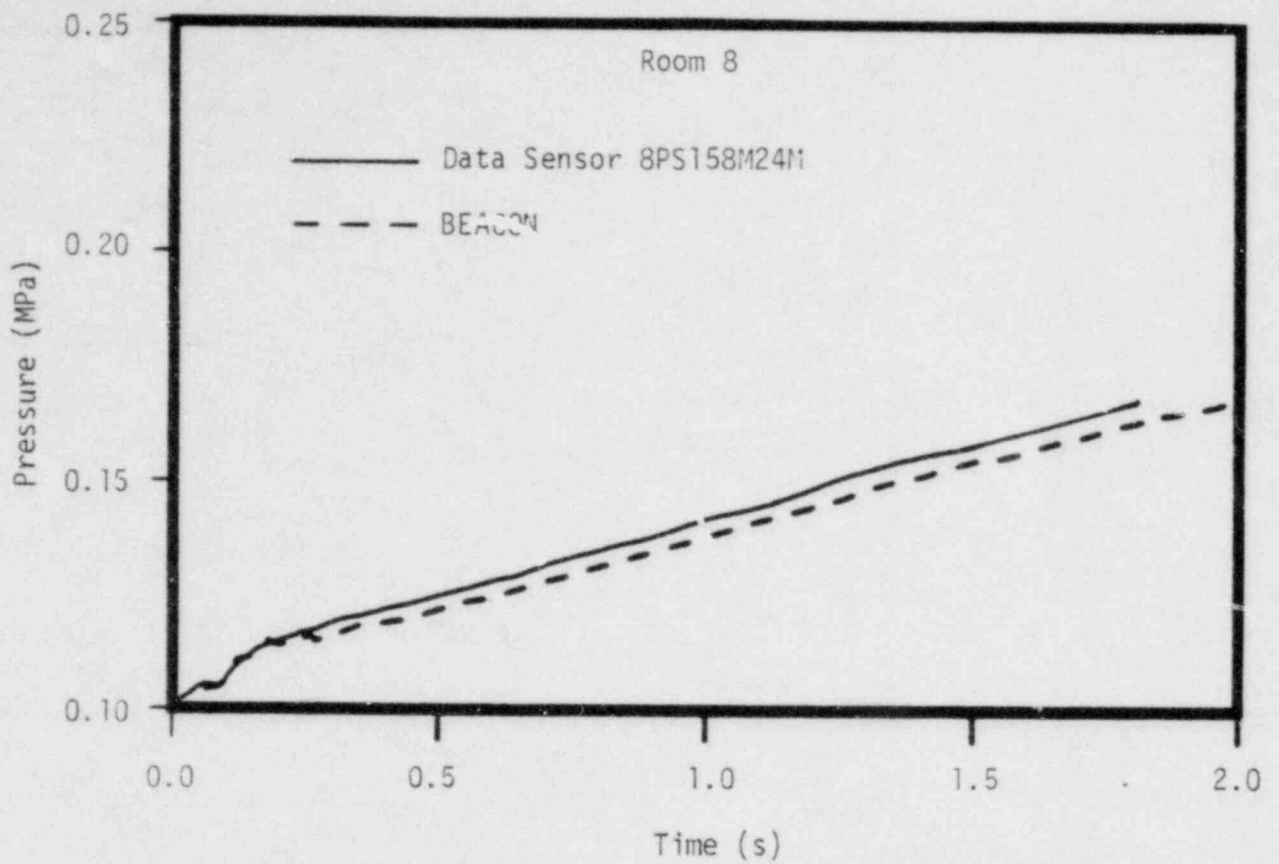


Figure D-8. Comparison of calculated and measured pressures in Room 8.

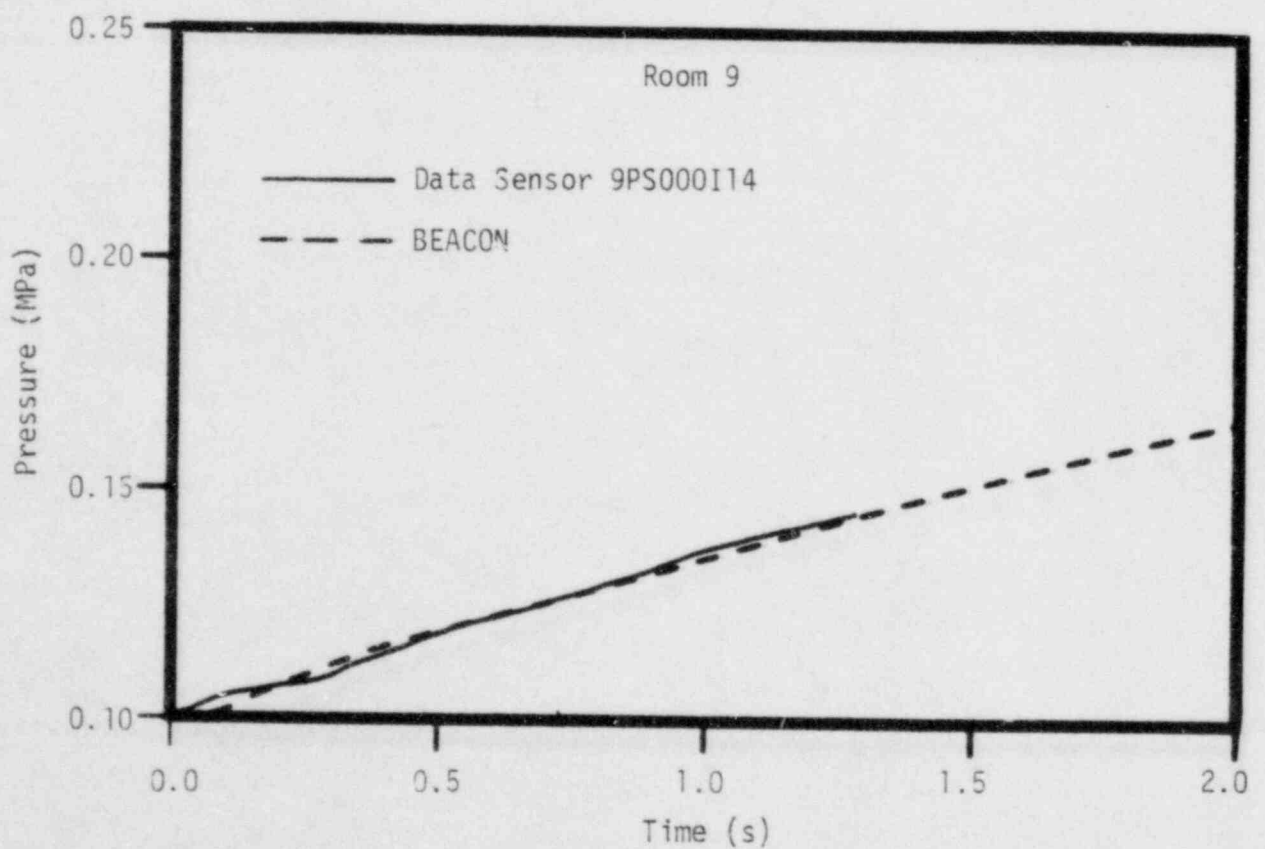


Figure D-9. Comparison of calculated and measured pressures in Room 9.

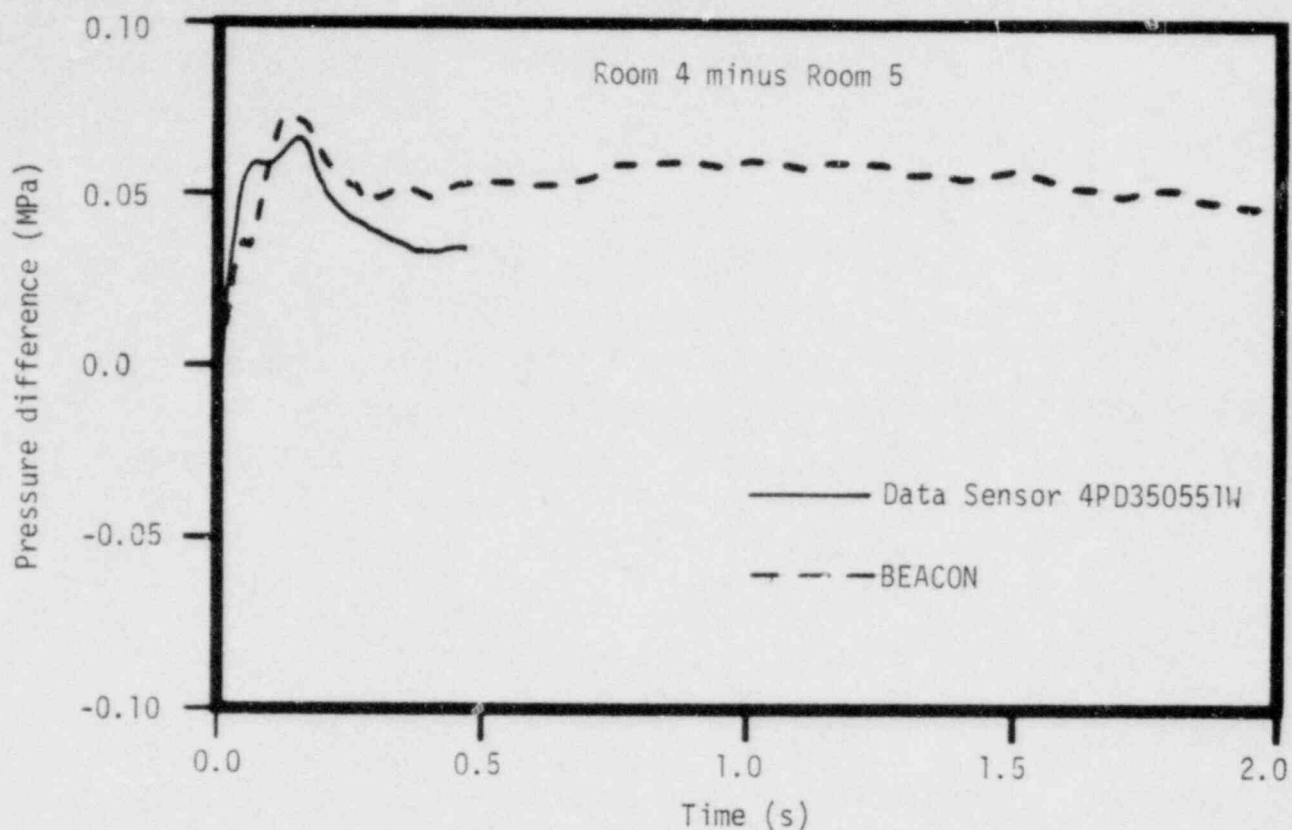


Figure D-10. Comparison of calculated and measured pressure differences between Rooms 4 and 5.

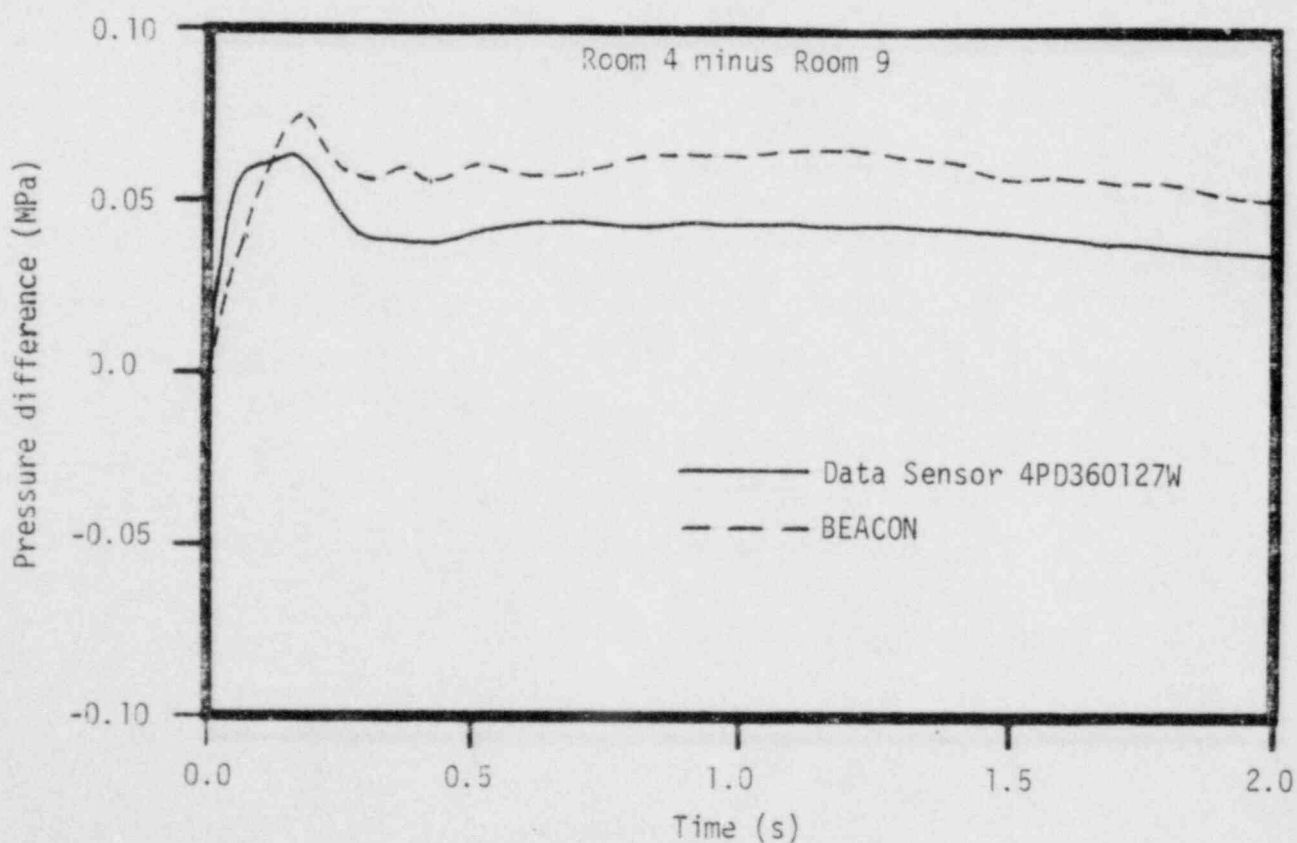


Figure D-11. Comparison between calculated and measured pressure differences between Rooms 4 and 9.

errors in calculated room pressures were due to incorrect calculation of losses between rooms. This further implied that the overpredicted pressure values were not due to insufficient heat transfer or to overflashing.

Temperature Comparisons

Temperature comparisons are shown in Figures D-12 through D-16. Excellent agreement between calculated and experimental data is seen in Room 4, after the initial temperature spikes (Figures D-12 and D-13). Similar results are observed in Rooms 5, 8, and 9, after an initial lag (Figures D-14 through D-16).

Previous studies have suggested that some of the differences between calculated and measured temperatures may be attributed to response time of the thermocouple (TC), location of the sensor, and condensation on the TC. The importance of two of these effects is illustrated by the C-9 results:

- (1) First, the exact location of the sensor may be either impracticable or difficult to model with a 2-D code such as BEACON. Correct choice of the BEACON cell to be used in the data comparison is necessary, as shown in Figure D-17. In this figure, calculated gas temperatures from two adjacent cells are compared with data. Results from one are excellent, from the other, poor.
- (2) Second, condensation on the thermocouple may cause saturation temperatures to be recorded during the test instead of gas temperatures. This is probably the effect seen in Room 8 as illustrated in Figure D-17. Here, BEACON saturation temperatures follow the data lag exactly, indicating that saturation temperatures instead of gas temperatures were probably being measured. Similar effects were observed in the other rooms but are not plotted.

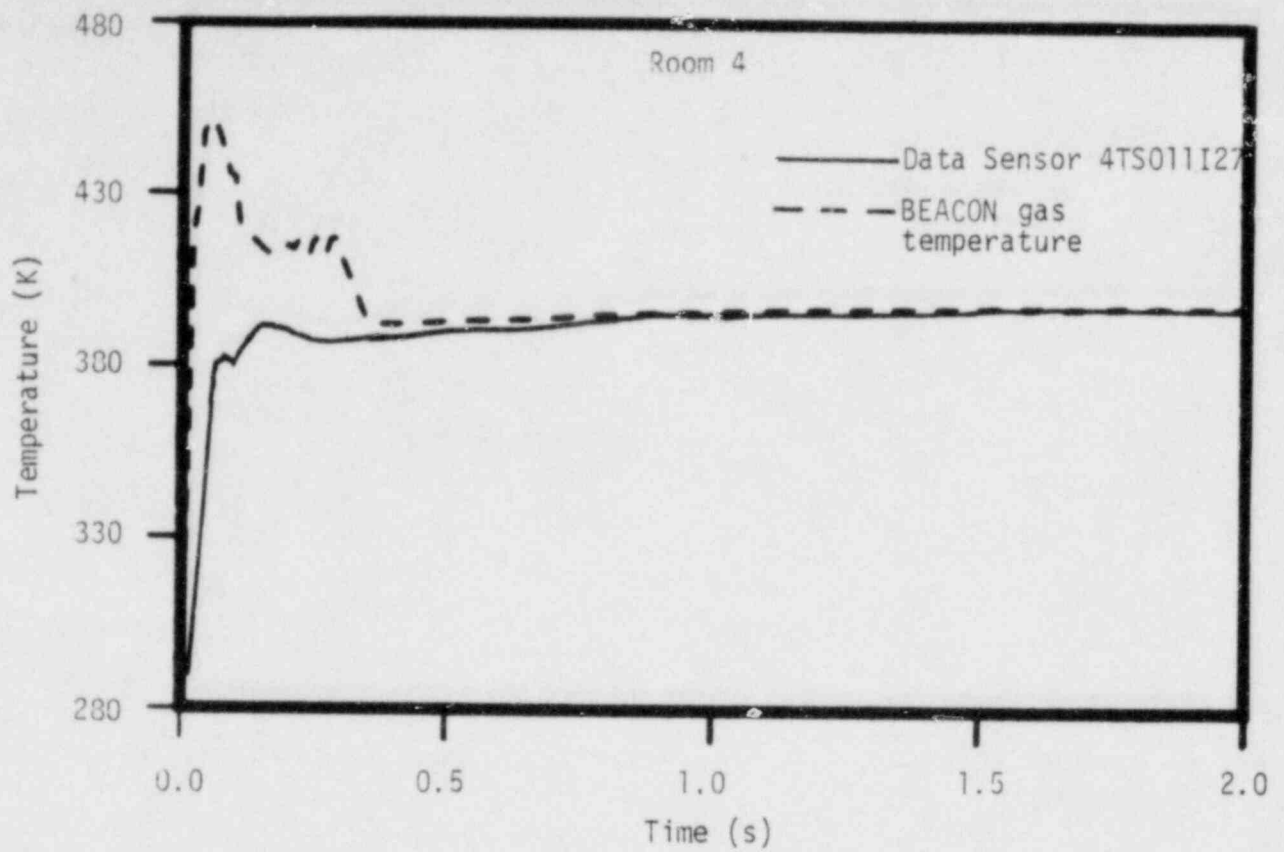


Figure D-12. Comparison of calculated and measured temperatures in Room 4 near the break.

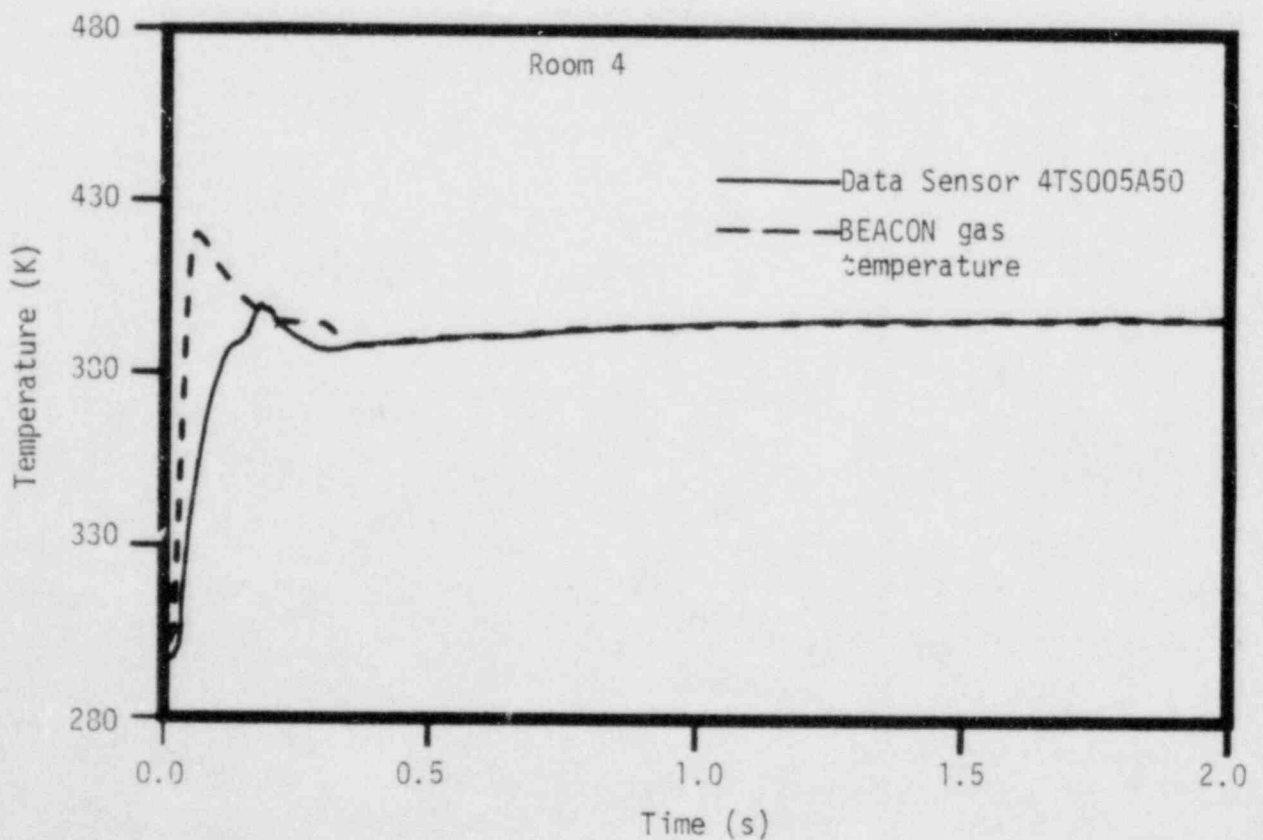


Figure D-13. Comparison of calculated and measured temperatures in Room 4 near the top of the room.

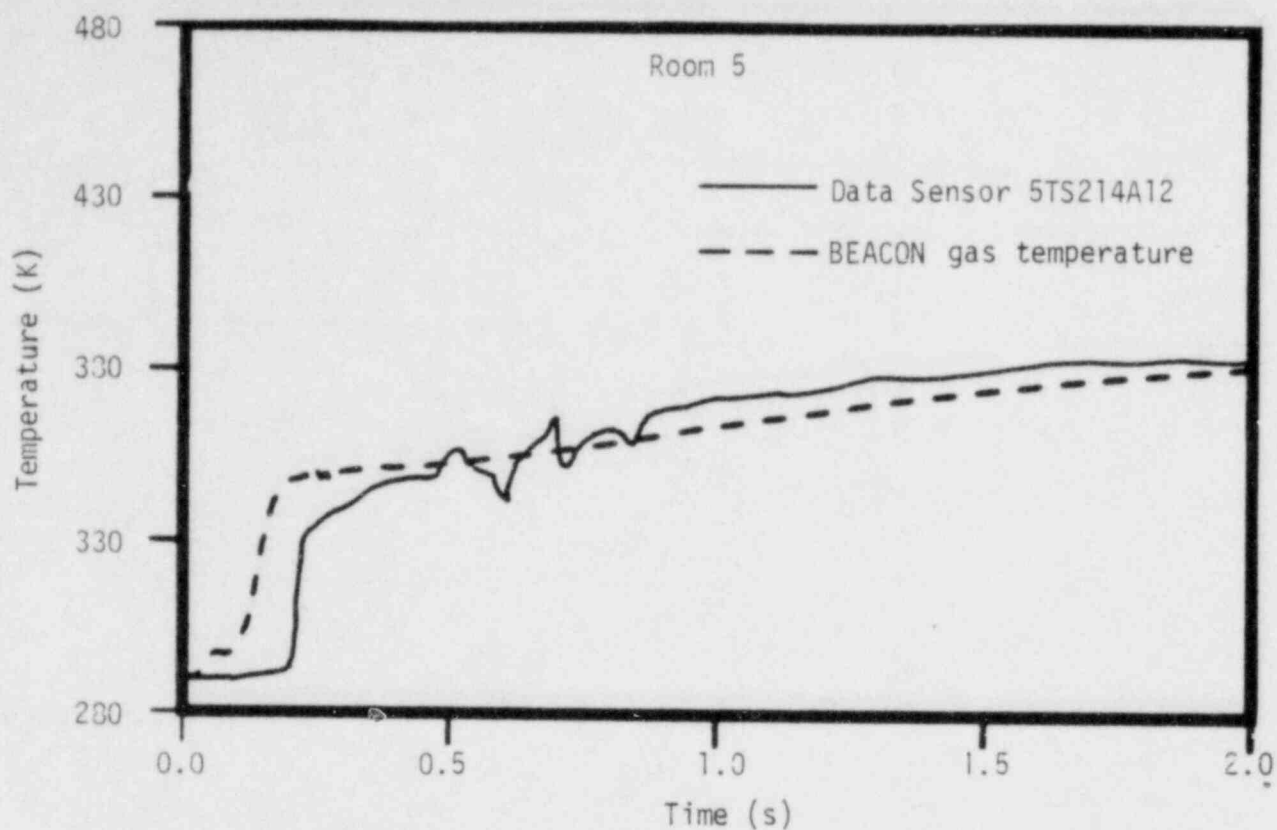


Figure D-14. Comparison of calculated and measured temperatures in Room 5.

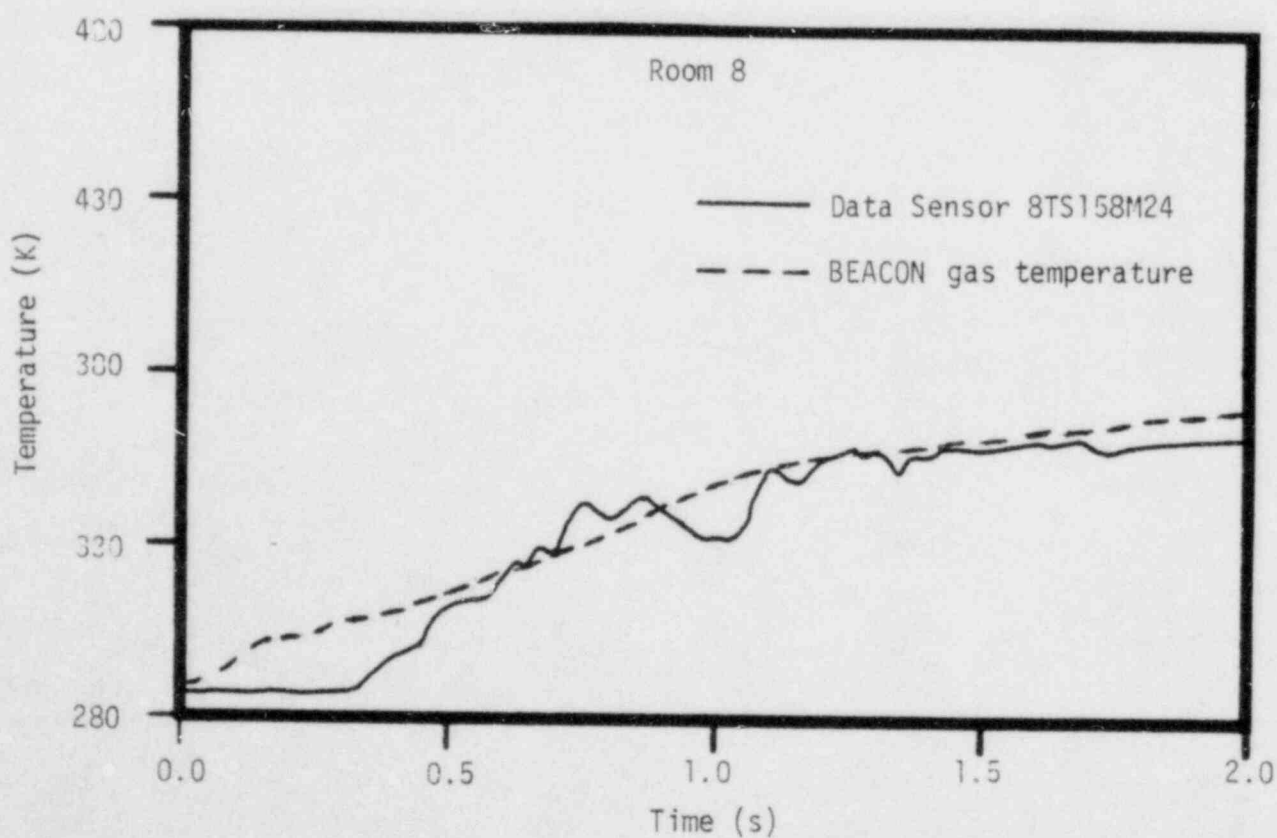


Figure D-15. Comparison of calculated and measured temperatures in Room 8.

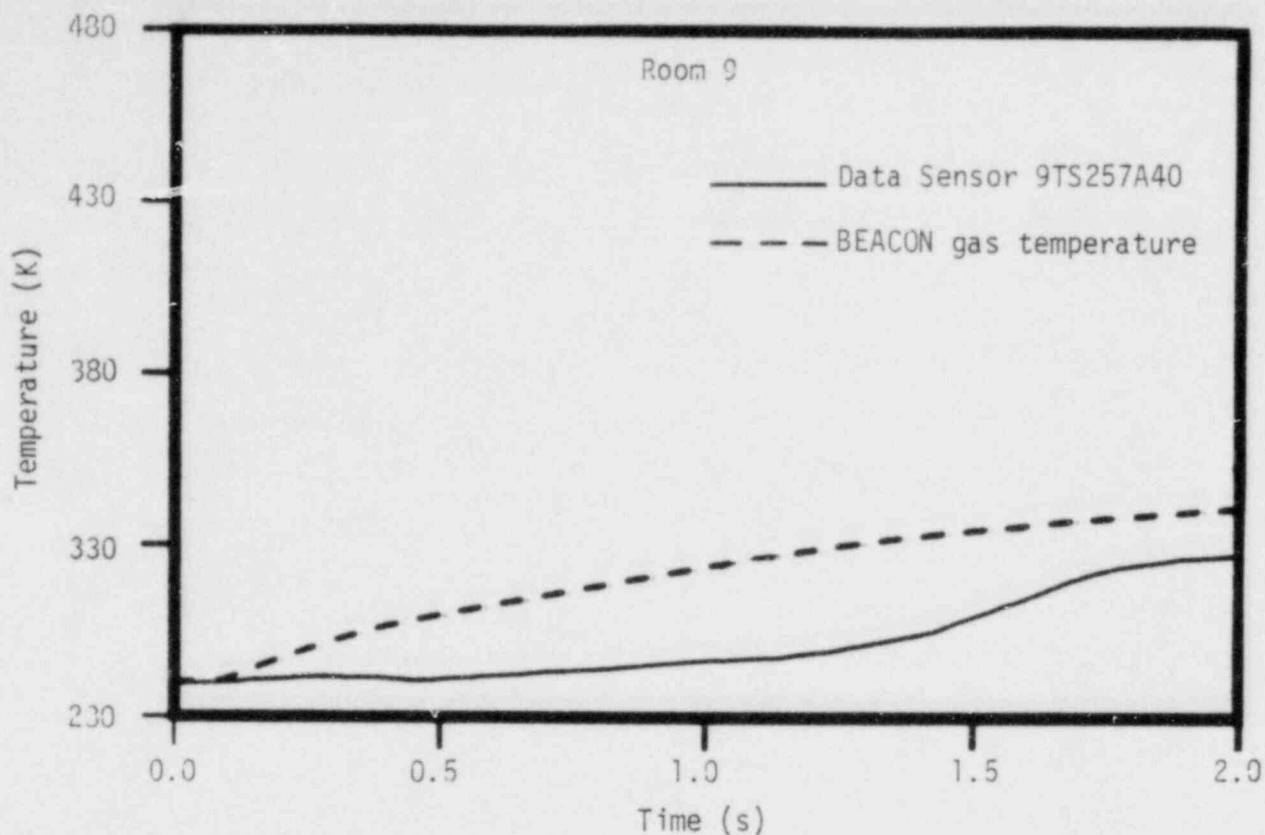


Figure D-16. Comparison of calculated and measured temperatures in Room 9.

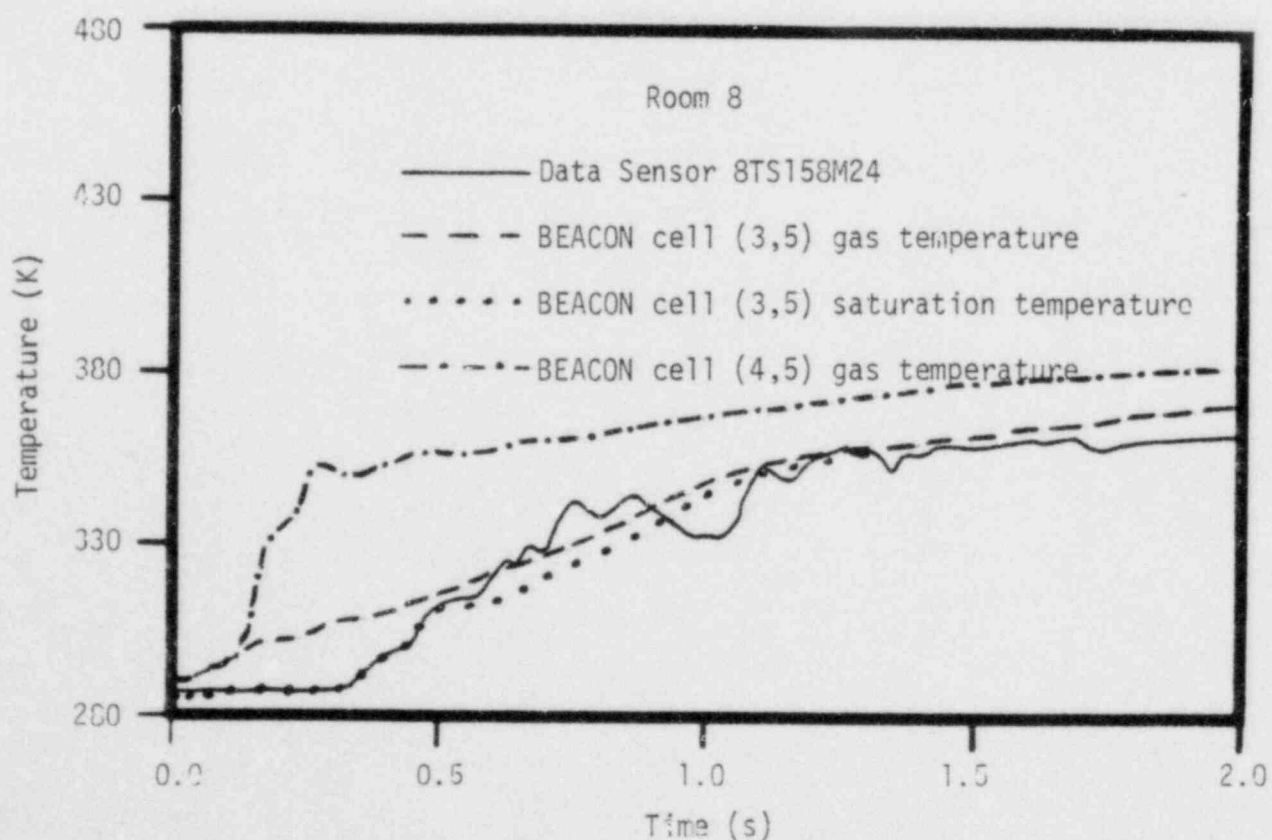


Figure D-17. Comparison of calculated and measured temperatures in Room 8 illustrating how choice of cell location and saturated conditions can affect BEACON results.

CONCLUSIONS

The BEACON/MOD3 best-estimate correlations appear to accurately predict the temperature and pressure response in the Battelle-Frankfurt C-9 experiment. Differences between calculated and measured values are small and explainable. Pressure differences are probably the result of overpredicted pressure losses where abrupt area changes are modeled. Temperature differences are thought to result partly from inexact representation of sensor locations. Additionally, it appears that the recorded data were possibly not gas temperatures, but saturation temperatures, representing condensation on the thermocouples. BEACON saturation temperatures show very close agreement with the data.

Several recommendations for the development and future use of the code have resulted from this study:

- (1) An investigation of the auto-timestep mode of calculation should be made to determine why the timestep must remain so small after nearly steady-state conditions have been attained.
- (2) If, as suspected, the overprediction of pressure losses for abrupt changes in flow area is inherent in the BEACON numerical scheme, a means of correcting this should be incorporated into the code. Also, an investigation of compressible flow behavior under similar conditions would be useful.
- (3) Running the code with a relaxation parameter of $\text{OMEGA} = 1.0$ generally will result in a CPU time savings.
- (4) The relative errors in the gas and liquid density calculations should be limited to a maximum of $\text{EPSG} = \text{EPSL} = 0.00001$ to ensure conservation of mass.

- (5) For the C-9 problem, the interphasic parameters which are presently used in the best-estimate correlations
(RLAME = RLAMC = 0.1 and FLCRIT = 0.0) give good results.

REFERENCES

- D-1. Maerkl, Hans, Study of the Processes Within a Multi-Partitioned Containment Model During Rupture of a Primary Cooling Circuit, Volume 2; Model Calculations to Verify the Short-Term Behavior of Absolute and Differential Pressures Measured in the RS 50 Experiments, Series C (Tests C1-C12, C14, C16), NUREG/TR-0035 (September 1977).
- D-2. Technischer Bericht RS 50-32-C9-1, Vorlaufiger Versuchsbericht C9 (March 1976).
- D-3. I. E. Idel'chk, Handbook of Hydraulic Resistance, AEC-TR-6630 (1966).
- D-4. Technischer Bericht BF RS 50-42-11, Specification of the Containment Standard Problem CASP2 (September 1979).
- D-5. W. C. Rivard and M. D. Torrey, Numerical Calculation of Flashing from Long Pipes Using a Two-Field Model, LA-6104-MS, 1977.

APPENDIX E

BATTELLE-FRANKFURT D-3 MATRIX

INTRODUCTION

When confronted with the task of modeling a reactor containment with a thermal-hydraulic code such as BEACON, the user must select which of the many options in the code are to be used. Frequently, the use of more options (i.e., wall film, heat structures, or finer nodalization) offers greater accuracy at the expense of running time and, therefore, cost. The prospective user must balance the costs and benefits of utilizing various code capabilities when defining the problem. The purpose of this study is to develop guidelines for the use of several BEACON modeling options. The effects of the following options on results and running time are examined:

- o Wall film
- o Heat structures
- o Degree of nodalization.

This evaluation was done by running a series of models of the Battelle-Frankfurt D-3 test and comparing the BEACON results with measured data. The D-3 experiment was chosen specifically because of the two-phase blowdown which occurred after 1.88 seconds of the test.

SYSTEM DESCRIPTION

The Battelle-Frankfurt D-3 test consisted of a steam and two-phase blowdown into the first room in a series of three coupled compartments. The following rooms formed the D-3 test configuration:

Room 6 (volume = 41.26 m^3)

Room 4 (volume = 13.0 m^3)

Room 9 (actually Rooms 1, 2, 3, 5, 7, 8, and 9 combined; total volume = 550 m^3).

Room 6 was connected to Room 4 via a converging nozzle with a minimum diameter of 0.6 m. Room 4 was connected to Room 9 with a similar nozzle. A schematic of the Battelle-Frankfurt test facility is shown in Figure E-1.

Initial conditions in the facility for the D-3 test were as follows:

Pressure = 0.1 MPa

Room 6 temperature = 287.6K

Room 9 temperature = 287.9K.^{E-1}

The initial temperature for Room 4 was assumed to be the same as for Room 6.

The blowdown was initiated by breaking a rupture disk in the high pressure system. The incoming steam and water then impinged upon a deflector plate, dispersing the flow. Because BEACON is a short-term containment code, only the first 2.5 seconds of the blowdown were used for this study.

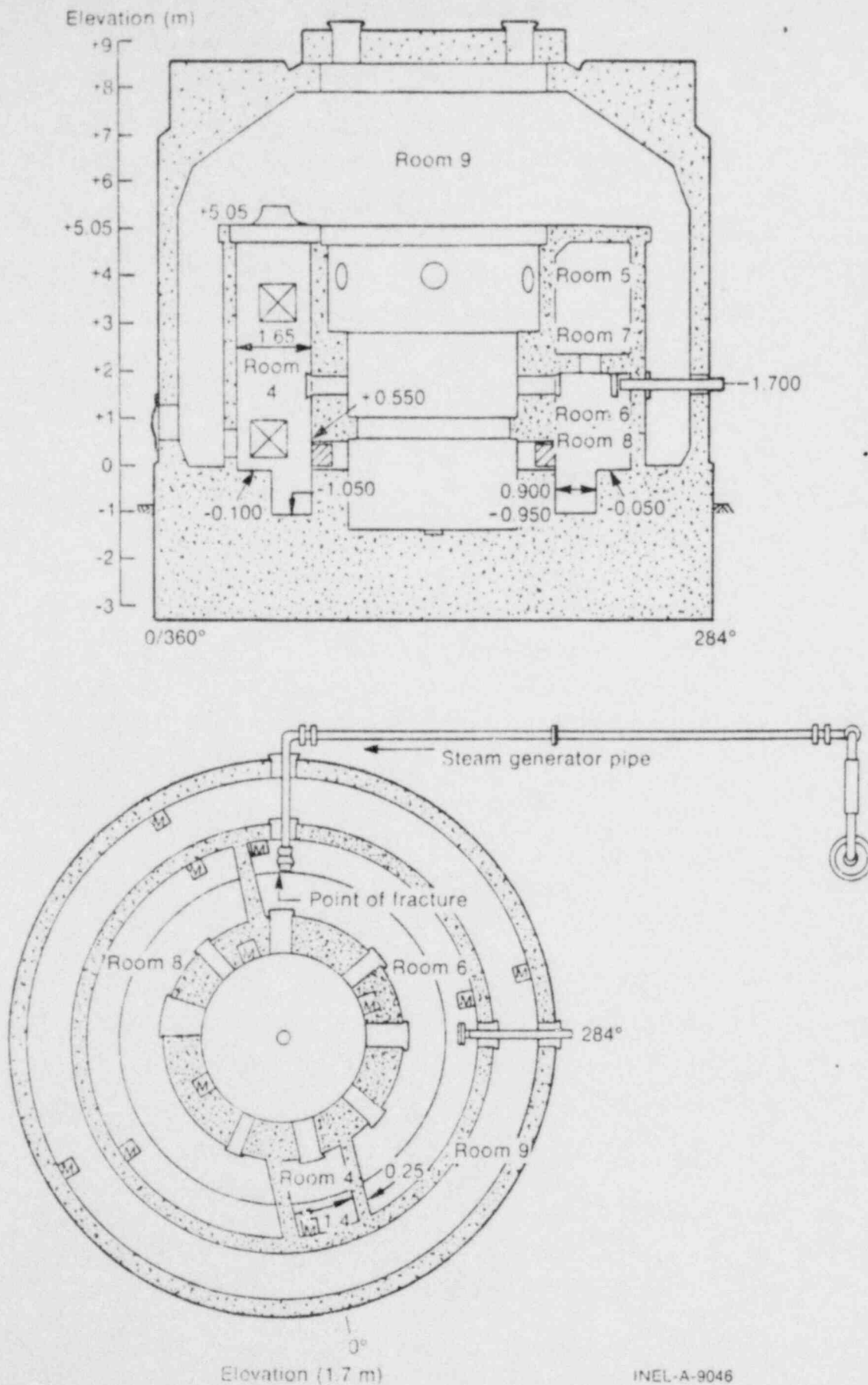


Figure E-1. Schematic of the Battelle-Frankfurt test facility.

MODEL DESCRIPTION

The cases which were modeled for the Battelle-Frankfurt D-3 matrix study are listed in Table E-1. Cases 1 through 4 were run to study the effects of using wall film and heat structures and Cases 5 through 7 were run for the nodalization study. Case 5 was also used as the "best-estimate" case for comparison with test data.

The fine nodalization used for the first five cases is shown in Figure E-2. The coarser nodalizations used for Cases 6a and 6b are shown in Figures E-3 and E-4, respectively. Both are shown as overlays on the fine nodalization case, for reference.

Restricted flow cells in the lower portions of Rooms 4 and 6 were used for Cases 1 through 6b. This option was used to model a projection of concrete which ran the lengths of both rooms.

Case 7 is a model of the same geometry as Cases 1 through 6b with both of the two-dimensional meshes replaced by lumped-parameter regions as shown in Figure E-5.

The configuration of the converging nozzles which connected the three rooms is shown in Figure E-6. The 0.6 m diameter portion had an effective flow area of 0.28 m^2 . The curvature of the entrance end of the nozzle was not known.

The nozzle models used in the BEACON calculations for Cases 1 through 6b are shown in Figures E-7 and E-8. The flow area used for both of these passages was 0.35 m^2 , or 1.26 times 0.28 m^2 . The factor 1.26 was determined from the relationship between the flow loss coefficient for a converging nozzle and for a thick orifice. The expectation was that the BEACON numerical scheme would calculate the effect of losses for an orifice, because of the two-dimensional nature of the equations, and that these orifice losses would be too high for the nozzles. Since the code did

TABLE E-1. BEACON D-3 MODEL MATRIX

<u>CASE NO.</u>	<u>FILM</u>	<u>HEAT STRUCTURES</u>	<u>ANALYSIS TIME(s)</u>	<u>NODALIZATION</u>
1	No	No	1.0	Fine
2	Yes	No	1.0	Fine
3	No	Yes	1.0	Fine
4	Yes	Yes	1.0	Fine
5	Yes	Yes	2.5	Fine
6a	Yes	Yes	1.0	Coarse
6b	Yes	Yes	1.0	Coarser
7	---	Yes	2.5	Lumped parameter

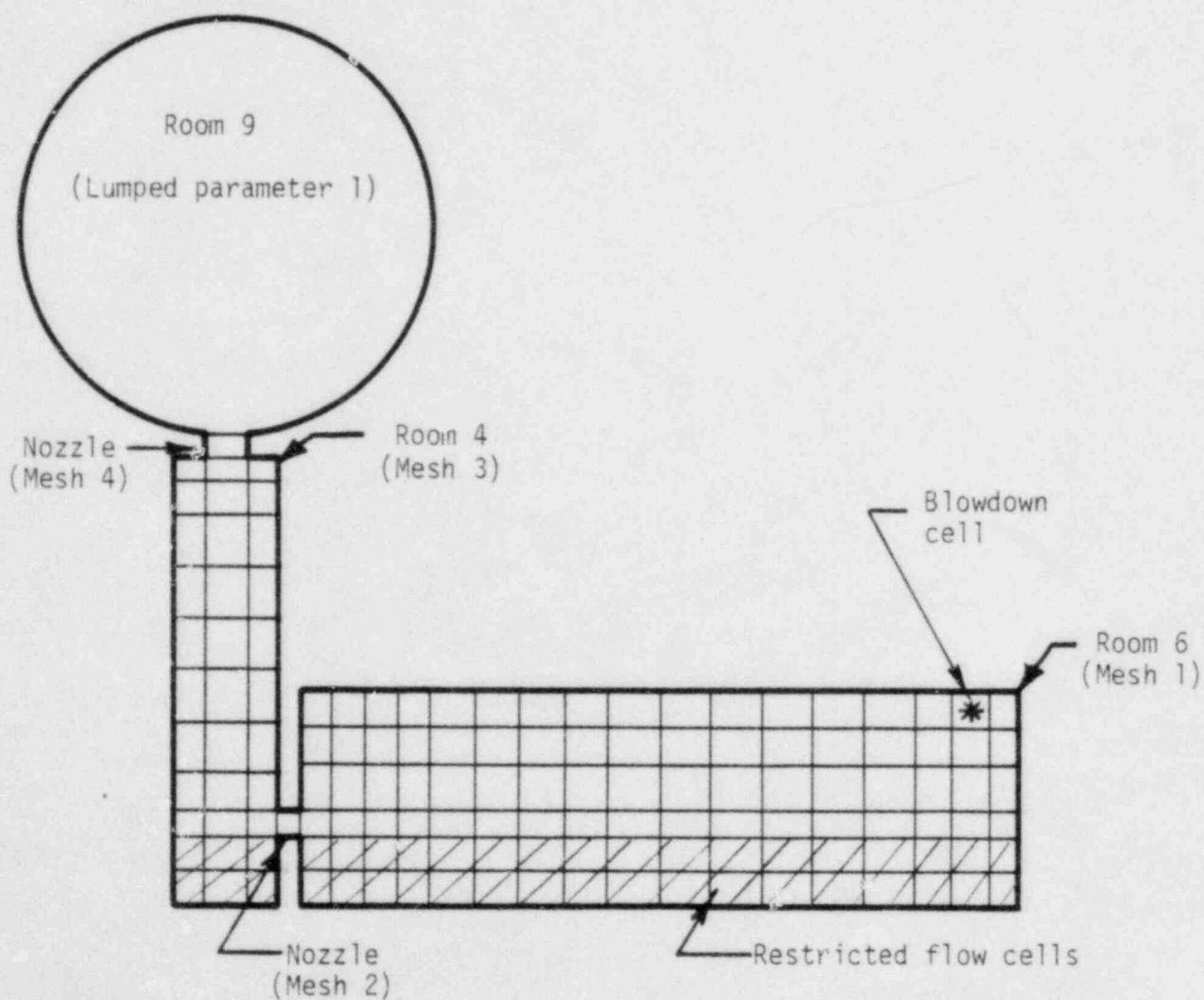


Figure E-2. Fine nodalization of the Battelle-Frankfurt D-3 facility used for Cases 1 through 5.

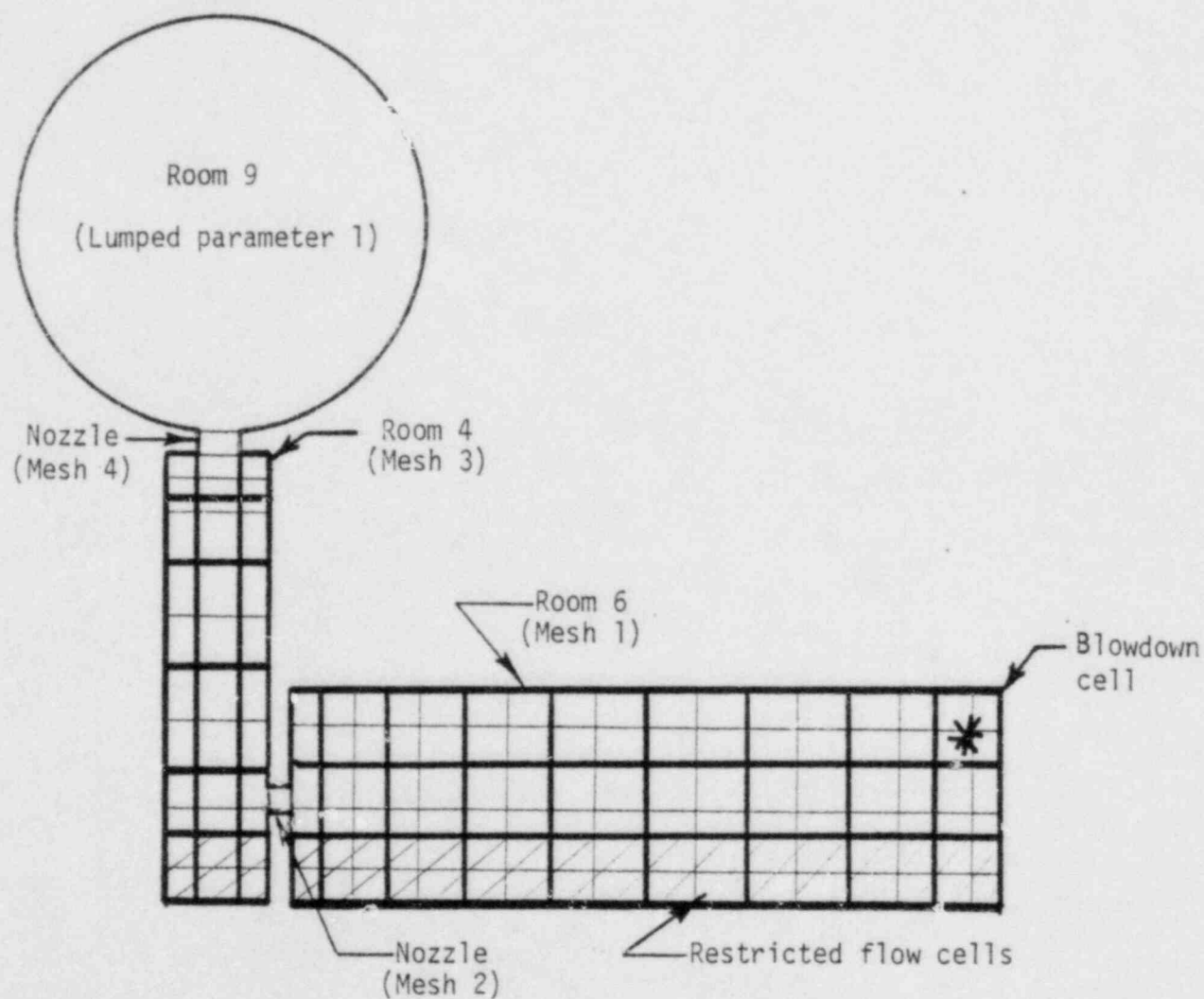


Figure E-3. Coarse nodalization of the Battelle-Frankfurt D-3 facility used for Case 6a.

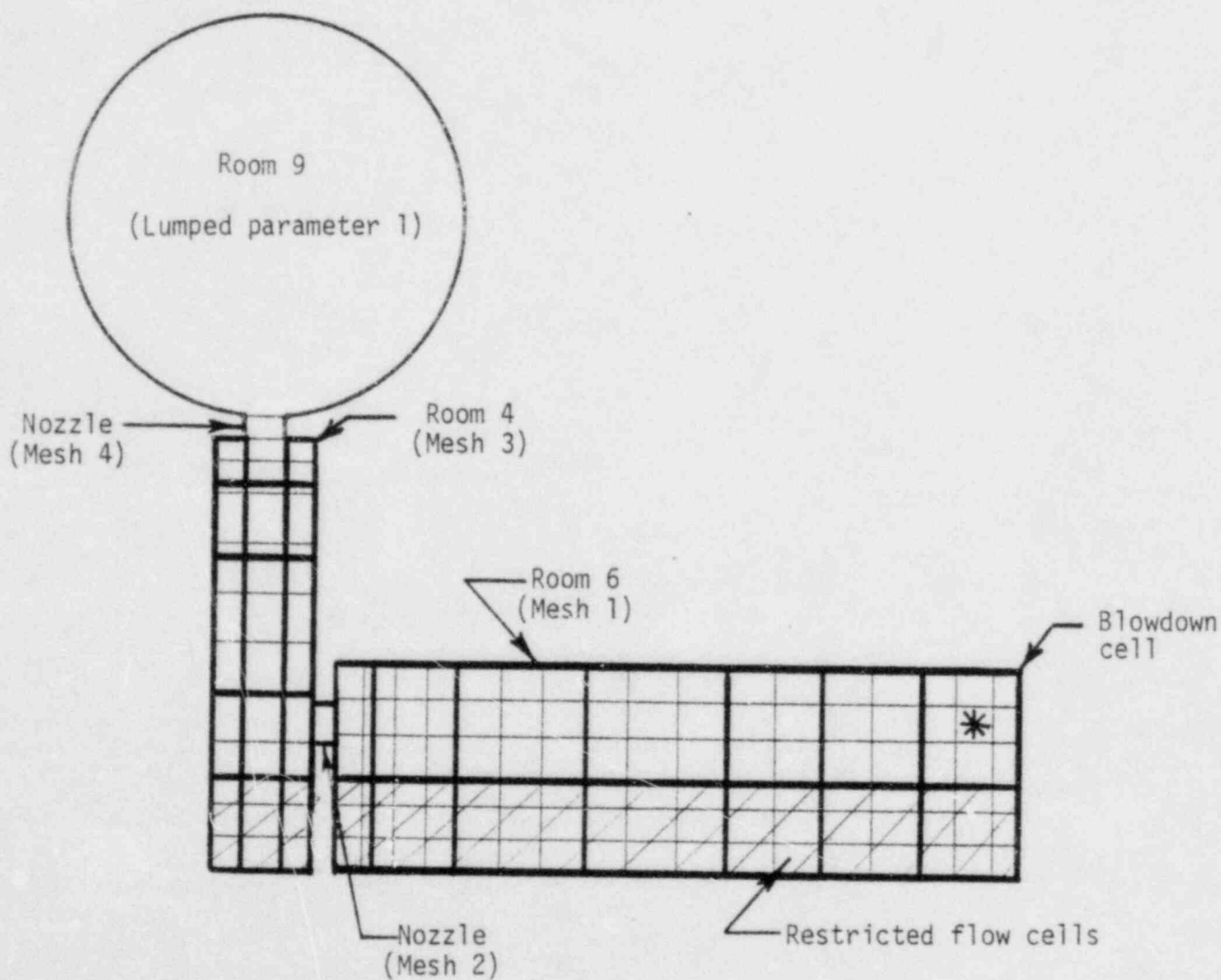


Figure E-4. Coarser nodalization of the Battelle-Frankfurt D-3 facility used for Case 6b.

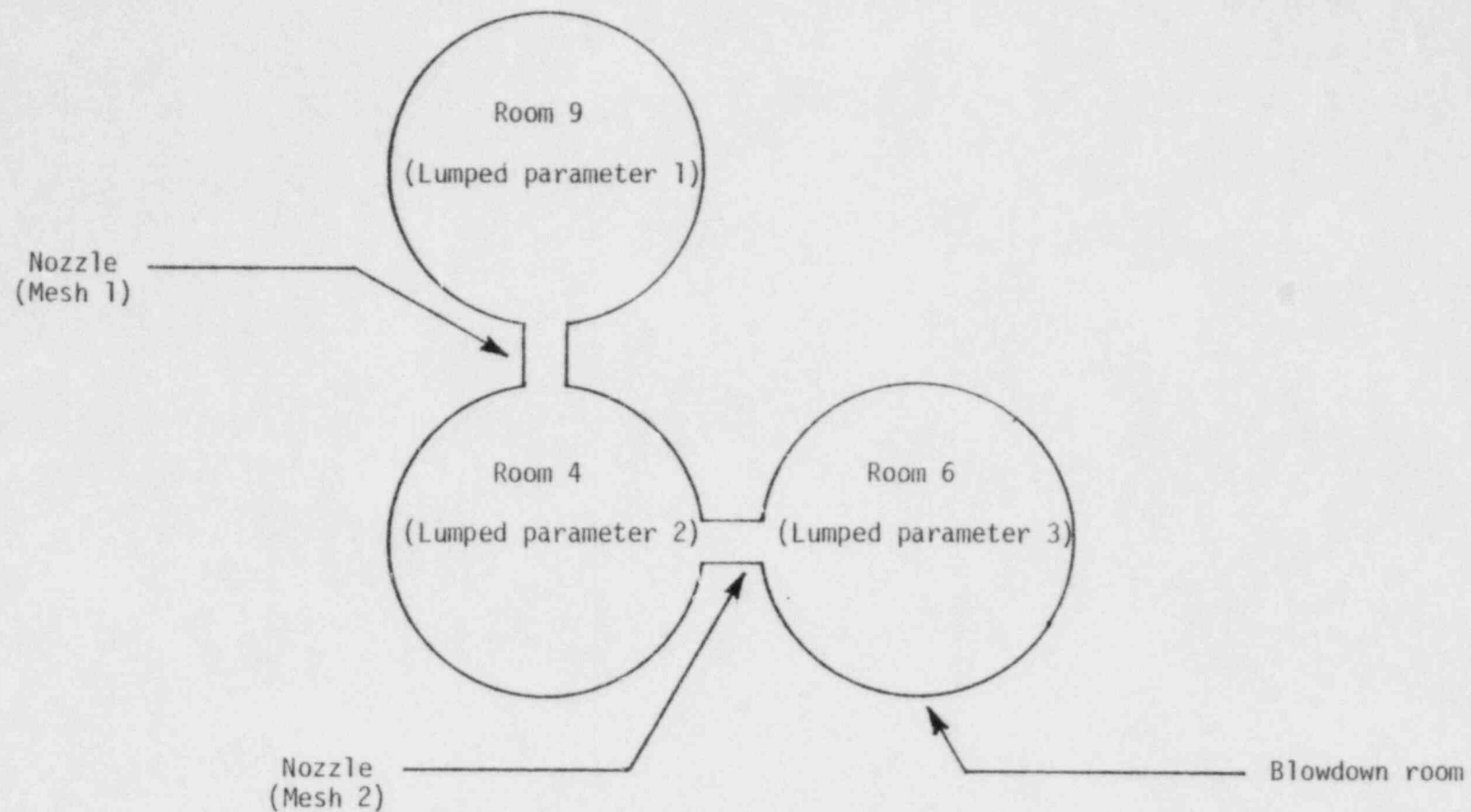


Figure E-5. Lumped parameter modeling of the Battelle-Frankfurt D-3 facility used for Case 7.

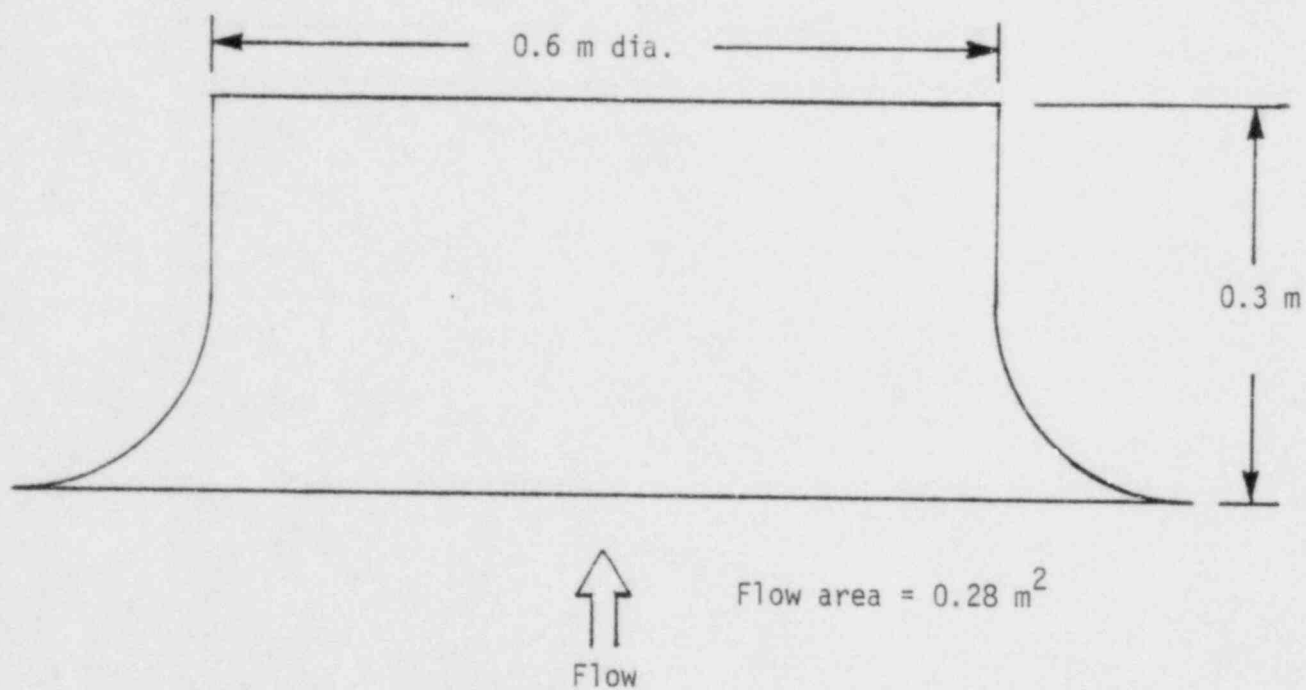


Figure E-6. Nozzle configuration for the D-3 test.

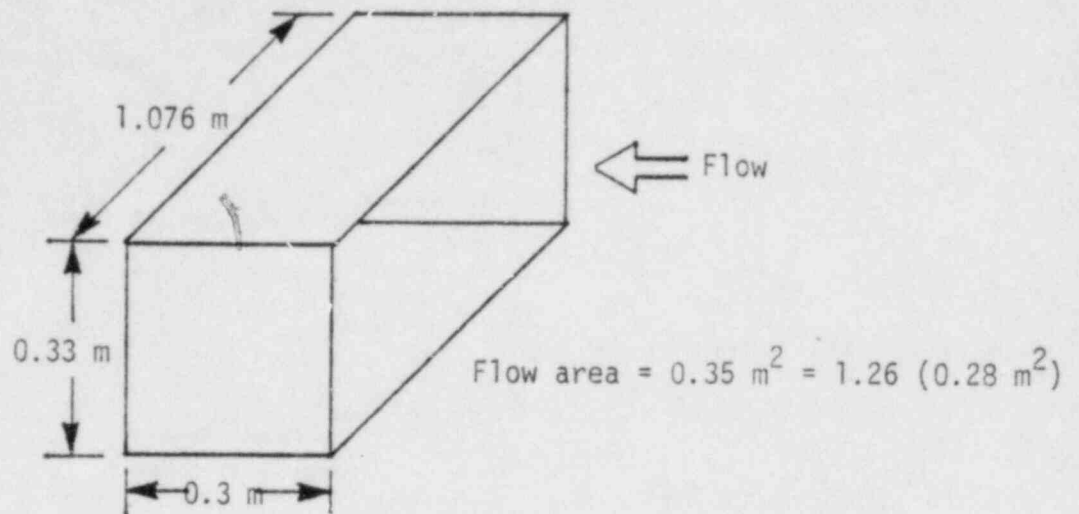


Figure E-7. Room 6 to Room 4 nozzle model for Cases 1 through 6b.

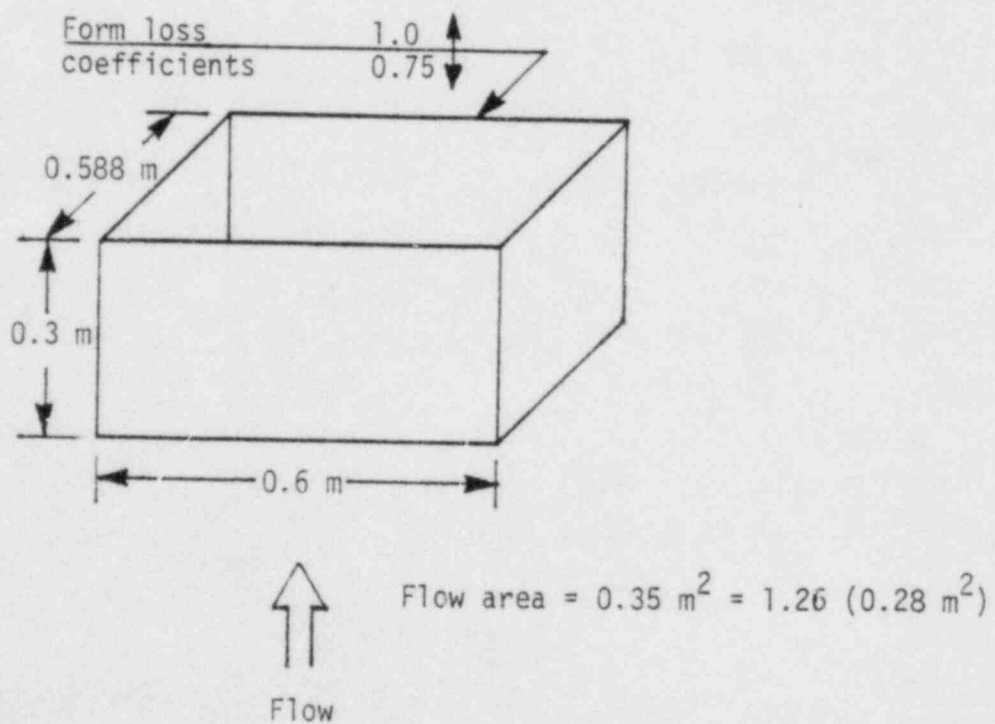


Figure E-8. Room 4 to Room 9 nozzle model for Cases 1 through 6b.

not allow input of negative flow losses, an artificial method was used. The flow areas of the nozzles were adjusted to reflect the ratio of the two loss coefficients. All of the coefficients were obtained from Reference E-2 and are as follows:

For a thick orifice of the D-3 nozzle dimensions:

$$\begin{array}{rcl} \text{Entrance loss} & = & 0.5 \\ \text{Exit loss} & = & \underline{1.0} \\ \text{Total Loss} & = & 1.5 \end{array}$$

For a converging nozzle of the D-3 dimension in foreword flow direction:

$$\begin{array}{rcl} \text{Entrance loss} & = & 0.1875 \\ \text{Exit loss} & = & \underline{1.0} \\ \text{Total Loss} & = & 1.1875 \end{array}$$

The areas were then adjusted by the factor:

$$\text{Factor} = \frac{1.5}{1.1875} = 1.26$$

This technique would be invalid for flow in the opposite direction from that expected, because the factor for the reverse flow would be 0.91. Because flow reversal was not expected to occur for the D-3 problem, this was not considered relevant.

The use of form loss coefficients was necessary for the lumped-parameter junctions, since these losses are not calculated by BEACON. The values used were 1.0 in the forward direction and 0.9 in the reverse flow direction.

The nozzle models for Case 7 (lumped-parameter case) are shown in Figures E-9 and E-10. The flow area for each nozzle was input as 0.28 m^2 . The 1.26 factor was not used because flow loss coefficients were input for all junctions. The values were:

In forward flow direction:

Entrance loss = 0.1875

Exit loss = 1.0

In reverse flow direction:

Entrance loss = 0.75

Exit loss = 0.9.

Tables for the blowdown mass flow rates and enthalpies were derived from Reference E-1. The inflow was pure steam until 1.88 seconds and was at saturated conditions with varying quality thereafter. Two sources were located in the upper right corner of Room 6 to model the blowdown. A steam source was used from the beginning of the test and a liquid source was added beginning at 1.88 seconds.

Heat structure information for Cases 3 through 7 was obtained from Reference E-3. Table E-2 shows the various heat structure areas, connections, and materials. The main structure of the Battelle facility was concrete with a protective coating on the test compartment surfaces. In the BEACON model, the concrete areas were attached to the faces of the two-dimensional meshes. The structural steel and piping, which was located along the upper portion of Room 6, was modeled at the top of the mesh. Assorted pieces of steel, which were stored in Rooms 4 and 6, were modeled at the bottom of the meshes. The steel nozzle heat structures were attached to the faces of the respective one-dimensional meshes. Remaining

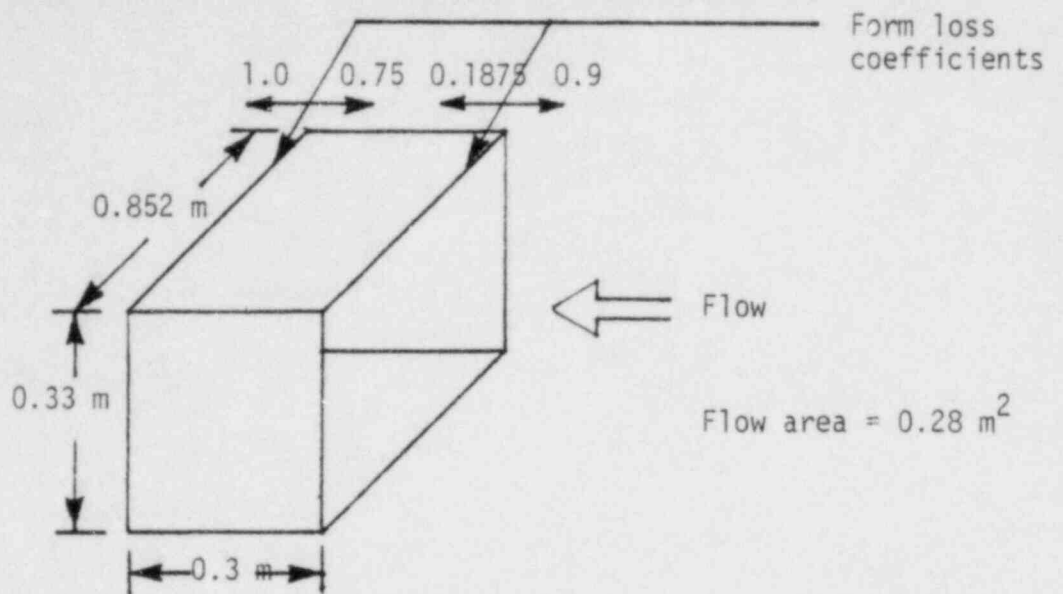


Figure E-9. Room 6 to Room 4 nozzle model for Case 7.

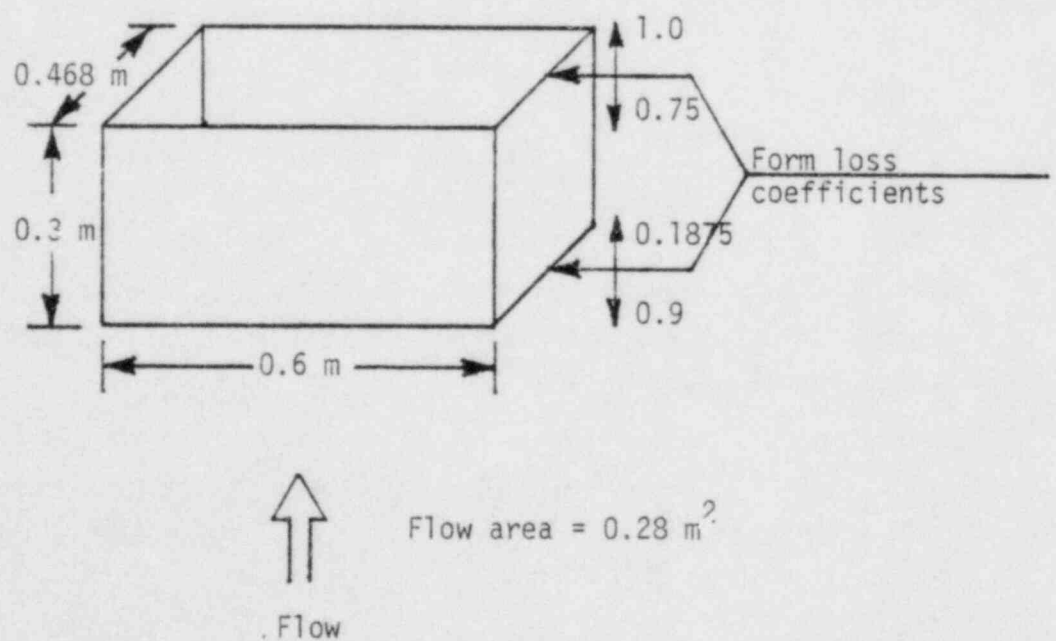


Figure E-10. Room 4 to Room 9 nozzle model for Case 7.

TABLE E-2. HEAT STRUCTURES FOR CASES 3 THROUGH 5

Heat Structure No.	Mesh No.	Lower Left Cell	Upper Right Cell	Connection Side	Area (m ²)	Thickness (m)	Material
1	3 (Room 4)	4,9	-	Right	1.745	.017	Steel
2		2,7	-	Left	0.6	.016	Aluminum
3		2,2	4,3	Faces	8.345	.013	Steel
4		2,4	4,12	Faces	38.631	.125	Concrete
5	1 (Room 6)	7,5	-	Faces	1.694	.020	Steel
6		13,5	-	Faces	1.918	.020	Steel
7		18,2	18,7	Right	3.600	.020	Aluminum
8		2,7	18,7	Top	6.781	.016	Steel
9		12,5	-	Faces	1.148	.016	Aluminum
10		2,2	18,2	Bottom	13.68	.008	Steel
11		2,2	6,7	Faces	22.16	.125	Concrete
12		7,2	7,4		3.33		
13		3,2	11,7		24.01		
14		12,2	13,4		7.76		
15		14,2	18,7		25.49		
16	LPR1 (Room 9)	-	-	None	890.059	.250	Concrete
17		-	-		120.848	.011	Steel
18		-	-		10.43	.016	Aluminum
19	2	2,2	-	Faces	0.990	.020	Steel
20	4	2,2	-	Faces	0.990	.020	Steel
21	1	7,6	7,7	Faces	5.19	.125	Concrete
22	1	12,6	13,7	Faces	5.17	.125	Concrete

cover plates and instrument junction boxes were connected to cells representative of their respective locations in the Battelle facility. For the lumped-parameter regions, the heat structure models have no spatial location.

All heat structures were connected to the walls on one side only. Connecting the heat structures in this way reduces the problem run time. For those structures which were, in reality, connected on both sides within the containment, this simplification should not have affected the results because of the short-term blowdown.

Listings of the BEACON input for Cases 4, 6a, 6b, and 7 are given in Figures E-11 through E-14.

[illegible]

Figure E-11. BEACON input listing for Case 4.

POOR ORIG

106

PC

107

[illegible]

108

POOR ORIGINAL

```

1200000 'R4-R9 NOZZLE'
1200001 8 1 0.0 0.0 100 0.01 0.
1200002 SINGLE 4 2 2 DUMMY
1200003 M2 0.490 FACES, NONE
1200009 11 11 0 0
1200200 0 2
1200201 2.175 4
1200301 2.175 4
1200401 2.175 4
1200601 2.32 0.3
1210000 'R8 CONCRETE'
1210001 8 1 0.0 0.0 100 0.01 0.
1210002 MULTI 1 7 8 7 7 DUMMY
1210003 M2 2.31 FACES, NONE
1210004 11 11 0 0
1210200 0 2
1210201 .00095 2 .025 7
1210301 0 1 1 7
1210401 0 1 7
1210601 2.32 0.3
1220000 'R8 CONCRETE'
1220001 8 1 0.0 0.0 100 0.01 0.
1220002 MULTI 1 1 12 6 13 7 DUMMY
1220003 M2 5.17 FACES, NONE
1220009 11 11 0 0
1220200 0 2
1220201 .00095 2 .025 7
1220301 0 1 1 7
1220401 0 1 7
1220601 2.32 0.3

```

Figure E-11. (continued).

[illegible]

110

POOR ORIGINAL

[illegible]

Figure E-12. (continued).

POOR ORIGINAL

[illegible]

Figure E-12. (continued).

POOR ORIGINAL

[illegible]

Figure E-12. (continued).

[illegible]

114


```

100 "BATTELLE-FRANKFURT TEST 0-3--CODE ADJUSTMENT--CASE SIX-3"
105 READ 30 WRITE 1 COPY
110 0.00,1.0, 0.0001, SEC, 10.0, 1, XEQ, BEST
120 0.01,0.5, 0.100, 2.5
130 AUTODT, 0, 0.20, 1.2, 3.0E-4
140 PRINT, NOPRINT, PRINT, NOPRINT, NOPRINT, PRINT
145 13 0 44 0
150 PLOTS 0.9 0 1 0 0 0 0 0 0 0 1 0 0 1 1
190 4 1 0.001
200 1.0, 0.00001, 0.00001, 100, 5, 5
240 LASL, PT, N/M2, DEGK, M, SEC-1
300 10
301 1 3 3 18 R07M6 PRESSURE
302 3 4 3 18 R07M4 PRESSURE
303 1 0 0 18 R07M9 PRESSURE
304 1 6 3 44 R07M5 TEMPERATUR
305 3 4 3 44 R07M4 TEMPERATUR
306 1 0 0 44 R07M2 TEMPERATUR
11005 ***** ROOM 6 *****
11000 CARTSN, 7, 2, 0.7, 0.5, 1.694, M, 0.0, 1.0
11020 .6 1.2 1.8 2.0 1.4 1.4 1.35
11030 1.28 1.67
11301 2 2 8 2 0.5 0.5 0.348
21005 * ROOM 6 TO ROOM 4 NOZZLE *
* DEPTH = 1.25*.852
21000 CARTSN, 1, 1, 0.3, 0.33, 1.076, M, 0.0, 1.0
31005 ***** ROOM 4 *****
31000 CARTSN, 3, 5, 0.5, 0.7, 1.649, M, 0.0, 1.0
31020 .4 .6 .4
31030 1.28 1.2 1.82 1.2 .5
31301 2 2 4 2 0.5 0.5 0.337
41005 ***** ROOM 4 TO ROOM 5 NOZZLE *****
* DEPTH = 1.26*.852
41000 CARTSN, 1, 1, 0.6, 0.3, 0.588, M, 0.0, 1.0
04001 4 2 2 TOP 1.0 .75
11101 MIXTURE, 2, 2, 8, 3, 0, 1.00E5, 287.60, 287.60, 1.0, 0.992976
21101 MIXTURE, 2, 2, 2, 2, 0, 1.00E5, 287.60, 287.60, 1.0, 0.992976
31101 MIXTURE, 2, 2, 4, 6, 0, 1.00E5, 287.60, 287.60, 1.0, 0.992976
41101 MIXTURE, 2, 2, 2, 2, 0, 1.00E5, 287.60, 287.60, 1.0, 0.992976
11010 NOSLIP NOSLIP NOSLIP NOSLIP
21010 NOSLIP NOSLIP NOSLIP NOSLIP
31010 NOSLIP NOSLIP NOSLIP NOSLIP
41010 NOSLIP NOSLIP NOSLIP NOSLIP
11050 FILM
21050 NOFILM
31050 FILM
41050 NOFILM
12005 ***** REMAINDER OF CONTAINMENT *****
12000 ZERO 550.0 M3 1.0E10 0.001 0.001
12010 MIXTURE 1.0E5 287.9 287.9 1.0 0.992976
6001 LEFT 1 2 3 1 2 2 1
6002 LEFT 2 2 2 1 3 4 1
6003 TOP 3 3 6 1 4 2 1
7001 TOP 4 2 2 1 2 2 1
3010 STEAM, 1, 8, 3, 3011
3011 SEC, KG/SEC, J/GM, M, SEC-1
3012 .000, 0.0, 2772.2, 0.0
3013 .020, 83.3, 2772.2, 0.0
3014 .050, 85.3, 2772.2, 0.0
3015 .075, 79.6, 2772.2, 0.0
3016 .100, 78.9, 2772.2, 0.0
3017 .200, 84.0, 2772.2, 0.0
3018 .300, 80.0, 2772.2, 0.0
3019 .500, 77.4, 2772.2, 0.0
3020 1.000, 73.6, 2772.2, 0.0
3021 1.500, 68.4, 2772.2, 0.0
3022 1.730, 65.1, 2772.2, 0.0
3023 1.880, 39.8, 2772.2, 0.0

```

Figure E-13. BEACON input listing for Case 6b.

Figure E-13. (continued).

[illegible]

ITEM	QTY	UNIT	PRICE	TOTAL	DESCRIPTION
1060000	1	COVER PLATE	1.00	1.00	COVER PLATE
1060001	5	1.00	5.00	1.00	1.00
1060002	1	1.00	1.00	1.00	1.00
1060003	1	1.00	1.00	1.00	1.00
1060009	1	1.00	1.00	1.00	1.00
1060200	1	1.00	1.00	1.00	1.00
1060201	1	1.00	1.00	1.00	1.00
1060301	2	1.00	2.00	1.00	1.00
1060401	1	1.00	1.00	1.00	1.00
1060601	1	1.00	1.00	1.00	1.00
1060601	282	0.5	141.00	1.00	1.00
1070000	1	1.00	1.00	1.00	1.00
1070001	5	1.00	5.00	1.00	1.00
1070002	1	1.00	1.00	1.00	1.00
1070003	1	1.00	1.00	1.00	1.00
1070009	1	1.00	1.00	1.00	1.00
1070200	1	1.00	1.00	1.00	1.00
1070201	1	1.00	1.00	1.00	1.00
1070301	3	1.00	3.00	1.00	1.00
1070401	1	1.00	1.00	1.00	1.00
1070601	1	1.00	1.00	1.00	1.00
1070601	282	0.5	141.00	1.00	1.00
1080000	1	1.00	1.00	1.00	1.00
1080001	5	1.00	5.00	1.00	1.00
1080002	1	1.00	1.00	1.00	1.00
1080003	1	1.00	1.00	1.00	1.00
1080009	1	1.00	1.00	1.00	1.00
1080200	1	1.00	1.00	1.00	1.00
1080201	1	1.00	1.00	1.00	1.00
1080301	2	1.00	2.00	1.00	1.00
1080401	1	1.00	1.00	1.00	1.00
1080601	1	1.00	1.00	1.00	1.00
1080601	282	0.5	141.00	1.00	1.00
1090000	1	1.00	1.00	1.00	1.00
1090001	5	1.00	5.00	1.00	1.00
1090002	1	1.00	1.00	1.00	1.00
1090003	1	1.00	1.00	1.00	1.00
1090009	1	1.00	1.00	1.00	1.00
1090200	1	1.00	1.00	1.00	1.00
1090201	1	1.00	1.00	1.00	1.00
1090301	3	1.00	3.00	1.00	1.00
1090401	1	1.00	1.00	1.00	1.00
1090601	1	1.00	1.00	1.00	1.00
1090601	282	0.5	141.00	1.00	1.00
1100000	1	1.00	1.00	1.00	1.00
1100001	3	1.00	3.00	1.00	1.00
1100002	1	1.00	1.00	1.00	1.00
1100003	1	1.00	1.00	1.00	1.00
1100009	1	1.00	1.00	1.00	1.00
1100200	1	1.00	1.00	1.00	1.00
1100201	1	1.00	1.00	1.00	1.00
1100301	2	1.00	2.00	1.00	1.00
1100401	1	1.00	1.00	1.00	1.00
1100601	1	1.00	1.00	1.00	1.00
1100601	282	0.3	84.60	1.00	1.00
1110000	1	1.00	1.00	1.00	1.00
1110001	6	1.00	6.00	1.00	1.00
1110002	1	1.00	1.00	1.00	1.00
1110003	1	1.00	1.00	1.00	1.00
1110009	1	1.00	1.00	1.00	1.00

```

1130000 'R6 CONCRETE'
1130001 6 1 0.0 0.0 100 0.01 0.
1130002 MULTI 1 7 3 8 3 DUMMY 0 0 0 0 0
1130003 M2, 30.88, FACES, NONE
1130009 11 11 0 0
1130200 0 2
1130201 .025 5
1130301 1 5
1130401 0.0 5
1130601 282.0 6
1140000 'R9, ETC. CONCRETE'
1140001 6 1 0.0 0.0 100 0.01 0.
1140002 LUMPED 1 0 0 0 0 DUMMY 0 0 0 0 0
1140003 M2, 890.059, NONE, NONE
1140009 11 11 0 0
1140200 0 2
1140201 .050 5
1140301 1 5
1140401 0.0 5
1140601 282.0 6
1150000 'R9, ETC. STEEL'
1150001 3 1 0.0 0.0 100 0.01 0.
1150002 LUMPED 1 0 0 0 0 DUMMY 0 0 0 0 0
1150003 M2, 120.848, NONE, NONE
1150009 11 11 0 0
1150200 0 2
1150201 .005 2
1150301 2 2
1150401 0.0 2
1150601 282.0 3
1160000 'R9, ETC. ALUMINUM'
1160001 5 1 0.0 0.0 100 0.01 0.
1160002 LUMPED 1 0 0 0 0 DUMMY 0 0 0 0 0
1160003 M2, 10.430, NONE, NONE
1160009 11 11 0 0
1160200 0 2
1160201 .004 4
1160301 3 4
1160401 0.0 4
1160601 282.0 5
1170000 'R6-R4 NOZZLE'
1170001 5 1 0.0 0.0 100 0.01 0.
1170002 SINGLE 2 2 2 0 0 DUMMY 0 0 0 0 0
1170003 M2, 0.990, FACES, NONE
1170009 11 11 0 0
1170200 0 2
1170201 .005 4
1170301 2 4
1170401 0.0 4
1170601 282.0 5
1180000 'R4-R9 NOZZLE'
1180001 5 1 0.0 0.0 100 0.01 0.
1180002 SINGLE 4 2 2 0 0 DUMMY 0 0 0 0 0
1180003 M2, 0.990, FACES, NONE
1180009 11 11 0 0
1180200 0 2
1180201 .005 4
1180301 2 4
1180401 0.0 4
1180601 282.0 5

```

Figure E-13. (continued).

```

100  "BATTELLE-FRANKFURT TEST 0-3--CODE ADJUSTMENT--CASE SEVEN"
101  NUREAD 12  KXITE 1  NOCLPY
110  C.CO,1.C, C.CO01, SEC, 10.C, 1, AEG, BEST
120  C.C1,U.5, C.100, 2.5
130  AUTCDT, C, C.20, 1.2, 3.0E-4
140  PRINT, NCPRI, PRINT, NUPRI, NUPRI, PRINT
150  2 3 0.0005
200  1.C, 0.0001, C.CO01, 100, 5, 5
240  LASL, PT, N/M2, DEGK, M, SEC-1
300  10
301  0 0 18 ROOM6 PRESSURE
302  0 0 18 ROOM4 PRESSURE
303  0 0 18 ROOM9 PRESSURE
304  0 0 44 ROOM6 TEMPERATURE
305  0 0 44 ROOM4 TEMPERATURE
306  0 0 44 ROOM9 TEMPERATURE
32005 ***** ROOM 6 *****
32000 ZERO, 41.20, M3, 1.0E10, 0.030, 0.030
32010 MIXTURE 1.0E5 287.6 287.6 1.C 0.992976
33005 ***** ROOM 6 TL ROOM 4 NOZZLE *****
33010 CARTSN, 1, 1, 0.3, 0.33, .852, M, C.0, 1.0
34005 MIXTURE, 2, 2, 2, 2, 0, 1.00E5, 287.60, 287.60, 1.0, 0.992976
34010 NOSLIP NOSLIP NOSLIP NOSLIP
34003 2 2 2 RIGHT .9 .1875
34004 2 2 2 LEFT .75 1.0
35005 NOFILM
35010 ***** ROOM 4 *****
35020 ZERO, 13.0, M3, 1.0E10, 0.001, 0.001
35030 MIXTURE 1.0E5 287.6 287.6 1.C 0.992976
35040 ***** ROOM 4 TL ROOM 9 NOZZLE *****
35050 CARTSN, 1, 1, 0.6, 0.3, 0.468, M, C.0, 1.0
35060 MIXTURE, 2, 2, 2, 2, 0, 1.00E5, 287.60, 287.60, 1.0, 0.992976
35070 NOSLIP NOSLIP NOSLIP NOSLIP
35080 1 2 2 BOTTOM .1875 .9
35090 2 2 2 TOP 1.C .75
36005 NOFILM
36010 ***** REMAINDER OF CONTAINMENT *****
36020 ZERO, 550.0, M3, 1.0E10, C.CO1, C.CO1
36030 MIXTURE 1.0E5 287.9 287.9 1.C 0.992976
37001 TOP 1 2 2 1 1.0
37002 BOTTOM 1 2 2 1 1.0
37003 LEFT 2 2 2 2 1.0
37004 RIGHT 2 2 2 3 1.0
38010 STEAM, 3, 0, 0, 3011
38011 SEC, KG/SEC, J/GM, M, SEC-1
38012 .000, 0.0, 2772.2, 0.0
38013 .020, 83.3, 2772.2, 0.0
38014 .050, 83.3, 2772.2, 0.0
38015 .075, 79.6, 2772.2, 0.0
38016 .100, 78.9, 2772.2, 0.0
38017 .200, 84.0, 2772.2, 0.0
38018 .400, 80.0, 2772.2, 0.0
38019 .500, 77.4, 2772.2, 0.0
38020 1.000, 73.6, 2772.2, 0.0
38021 1.500, 68.4, 2772.2, 0.0
38022 1.733, 65.1, 2772.2, 0.0
38023 1.880, 39.8, 2772.2, 0.0
38024 QUALITY = .500 AT T = 2.000 SEC 0.0
38025 QUALITY = .350 AT T = 2.700 SEC 0.0
38026 QUALITY = .370 AT T = 4.000 SEC 0.0
38027 4.000, 38.4, 2772.2, 0.0
38030 LIQUID, 3, C, 0, 3011
38031 SEC, KG/SEC, J/GM, M, SEC-1
38032 0.000, C.C, 735.9, 0.0
38033 1.680, 0.0, 735.9, 0.0
38034 2.000, 39.6, 735.9, 0.0
38035 2.700, 77.1, 735.9, 0.0
38036 4.000, 63.8, 735.9, 0.0

```

Figure E-14. BEACON input listing for Case 7.

```

*
10000001 HEAT SLAB INPUT
10000002 K, MAT, DEGK
10000003 C, SEC, C.CC1
10000004 BTU/HR-FT-DEGF, BTU/FT3-DEGF, BTU/HK-FT2-DEGF
*
10001001 CONCRETE STEEL ALUMINUM STAINLESS NG02
10001002 1.00 33.02 30.00 55.01 119.00 35.48 10. 58.44 .32 1.09
10001003 'R4 STEEL'
10001004 5 1 0.0 0.0 100 0.01 0.
10001005 LUMPED 2 0 0 0 0 DUMMY 0 0 0 0
10001006 M2, 10.090, NONE, NONE
10001007 11 11 0 0
10001008 C 2
10001009 .CC32 4
10001010 2 4
10001011 C.C 4
10001012 282.0 5
10001013 'R4 INSTRUMENTATION PULL BOX'
10001014 5 1 0.0 0.0 100 0.01 0.
10001015 LUMPED 2 0 0 0 0 DUMMY 0 0 0 0
10001016 M2, 0.600, NONE, NONE
10001017 11 11 0 0
10001018 C 2
10001019 .CC4 4
10001020 2 4
10001021 C.C 4
10001022 282.0 5
10001023 'R4 CONCRETE'
10001024 6 1 0.0 0.0 100 0.01 0.
10001025 LUMPED 2 0 0 0 0 DUMMY 0 0 0 0
10001026 M2, 38.831, NONE, NONE
10001027 11 11 0 0
10001028 C 2
10001029 .CC5 5
10001030 1 5
10001031 C.C 5
10001032 282.0 6
10001033 'R6 STEEL'
10001034 5 1 0.0 0.0 100 0.01 0.
10001035 LUMPED 3 0 0 0 0 DUMMY 0 0 0 0
10001036 M2, 24.073, NONE, NONE
10001037 11 11 0 0
10001038 C 2
10001039 .CC3 4
10001040 2 4
10001041 C.C 4
10001042 282.0 5
10001043 'R6 ALUMINUM'
10001044 5 1 0.0 0.0 100 0.01 0.
10001045 LUMPED 3 0 0 0 0 DUMMY 0 0 0 0
10001046 M2, 4.748, NONE, NONE
10001047 11 11 0 0
10001048 C 2
10001049 .CC5 4
10001050 2 4
10001051 C.C 4
10001052 282.0 5
10001053 'R6 CONCRETE'
10001054 6 1 0.0 0.0 100 0.01 0.
10001055 LUMPED 3 0 0 0 0 DUMMY 0 0 0 0
10001056 M2, 90.12, NONE, NONE
10001057 11 11 0 0
10001058 C 2
10001059 .CC5 5
10001060 1 5
10001061 C.C 5
10001062 282.0 6

```

Figure E-14. (continued).


```

1C70000 'K9, ETC. CONCRETE'
1C70001 6 1 0.0 0.0 100 0.01 0.
1C70002 LUMPED 1 0 0 0 0 DUMMY 0 0 0 0
1C70003 M2, 890.059, NONE, NONE
1C70009 11 11 0 0
1070200 0 2
1C70201 .050 5
1C70301 1 5
1C70401 C.C 5
1070601 282.0 6
1C80000 'K9, ETC. STEEL'
1C80001 3 1 0.0 0.0 100 0.01 0.
1C80002 LUMPED 1 0 0 0 0 DUMMY 0 0 0 0
1C80003 M2, 120.848, NONE, NONE
1C80009 11 11 0 0
1C80200 0 2
1C80201 .005 2
1080301 2 2
1C80401 C.C 2
1C80601 282.0 3
1C90000 'K9, ETC. ALUMINUM'
1C90001 5 1 0.0 0.0 100 0.01 0.
1C90002 LUMPED 1 0 0 0 0 DUMMY 0 0 0 0
1C90003 M2, 10.430, NONE, NONE
1C90009 11 11 0 0
1C90200 0 2
1C90201 .004 4
1090301 3 4
1C90401 C.C 4
1C90601 282.0 5
1100000 'K6-K4 NOZZLE'
1100001 5 1 0.0 0.0 100 0.01 0.
1100002 SINGLE 2 2 2 0 0 DUMMY 0 0 0 0
1100003 M2, 0.990, FACES, NONE
1100009 11 11 0 0
1100200 0 2
1100201 .005 4
1100301 2 4
1100401 C.C 4
1100601 282.0 5
1110000 'K4-K9 NOZZLE'
1110001 5 1 0.0 0.0 100 0.01 0.
1110002 SINGLE 1 2 2 0 0 DUMMY 0 0 0 0
1110003 M2, 0.990, FACES, NONE
1110009 11 11 0 0
1110200 0 2
1110201 .005 4
1110301 2 4
1110401 C.C 4
1110601 282.0 5

```

Figure E-14. (continued)

RESULTS

The results are discussed in three-sections. First, a comparison among the first four cases is made, thereby focusing on the effects of heat structures and film. Second, a comparison of the effects of nodalization (Cases 5 through 7) is made. Experimental data are included on the time history plots for these two studies but will not be addressed in the text and are for reference only. Last, the performance of the "best" model is compared to recorded test data to assess the overall performance of the code.

Effects of Heat Structures and Film

The options used in the first four cases were:

	<u>Film</u>	<u>Heat Structures</u>
Case 1	No	No
Case 2	Yes	No
Case 3	No	Yes
Case 4	Yes	Yes

Figure E-15 shows pressures in the break room for the first four cases. The presence of film in the absence of heat structures (comparing Cases 1 and 2), has negligible effect on the results. This is because virtually no film was formed when heat structures were absent. In Case 3, the addition of heat structures caused significantly lower pressures to be calculated. This was not due to a decrease in temperature, but to a marked increase in condensation, thereby removing mass from the gas-phase and depressurizing the room. In Case 4, the addition of film increased the pressure moderately from Case 3. This was due to the insulating effect the film had between the fluid regions and the heat structures, and its subsequent effect on temperatures. This is illustrated in Figure E-16, which shows gas temperatures (T_G) and wall temperatures (T_W) for

TEST D-3
PRESSURE IN ROOM 6 - CELL (5,6)

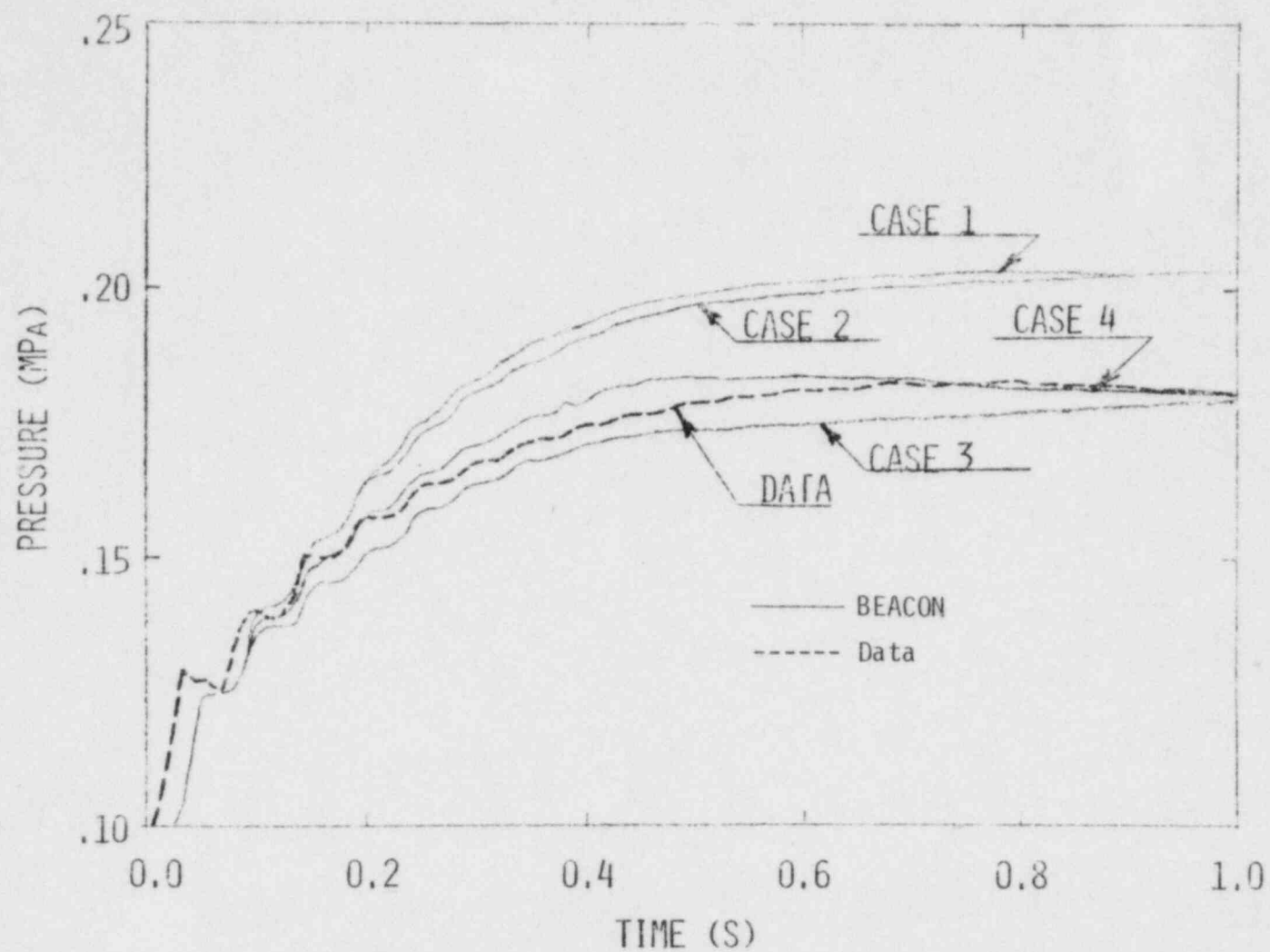


Figure E-15. Pressures in Room 6, Cell (5,6) for Cases 1 through 4.

GAS TEMPERATURE AND WALL TEMPERATURE IN ROOM 6

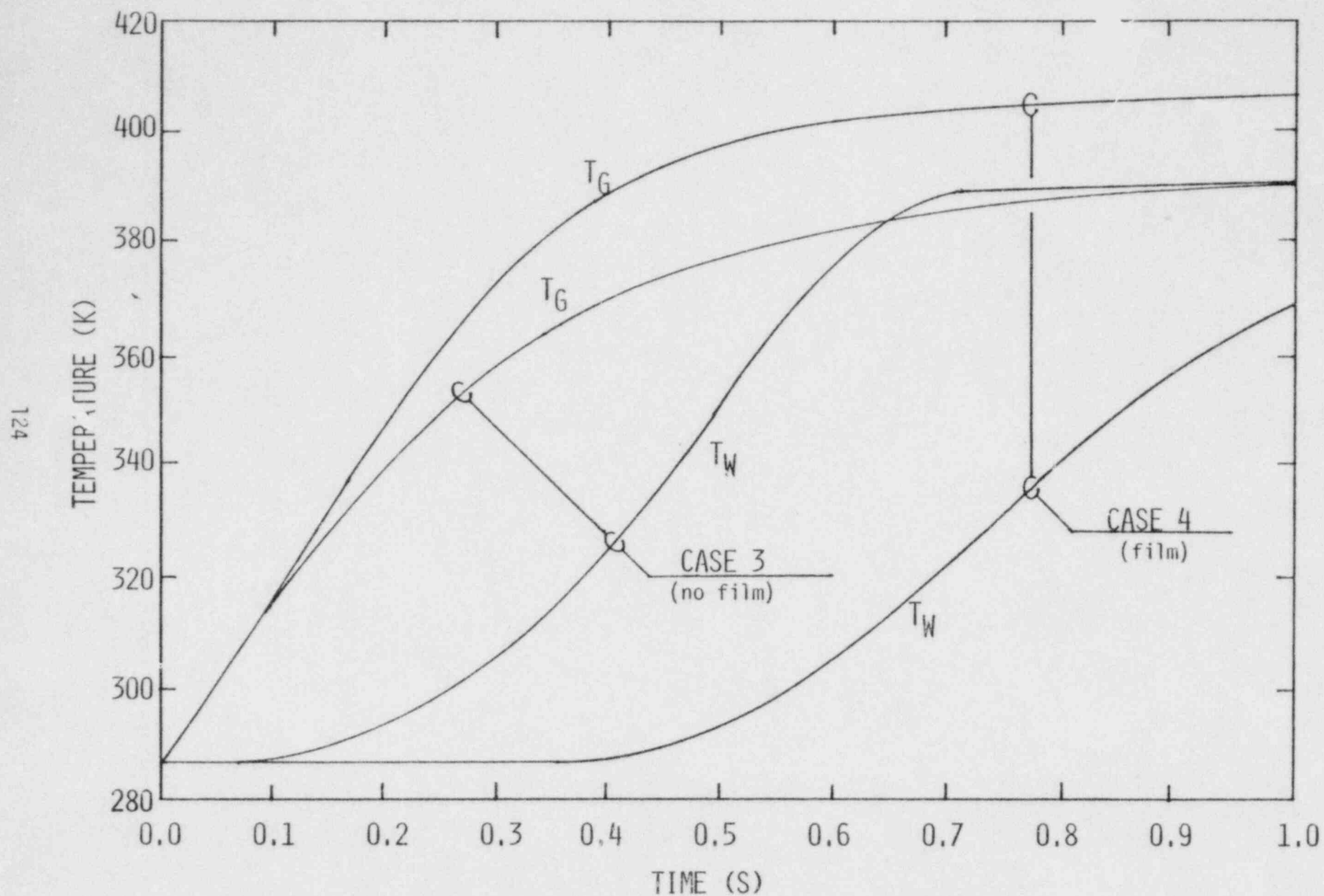


Figure E-16. Comparison between gas temperatures and wall temperatures for Cases 3 and 4 in Room 6.

Cases 3 and 4 for a typical fluid cell in Room 6. The temperature difference at any given time was substantially greater for the film-insulated case than for the no-film model.

The temperatures for the break room displayed the same trend as the pressures. Figure E-17 shows the temperatures near the break. The transient responses which occurred between 0 and 0.2 second show a sensitivity to the use of film and heat structures which varied the results over a range of approximately 25 Kelvin. Cases 1 and 2 have identical peak temperatures, but the second case falls further below the peak for the next 0.2 second. This is not an overall temperature response but is symptomatic of a redistribution of energy due to the film. Both heat structure cases have lower peak temperatures than the non-heat structure cases, while the insulating effects of the film appear in the form of slightly higher temperatures. The longer term responses show little differences among the models. The no-film heat structure case gives slightly lower temperatures.

Figure E-18 shows temperatures for Room 6 further from the break (Cell 13,4 - approximately 2.5 m from break). At this location, the difference in results among the cases was much more pronounced. The proximity of the previously described cell to the source caused the temperature to show very little sensitivity to the models used. In this cell, however, the effects of the options were more clearly seen. The primary differences between this and the previous cell were the wider spread of temperatures (approximately 70 K) and the medium-term response in Case 4 (at approximately 0.8 s).

The response of Case 4 with respect to Case 2 seems to be contrary to intuitively expected results. The temperature of the film/heat structure model is higher, for a short time, than that for the film only model. The reason for this is that the temperatures in this cell represent those of approximately 1% of the total mass of the room. The most realistic model (Case 4) shows that the dynamics of the problem were more complex than the simpler models predicted. This effect is seen in Figure E-19, which shows

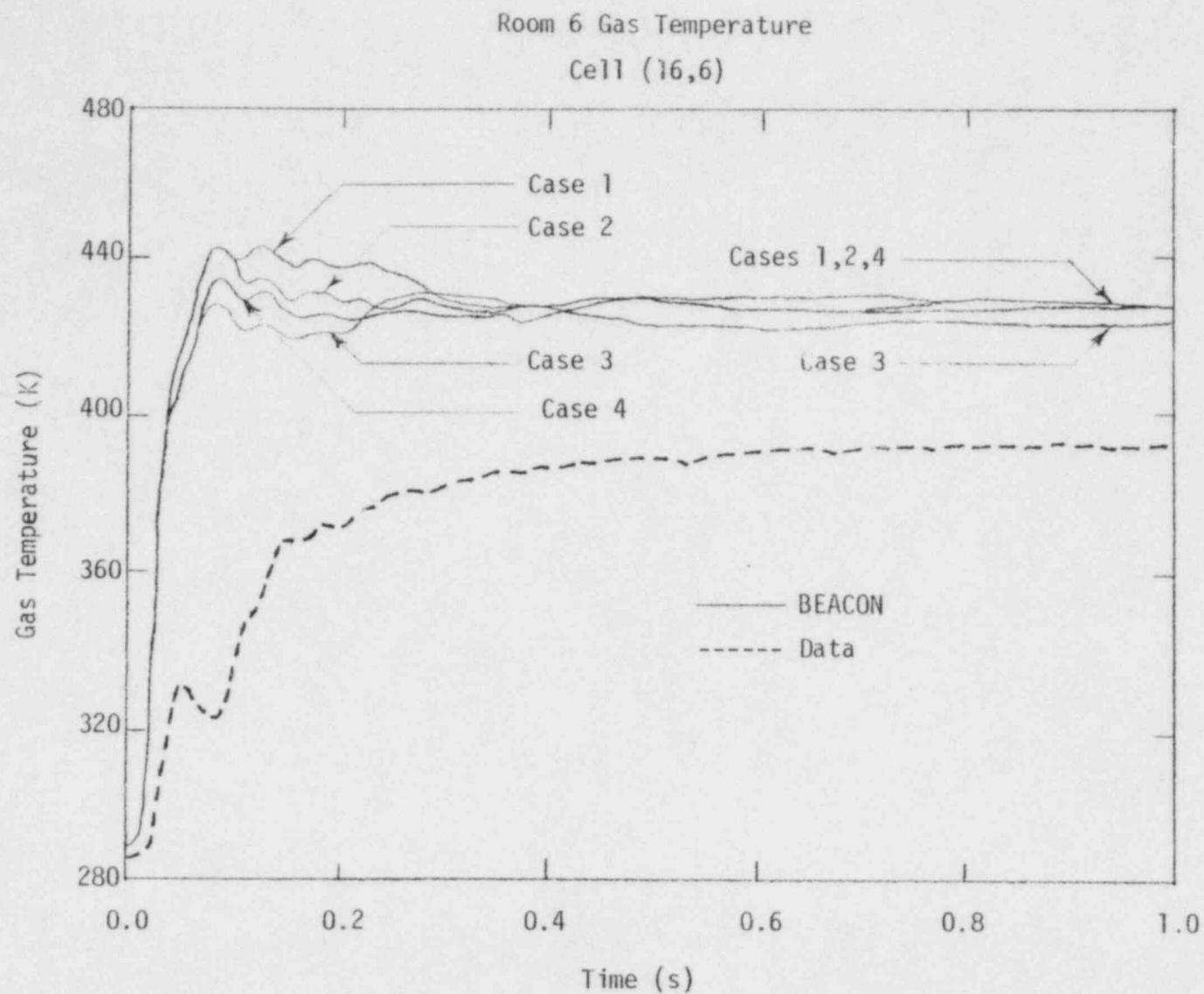


Figure E-17. Gas temperatures near the break in Room 6, Cell (16,6) for Cases 1 through 4.

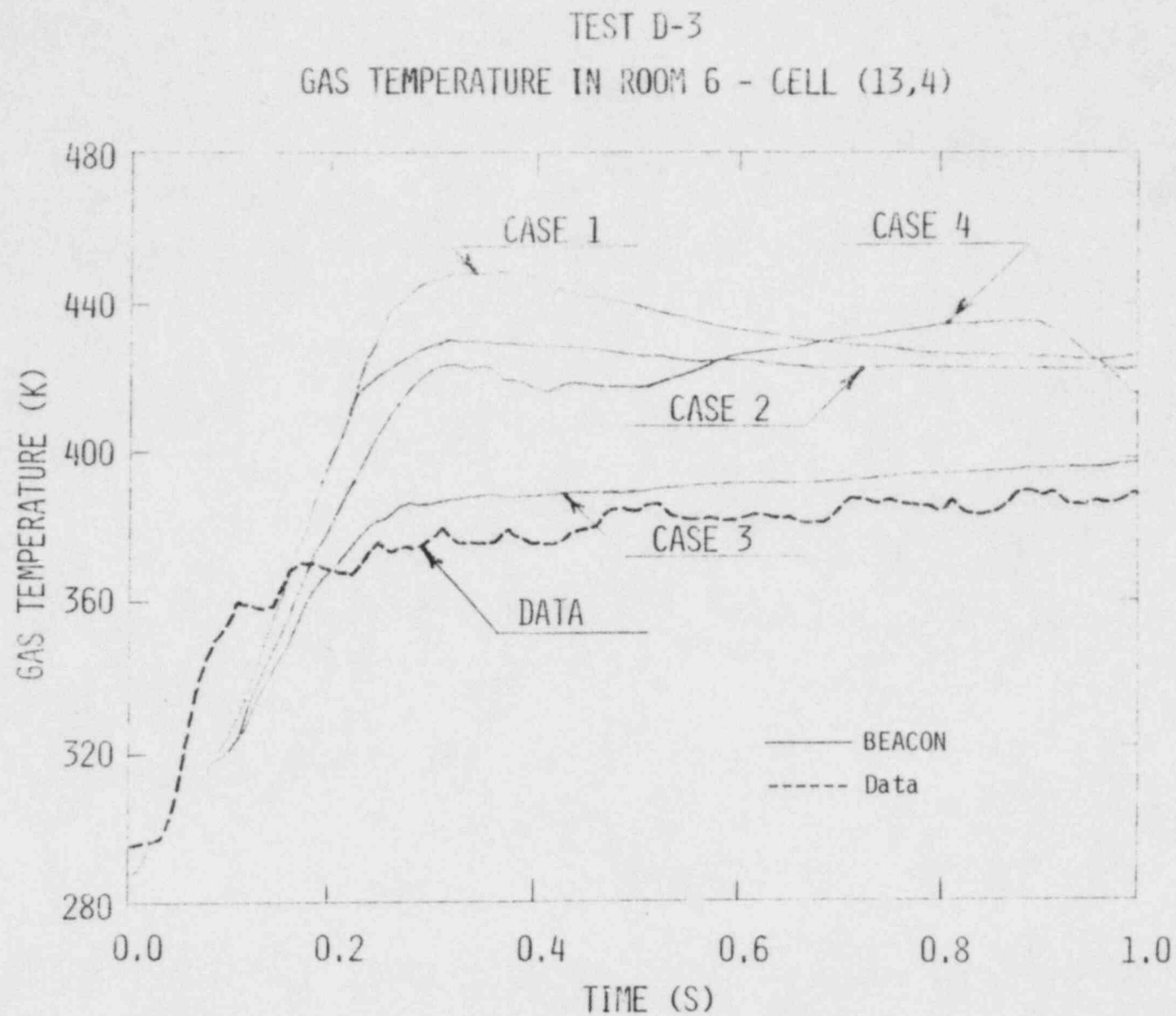


Figure E-18. Gas temperatures in Room 6, Cell (13,4).

TEST D-3

TEMPERATURE DISTRIBUTION IN ROOM 6 AT 2.8 S

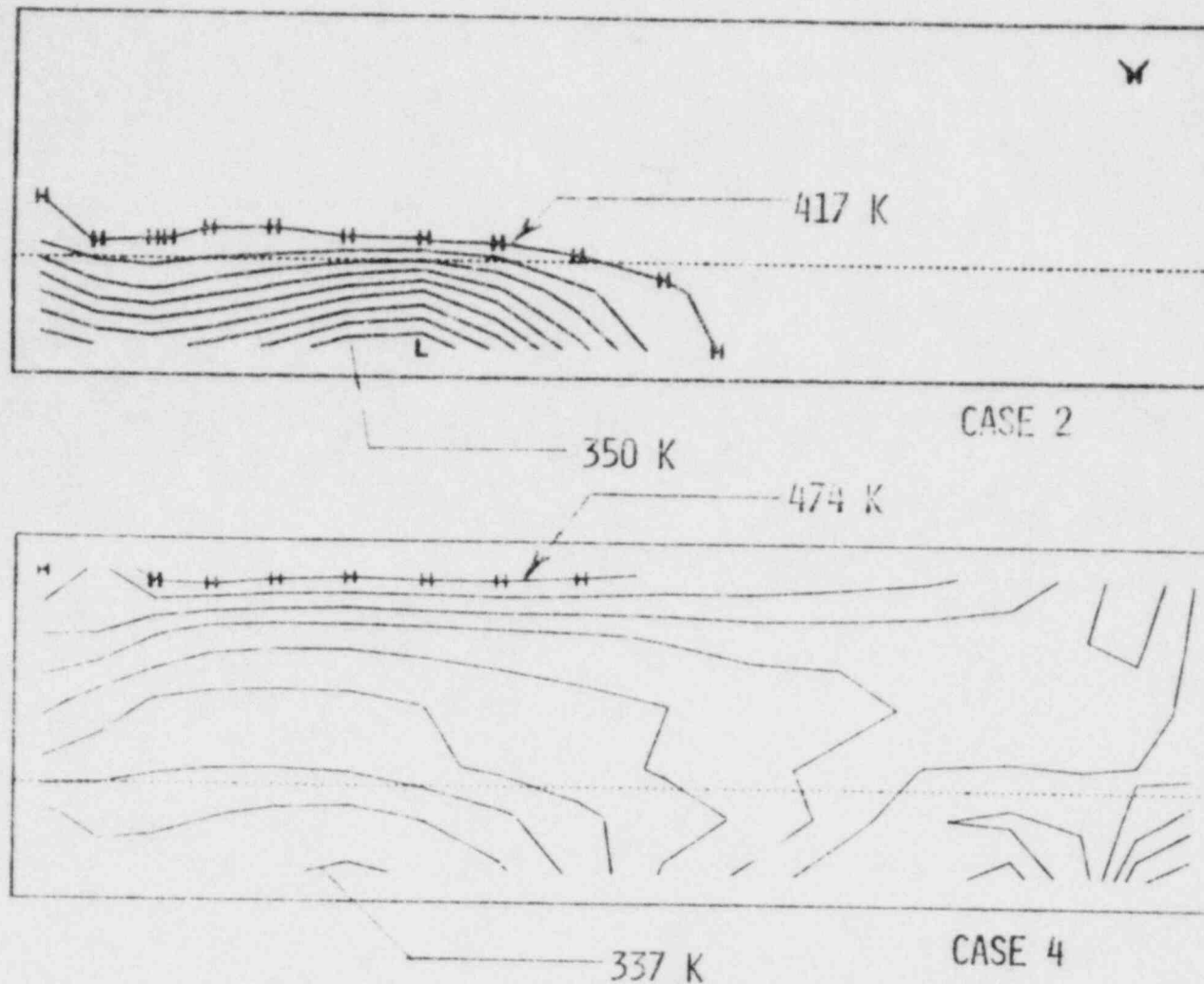


Figure E-19. Temperature distribution in Room 6 for Case 2 (with film, without heat structures) and Case 4 (with film and heat structures).

temperature contours in Room 6 at 0.8 s for Cases 2 and 4. Without the presence of heat structures, the film model (Case 2) gives results that agree with an intuitive prediction. The addition of heat structures (Case 4) had the effect of making the film more of a factor in the calculation and shows a much more complex temperature distribution. A pocket of high-temperature steam has traveled across the top of the room and become somewhat isolated in temperature due to mass-transfer effects. The steam pocket is probably unrealistically elongated because it was traveling along a single steel heat structure at the top of the room. Using this type of representation in BEACON tends to equalize temperatures along the surface. The final difference seen is the much wider temperature variation across the room for Case 4, with both a higher peak temperature and a lower minimum.

Pressures in Room 4 show trends similar to those in Room 6 for the same reasons (Figure E-20). The temperatures, however, show a reversal of results for Cases 3 and 4 (Figure E-21). In examining the printed output for these cases, it was discovered that the total water mass (steam + liquid) in Room 4 was 14% greater for Case 3 than for Case 4. This was due to liquid transport from Room 6 to Room 4 being greater in the no-film case. When film was present, liquid was "trapped" on the walls of the mesh and was inhibited from traveling with the fluid flow. As a result, in this case, the greater mass increased the thermal inertia in Room 4, and the effects of heat removal via heat transfer became somewhat less pronounced. This resulted in higher temperatures for the no-film case.

In Room 9, pressures and temperatures were not a function of film presence (Figures E-22 and E-23). This is reasonable since Room 9 was modeled as a lumped-parameter region and BEACON does not have the option of film for lumped-parameter regions. Pressures and temperatures were functions of the use of heat structures in the lumped-parameter case, with the heat structure option reducing the magnitude of both. This is consistent with the simpler fluid model used for lumped-parameter regions. Conducting heat from the volume reduces temperature, and consequently, pressure.

Pressure in Room 4

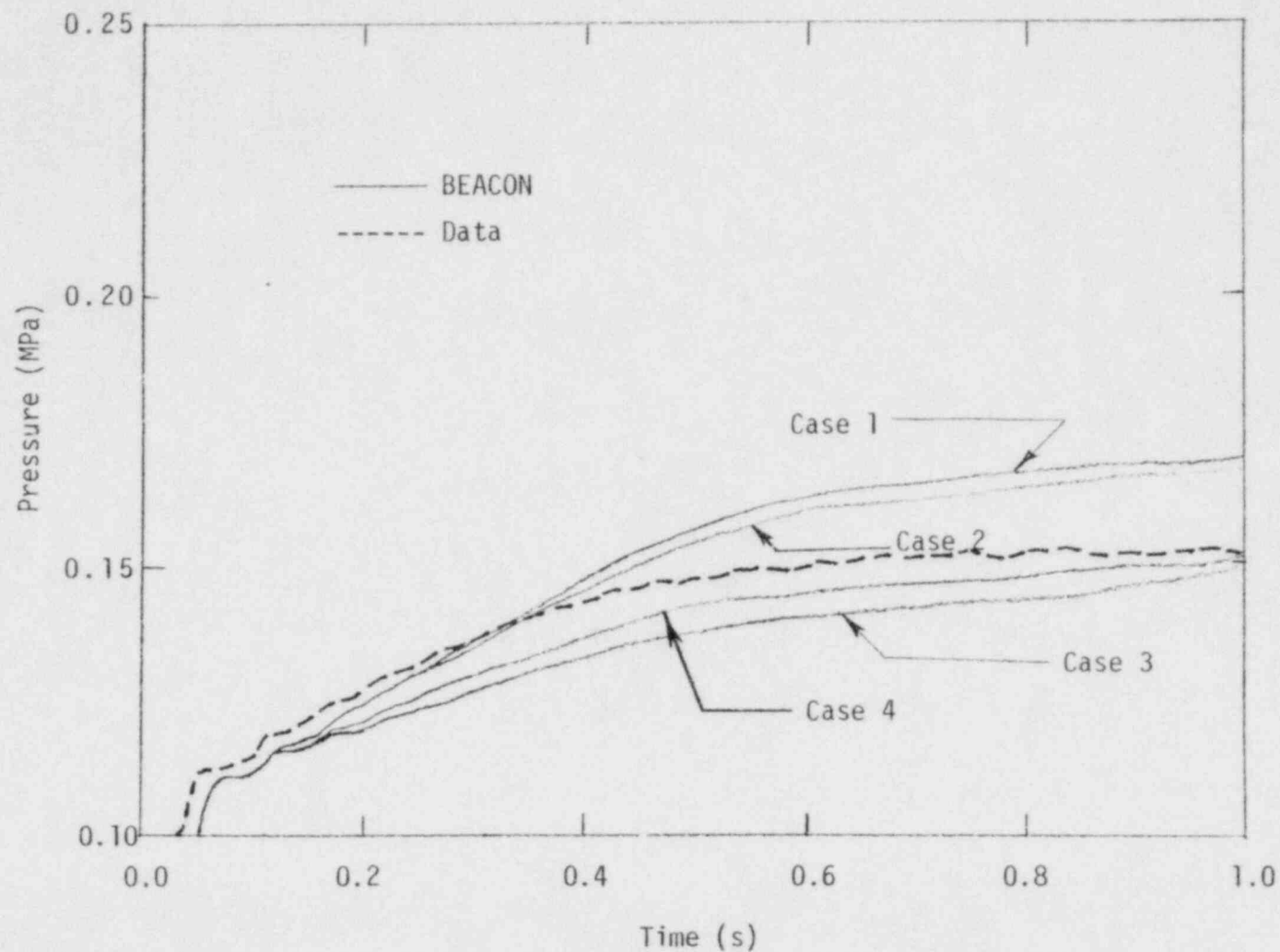


Figure E-20. Pressures in Room 4 for Cases 1 through 4.

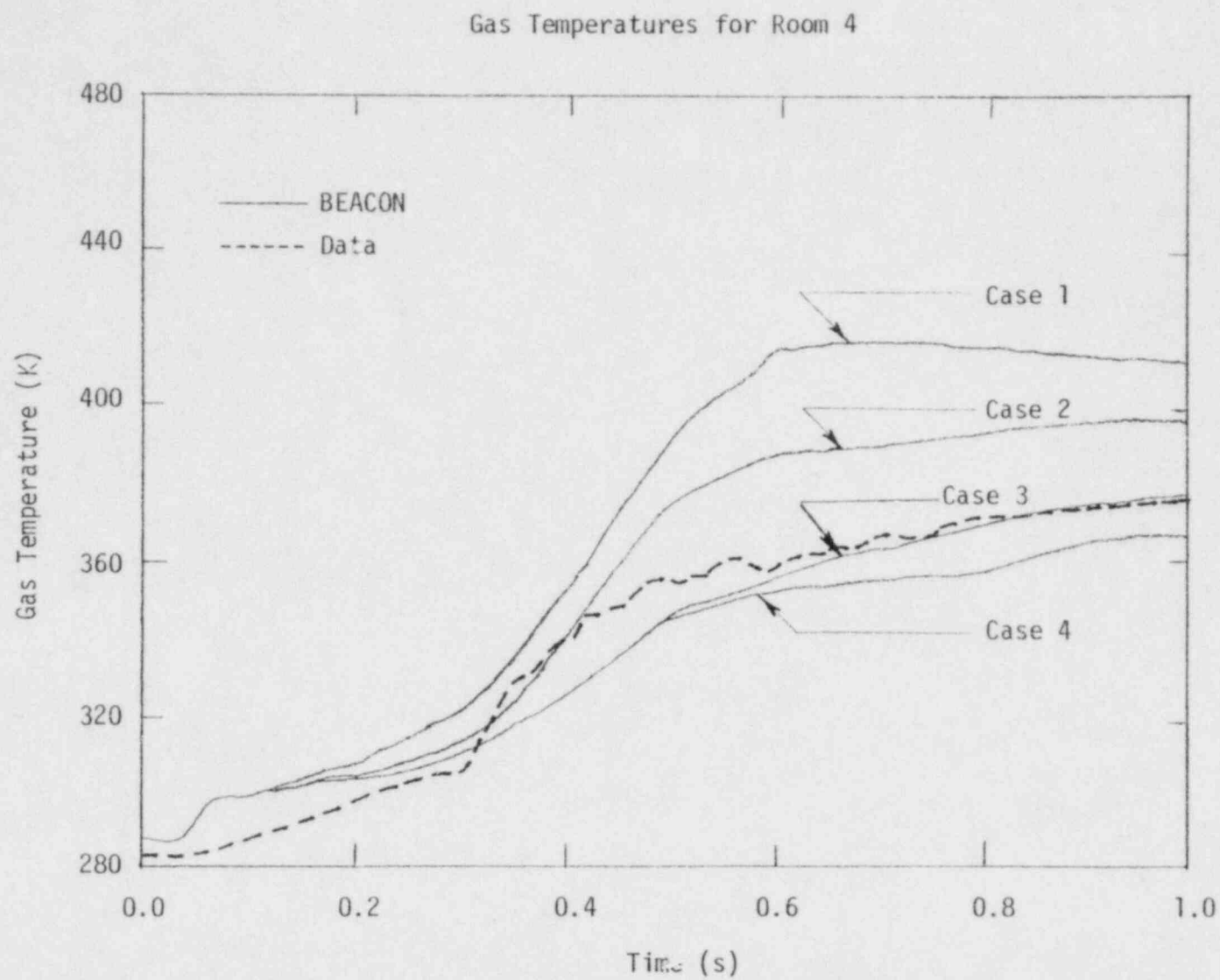


Figure E-21. Gas temperatures in Room 4 for Cases 1 through 4.

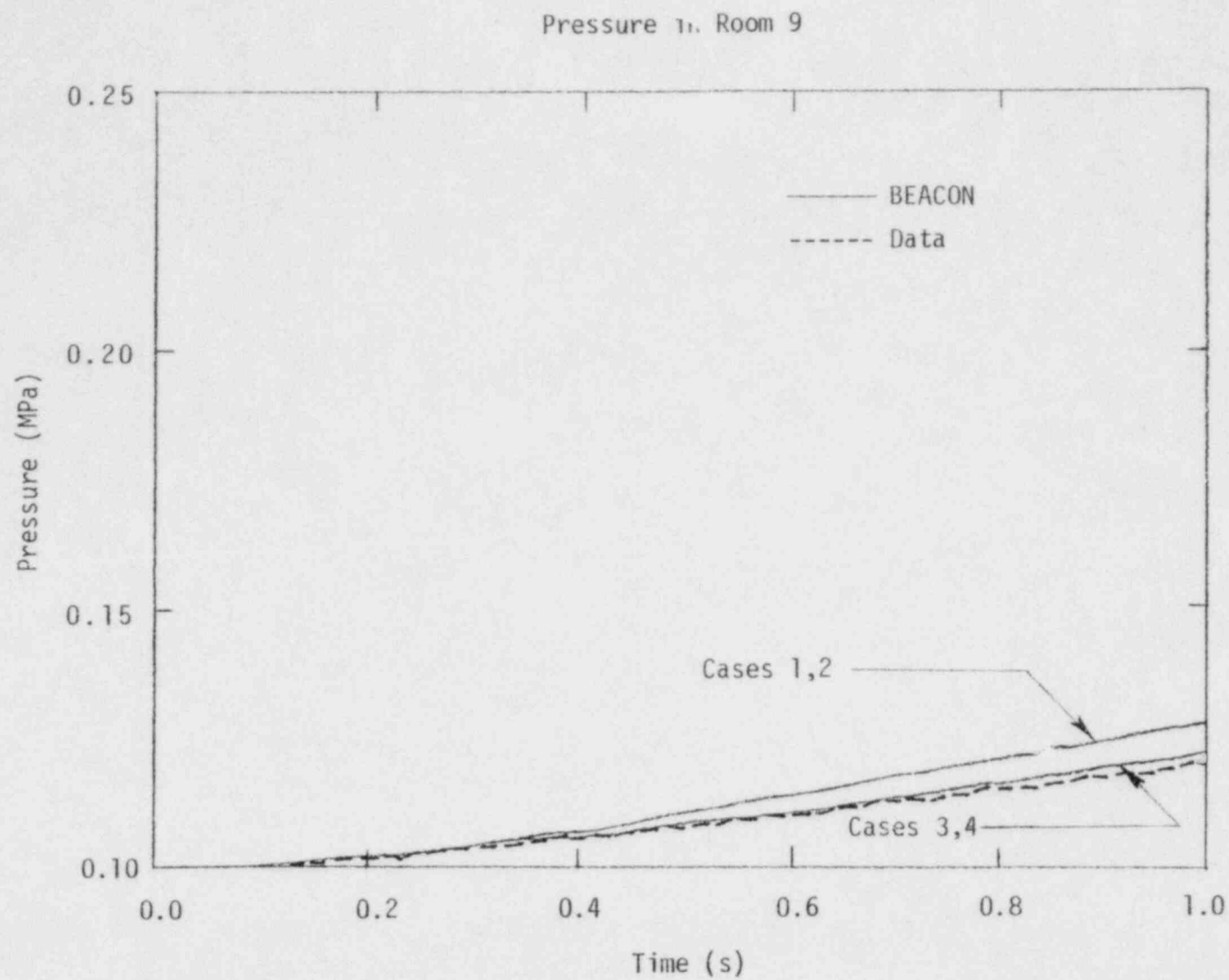


Figure E-22. Pressures in Room 9 for Cases 1 through 4.

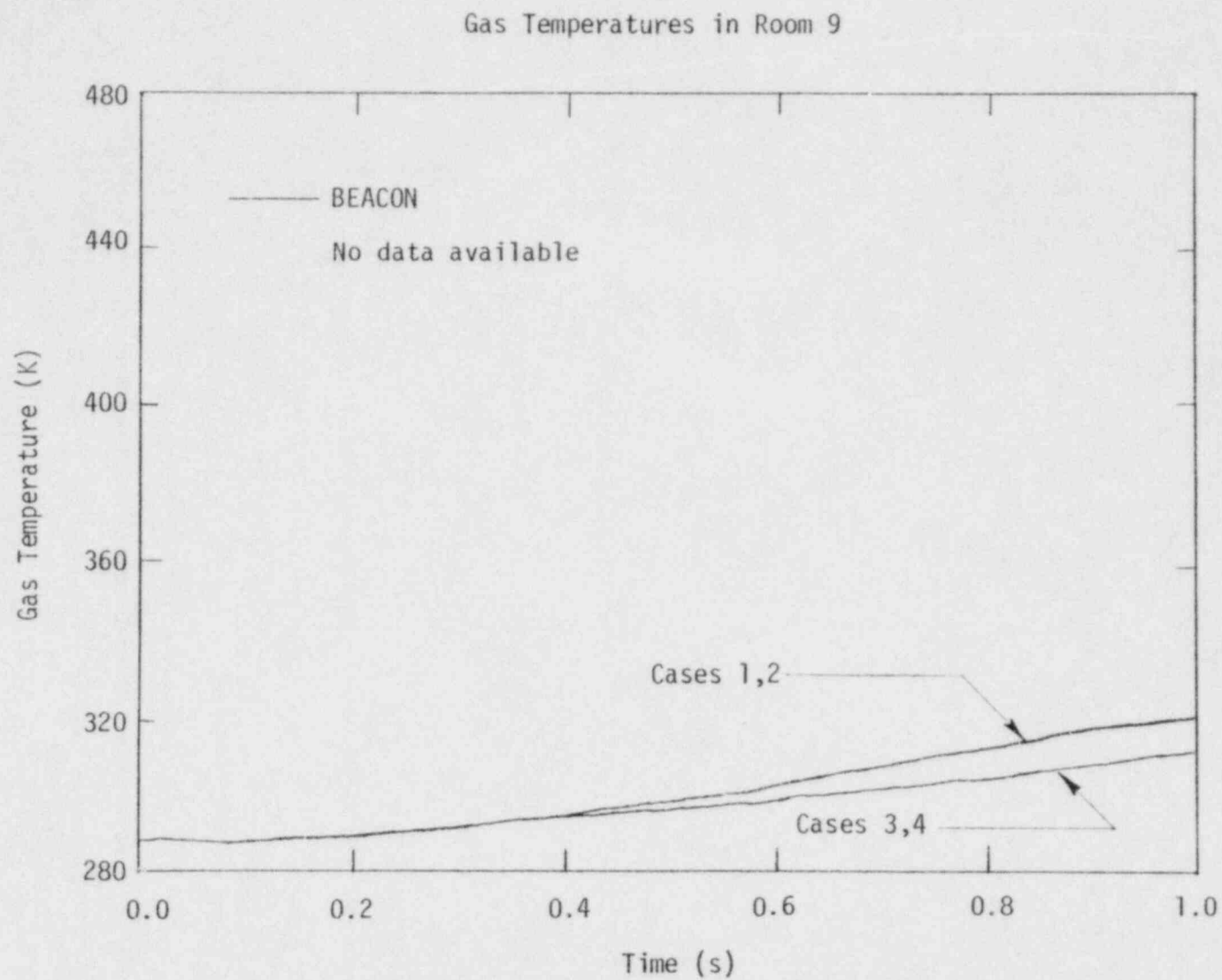


Figure E-23. Gas temperatures in Room 9 for Cases 1 through 4.

A comparison of the BEACON computation times for the D-3 study is given in Table E-3. The effects of adding film and heat structures to the no-film, no-heat structure model (Case 1) can be seen by comparing the computation times for Cases 1 through 4. The addition of film in Case 2 required a large increase in run time (82%). Interestingly, the addition of only heat structures in Case 3 caused an 11% decrease in computing time. This decrease occurred because the average timestep calculated in Case 3 was larger than that in Case 1. The Courant timestep, upon which the BEACON timestep is based, is inversely proportional to the velocity. The calculated velocities in Case 3 were lower because of lower driving pressures, as seen in Figures E-15 and E-20. The addition of both film and heat structures (Case 4) required a 100% increase in computation time over Case 1. Probably the interactions between the film and heat structure models require more time cumulatively than the addition of each model individually.

Effects of Nodalization

In addition to the use of the film and heat structure options in running BEACON, the user also must select the degree of nodalization to be used for the problem. Because of the nature of the finite difference numerical scheme used in BEACON, increasing the coarseness of the model will increase the calculational error in the code. The nodalization study was used to determine the magnitude of this error and whether the code produces higher or lower results with coarser nodalization.

There are two obvious ways to quantitatively discuss a degree of nodalization. One is to describe the average cell size for a given problem. The other is to define the number of cells used to describe a particular room. Neither of these is adequate for describing nodalization for a two-dimensional code. For example, because of the use of a two-dimensional numerical scheme with momentum-exchange functions, BEACON will behave as though form losses exist at junctions with unequal flow areas, if the inequality is sufficiently modeled in the two-dimensional

TABLE E-3. COMPARISON OF COMPUTATION TIMES FOR CASES 1 THROUGH 7

Case No.	Nodalization	Film	Heat Structures	Total No. of Interior Cells	Analysis Time(s)	Computation Time(s)
1	Fine	no	no	138	1.0	2684
2		yes	no			4873
3		no	yes			2382
4		yes	yes			5405
5		yes	yes			13131 (5405 to 1.0 s)
6a	Coarse	yes	yes	48	1.0	1591
6b		yes	yes			906
7	Lumped-parameter modeling	--	yes	5	2.5	348 (148 to 1.0 s)

direction. In short, fine nodalization in both dimensions is required near flow junctions. For this reason, nodalization for BEACON must be considered in a two-dimensional form.

The nodalization of Cases 5, 6a, 6b, and 7 is shown in Figures E-2 through E-5. The nodalization was changed only for Rooms 6 and 4, and is summarized in Table E-4.

Figures E-24, E-25 and E-26 show pressures in Rooms 6, 4, and 9, respectively, for Cases 5 through 7. The two-dimensional models show appreciable decreases in pressure in Rooms 6 and 9 and overpressurization of Room 9, with increasingly coarse nodalization. The lumped-parameter case shows sizable overpressurization in Rooms 6 and 4, and lower pressure in Room 9. All of these are a result of the flow rates through the one-dimensional regions.

In Cases 6a and 6b, the flow through these junctions was too large. As the nodalization becomes coarser, the flow rate increases because the entrance and exit losses at the junctions are no longer adequately modeled. The lumped-parameter model relies solely on the flow loss coefficients which have been input and these may be higher than in the actual experiment.

Figures E-27, E-28, and E-29 show temperatures in Rooms 6, 4, and 9 for Cases 5 through 7. For Cases 6a and 6b, the trend is the same as for the pressures, with the exception of Room 4 temperatures for Case 6a. This was the only case run with the film option enabled in the nozzles. With film enabled, the heat between the fluid and the nozzle itself was greatly inhibited, keeping the fluid temperature quite high in Room 4. For the lumped-parameter case, temperatures were kept at saturation temperature for the entire problem.

TABLE E.4. NODALIZATION FOR CASES 5 THROUGH 7.

	<u>Room 6</u>	<u>Room 4</u>
Case 5	17 x 6	3 x 11
Case 6a	9 x 3	3 x 6
Case 6b	7 x 2	3 x 5
Case 7	Lumped-parameter	Lumped-parameter

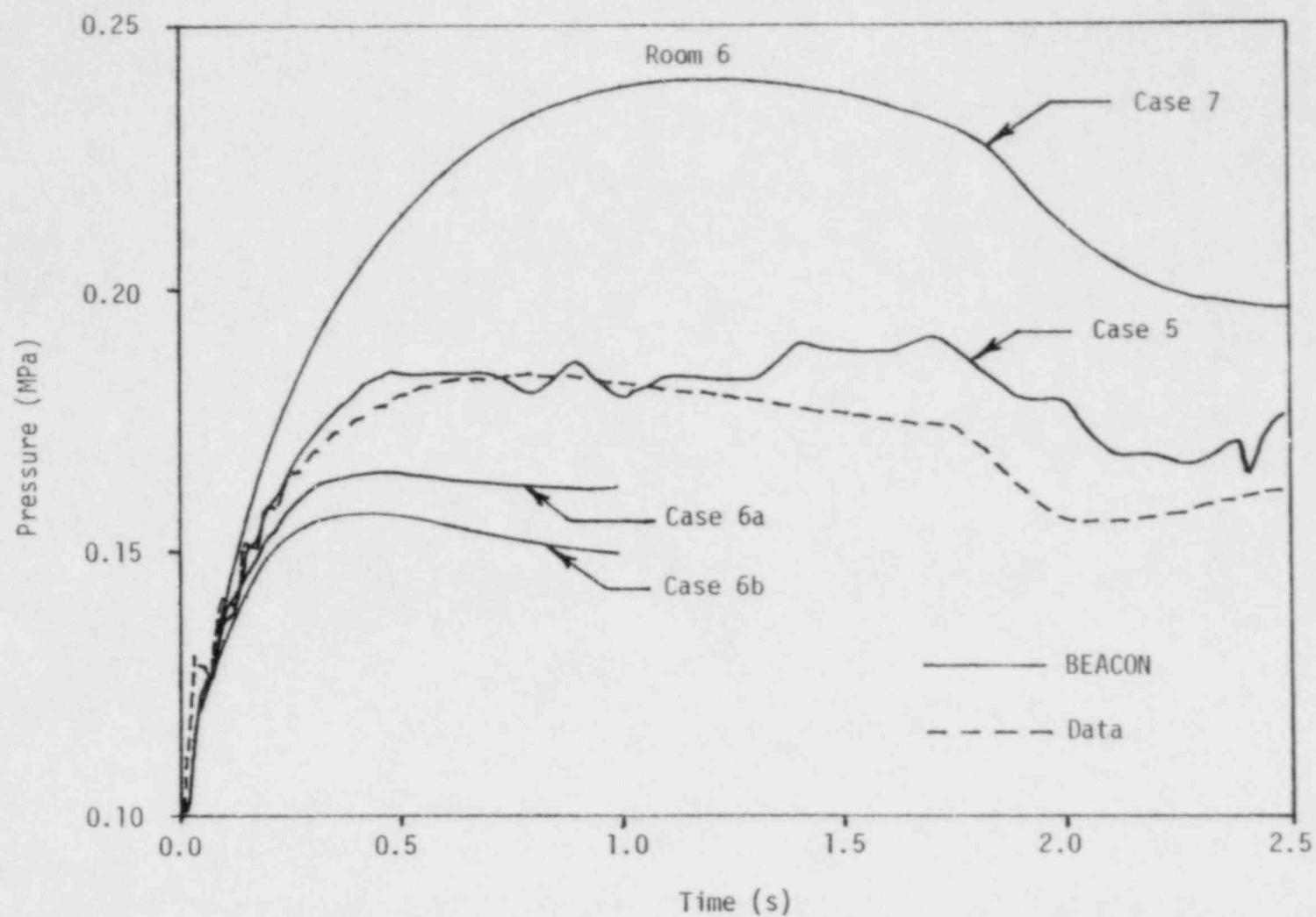


Figure E-24. Comparison of effects of nodalization on calculated pressures in Room 6.

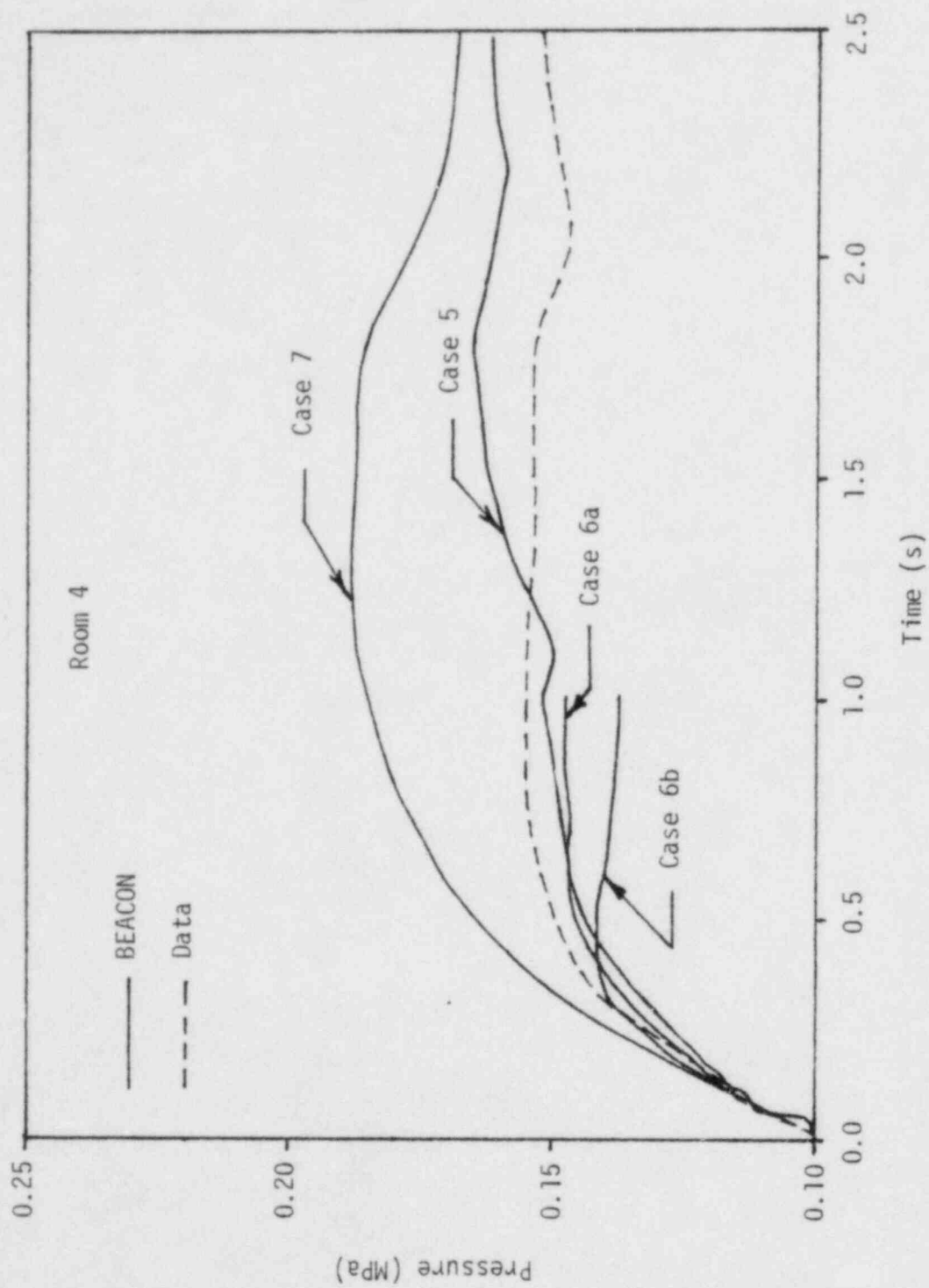


Figure E-25. Comparison of effects of nodalization on calculated pressures in Room 4.

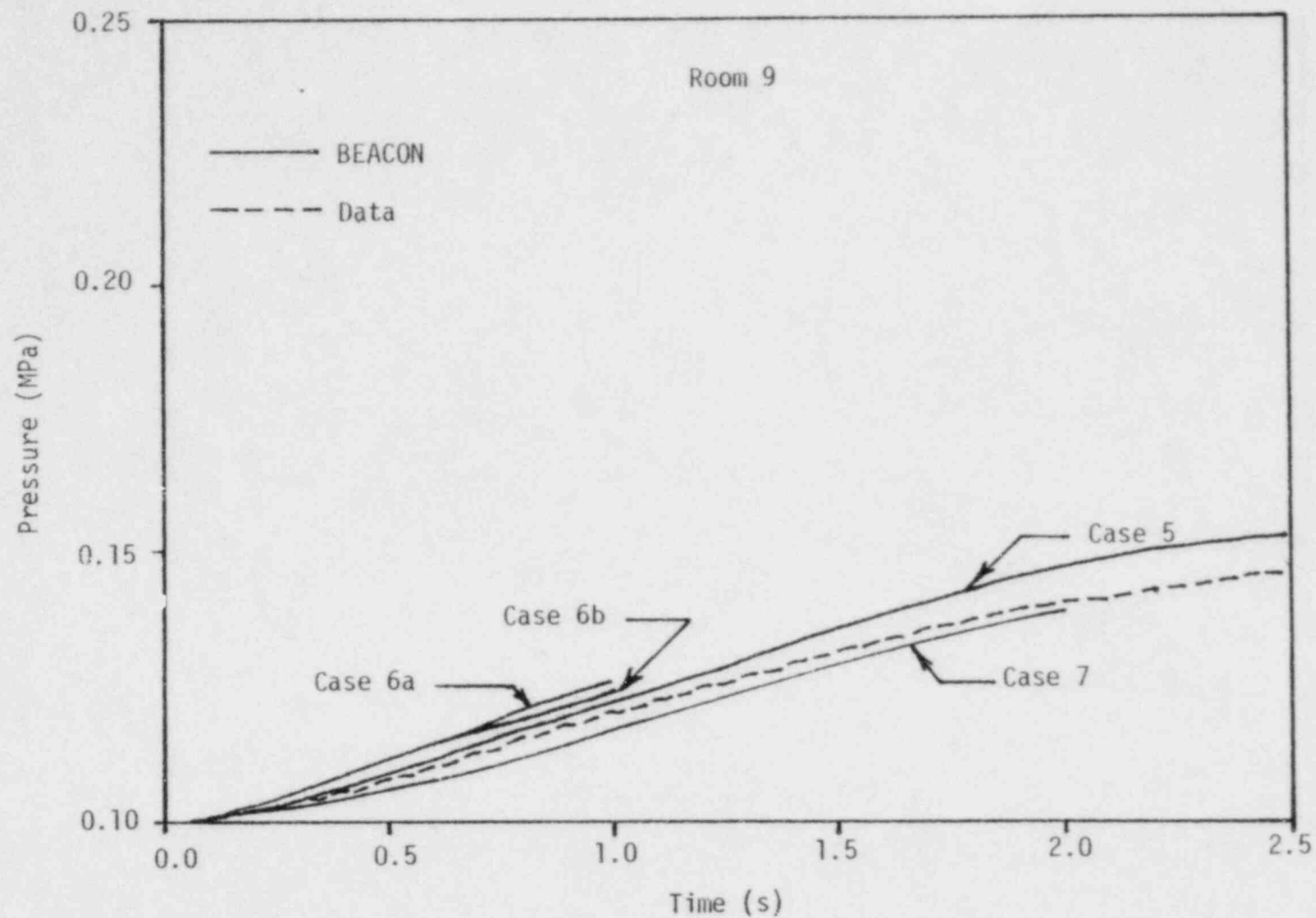


Figure E-26. Comparison of effects of nodalization on calculated pressures in Room 9.

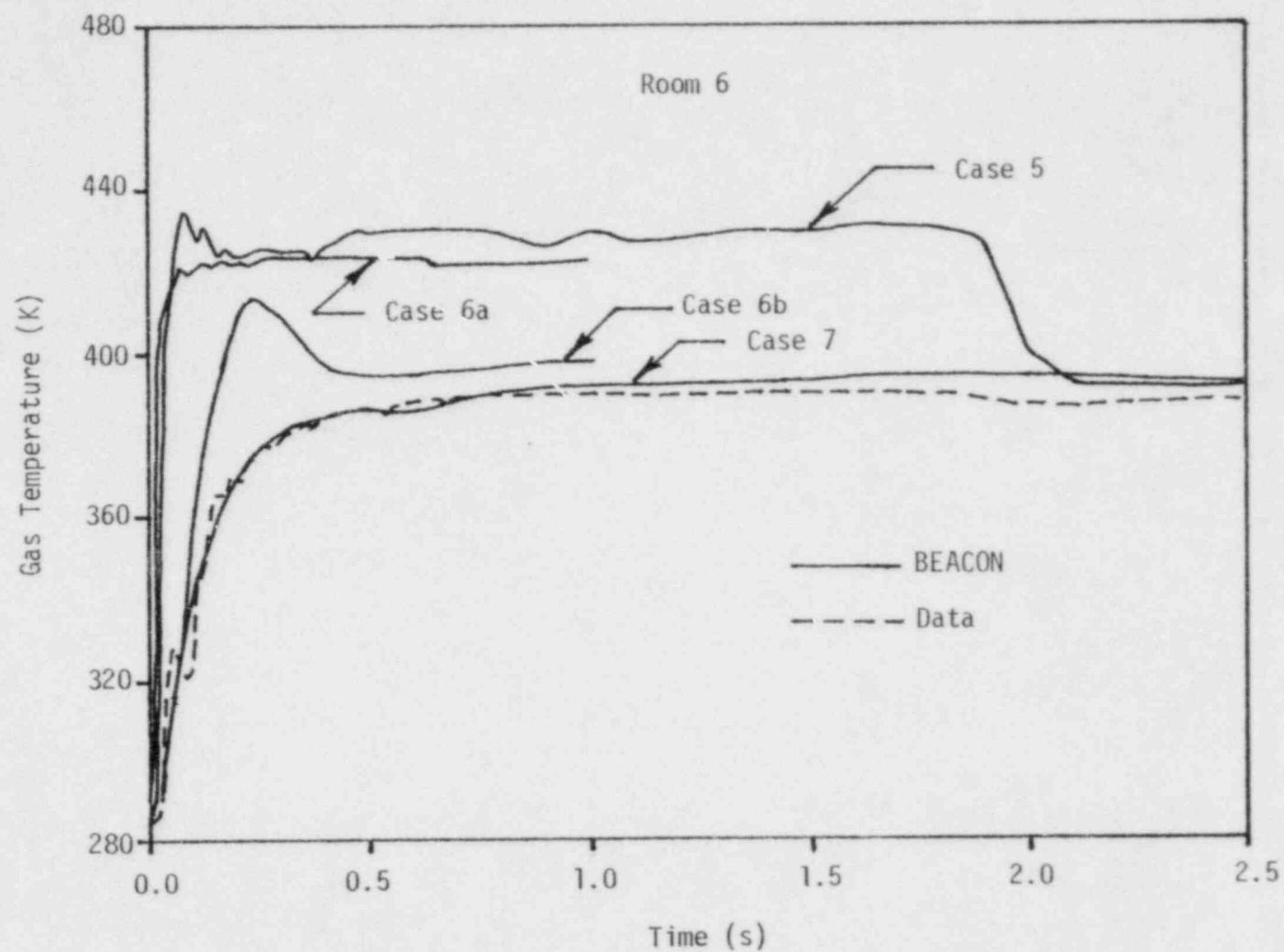


Figure E-27. Comparison of effects of nodalization on gas temperatures in Room 6.

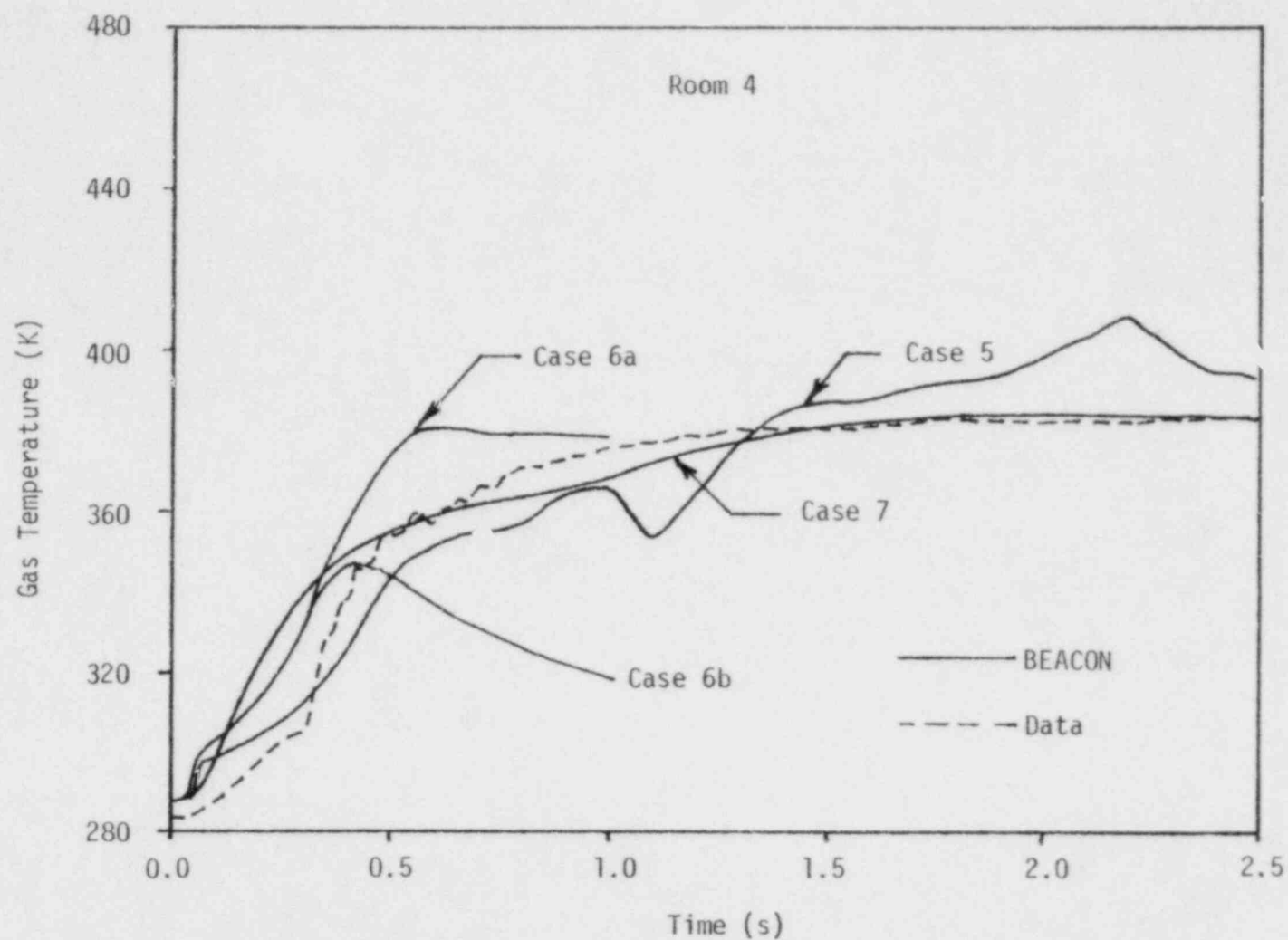


Figure E-28. Comparison of effects of nodalization on calculated gas temperatures in Room 4.

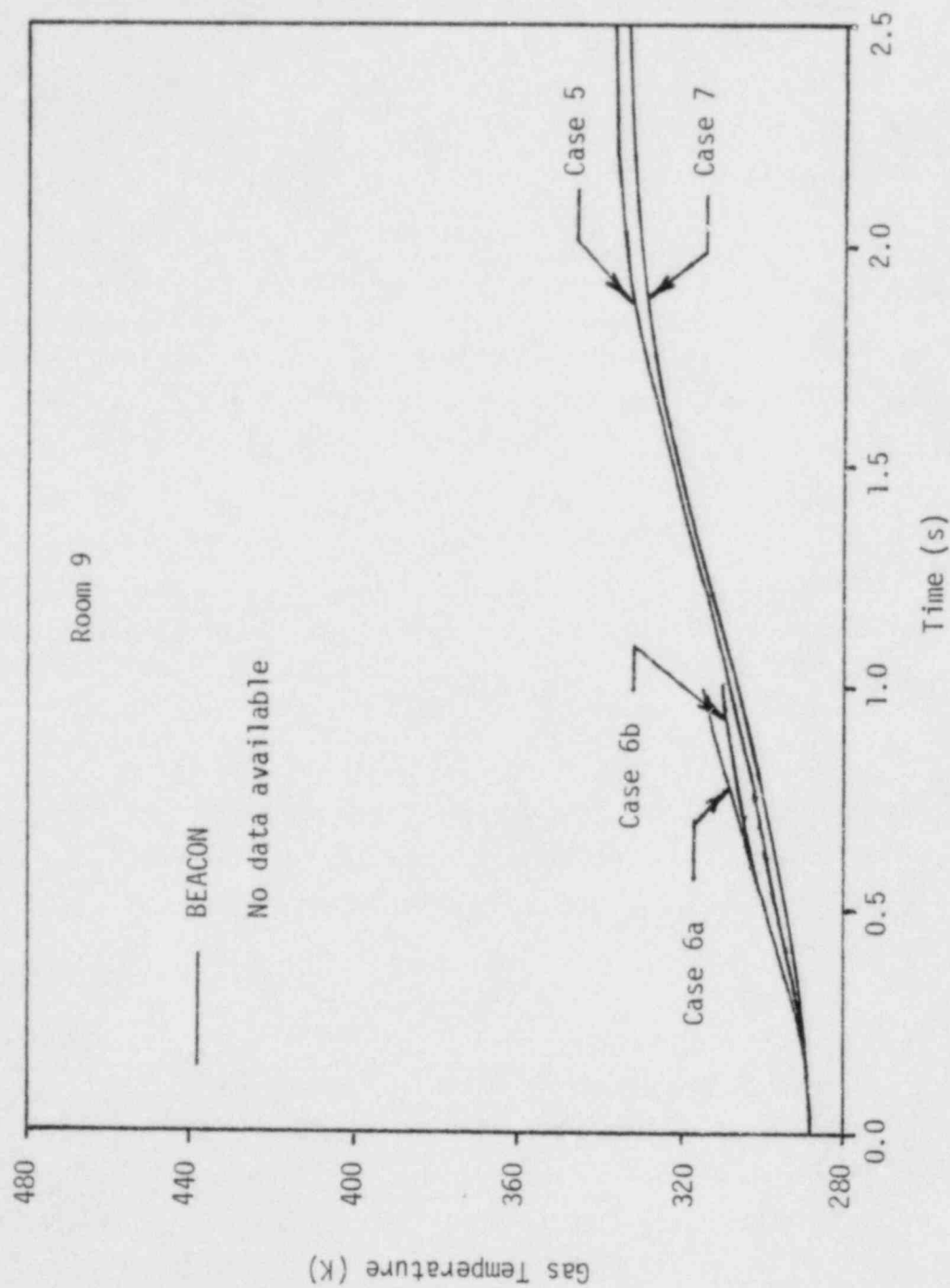


Figure E-29. Comparison of effects of nodalization on calculated gas temperatures in Room 9.

A comparison of the computation times for Cases 5 through 7 is given in Table E-3. Significant savings in computing time (83%) resulted from using the coarser mesh (Case 6b) instead of the fine mesh (Case 5). Further computation time savings were also obtained by using lumped-parameter modeling (Case 7) at the expense of accuracy (see Figure E-24). An analysis of Table E-3 results suggests that BEACON computation times are directly proportional to the number of interior cells defined for a problem. This relationship holds only for cases having the same modeling options.

"Best Estimate" Model Comparisons with Data

The "best-estimate" case selected for the comparison with test data, was modeled with fine nodalization, wall film, and heat structures (Case 5). This model was run to 2.5 seconds and the results are compared with test data in Figures E-30 through E-35. No comparisons are plotted for the Room 9 temperatures, since test data were not available. BEACON saturation temperatures (T_s) were included in the temperature plots because these were believed to be the values actually recorded by the thermocouples.

Figure E-30 shows the pressure history in Room 6 for the problem. BEACON results show close agreement with data to about 1.3 seconds, at which time the code slightly overpressurizes the room. Pressure oscillations which occurred in the early transient were also calculated by the code.

Room 4 pressures, shown in Figure E-31, are slightly low until approximately 1.1 seconds, when they suddenly increase. Since the pressure pulse occurs in this mesh first, the cause of the pressure rise throughout the problem for the later transient (1.1 second) appears to originate with the temperatures calculated for this mesh (discussed below).

Room 6

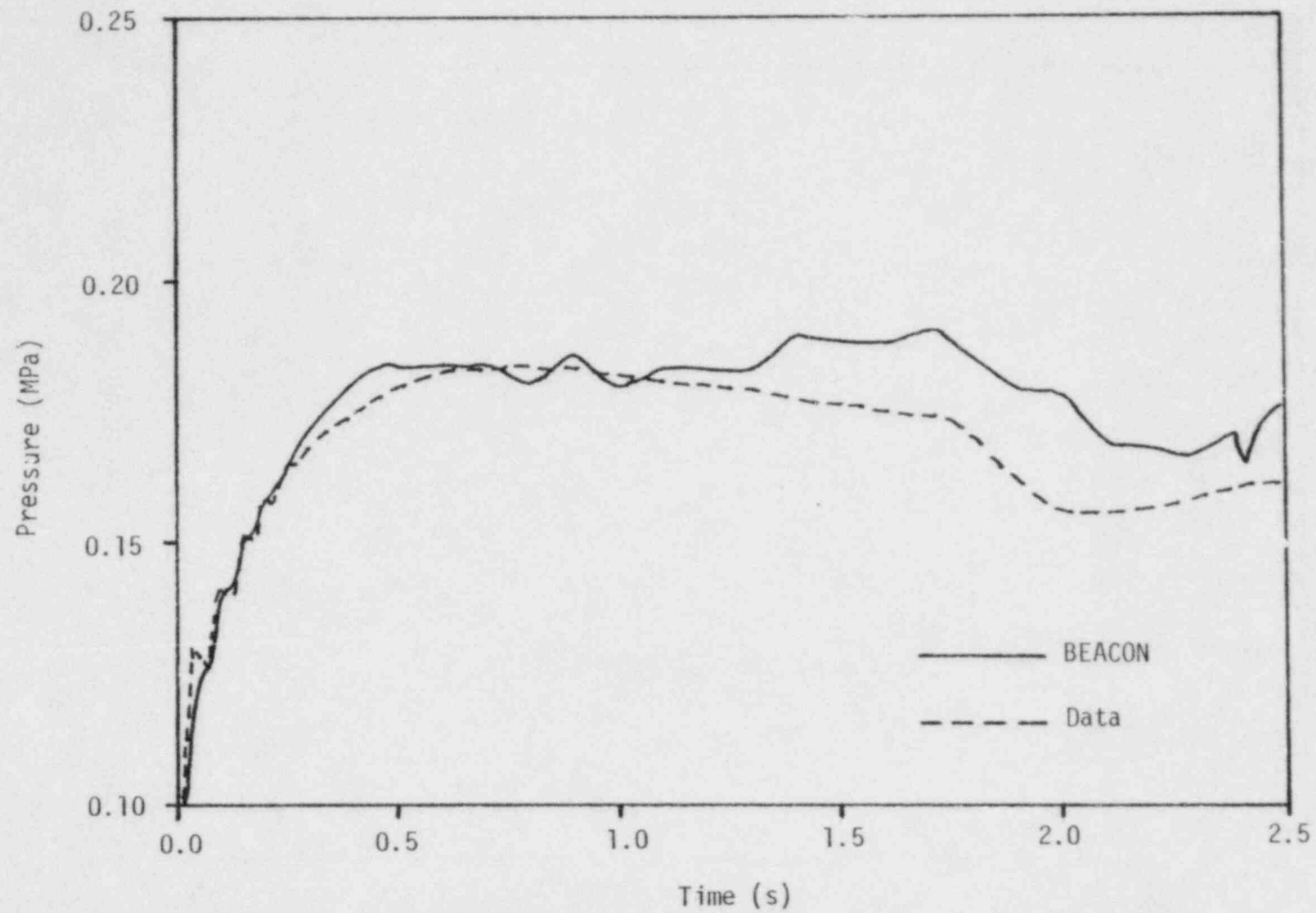


Figure E-30. Comparison between BEACON "best-estimate" pressures and test data for Room 6.

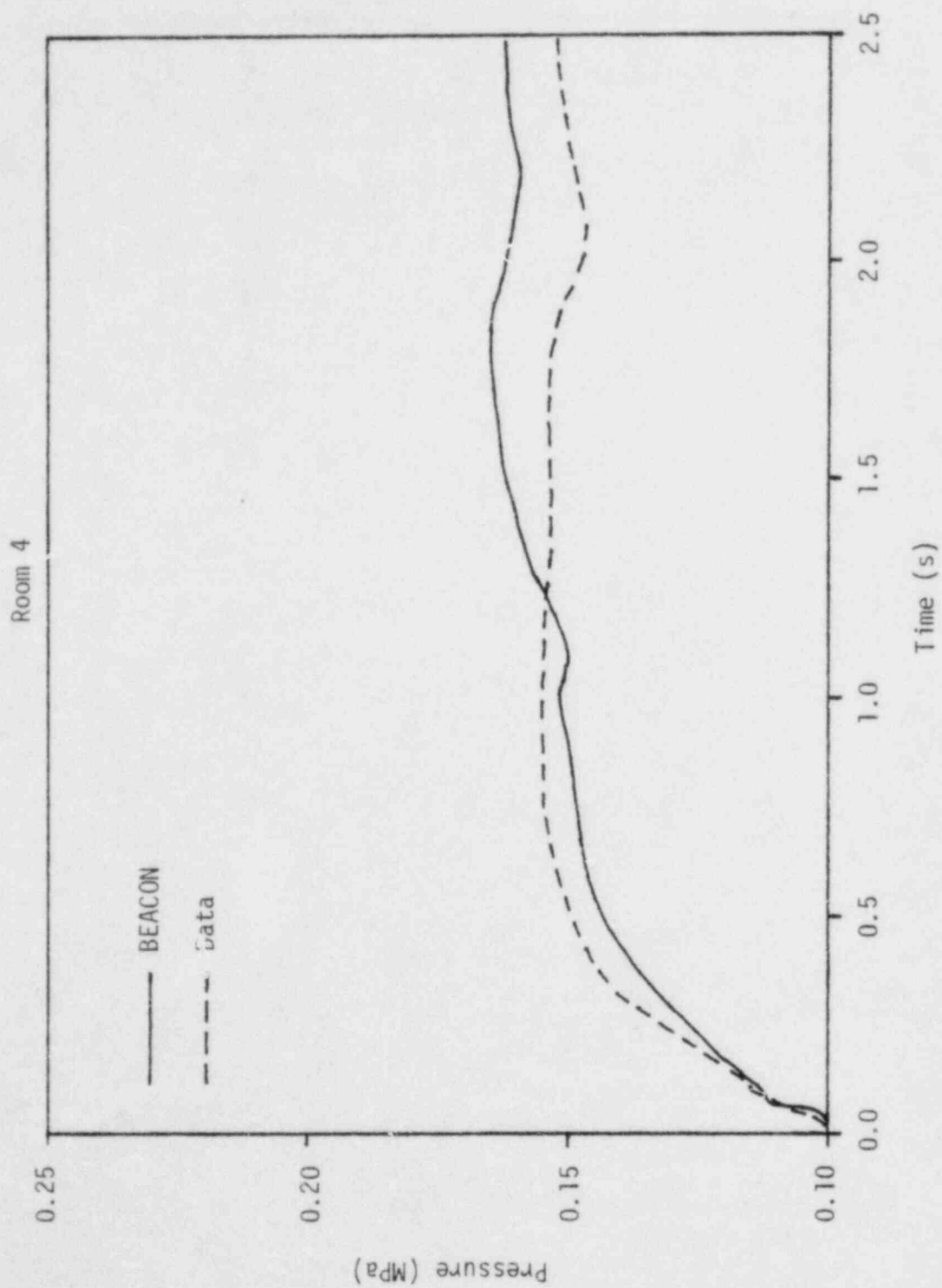


Figure E-31. Comparison between BEACON "best-estimate" pressures and test data for Room 4.

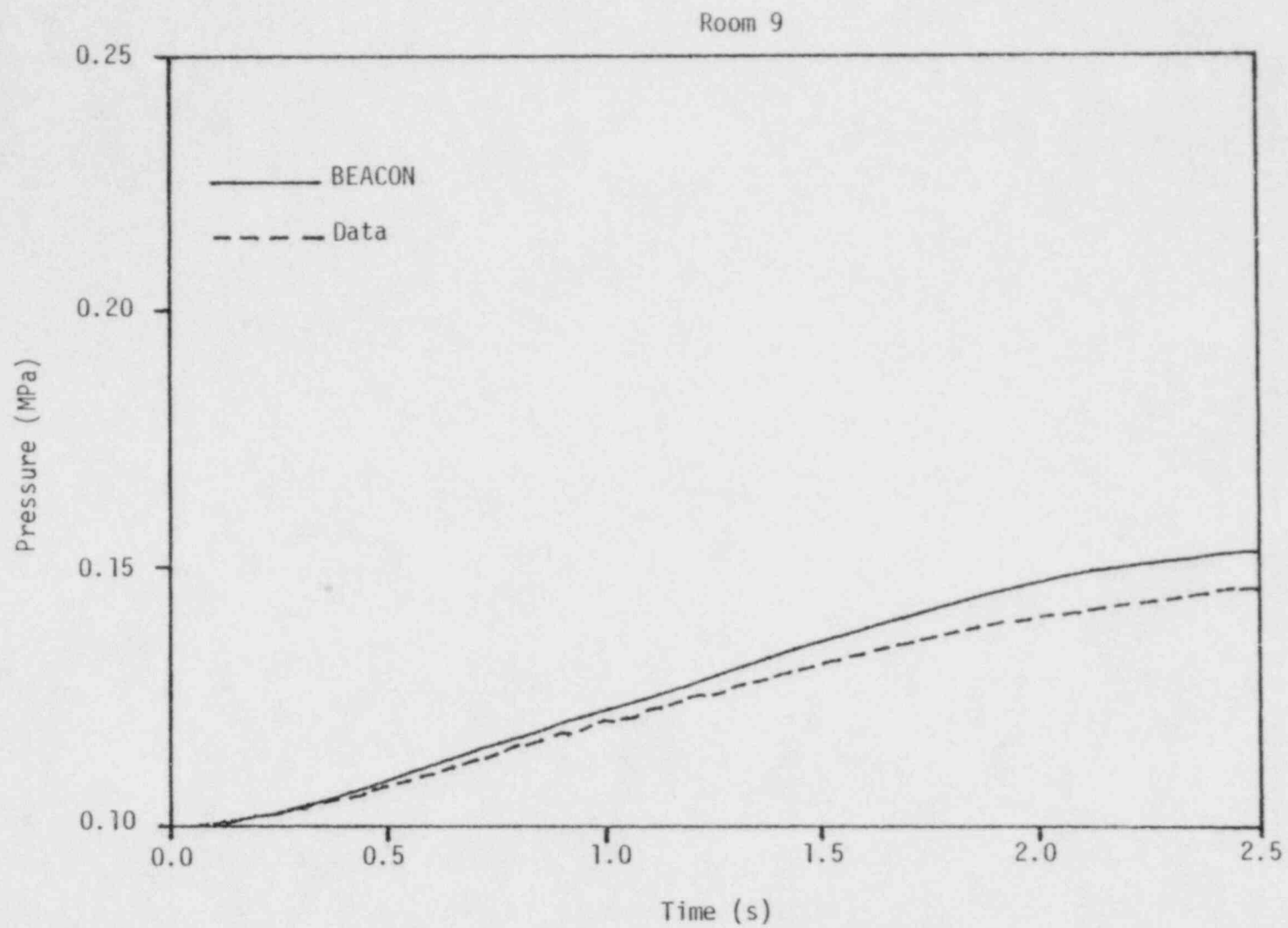


Figure E-32. Comparison between BEACON "best-estimate" pressures and test data for Room 9.

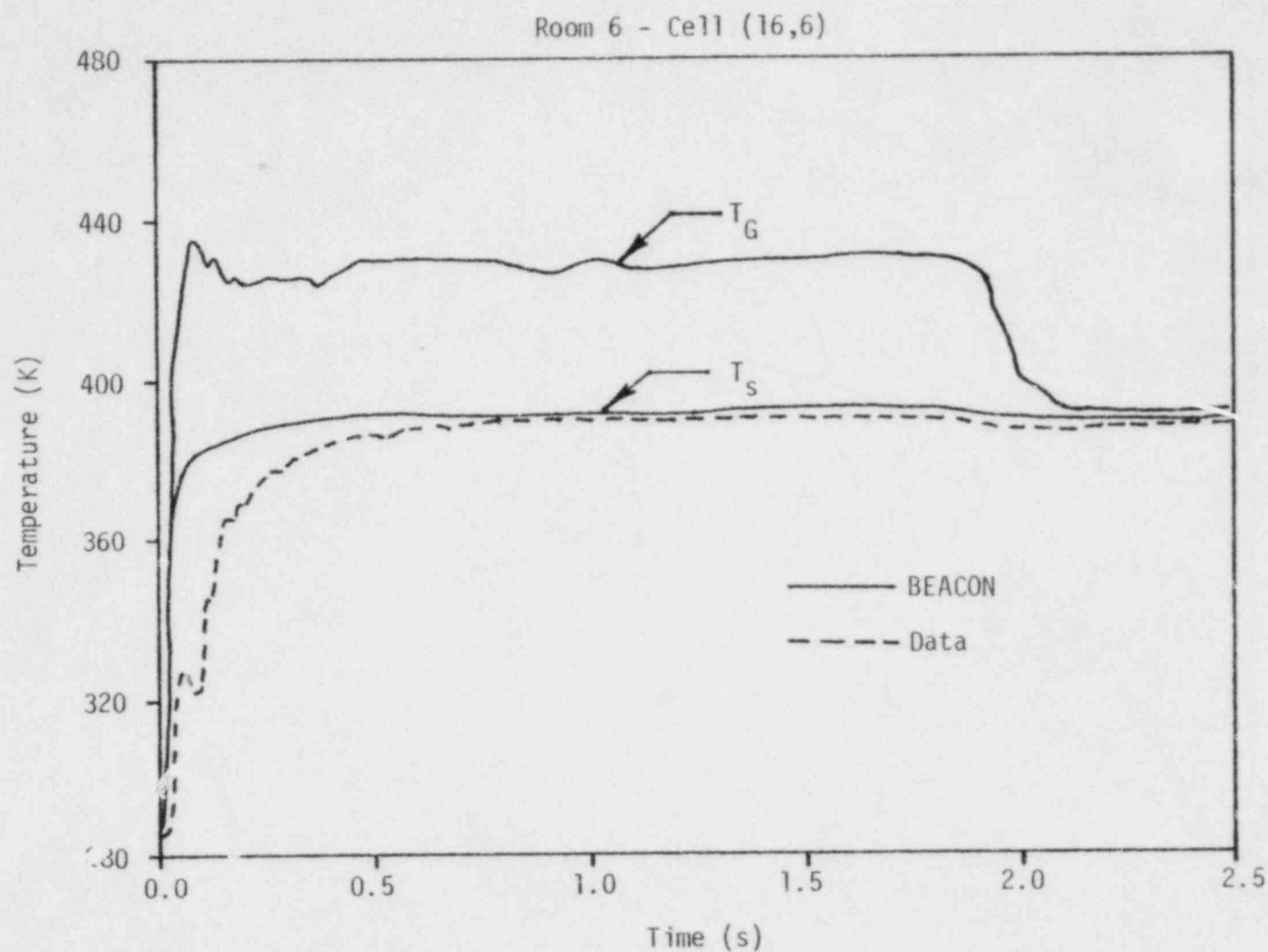


Figure E-33. Comparison between BEACON "best-estimate" temperatures and test data for Room 6 - Cell (16,6).

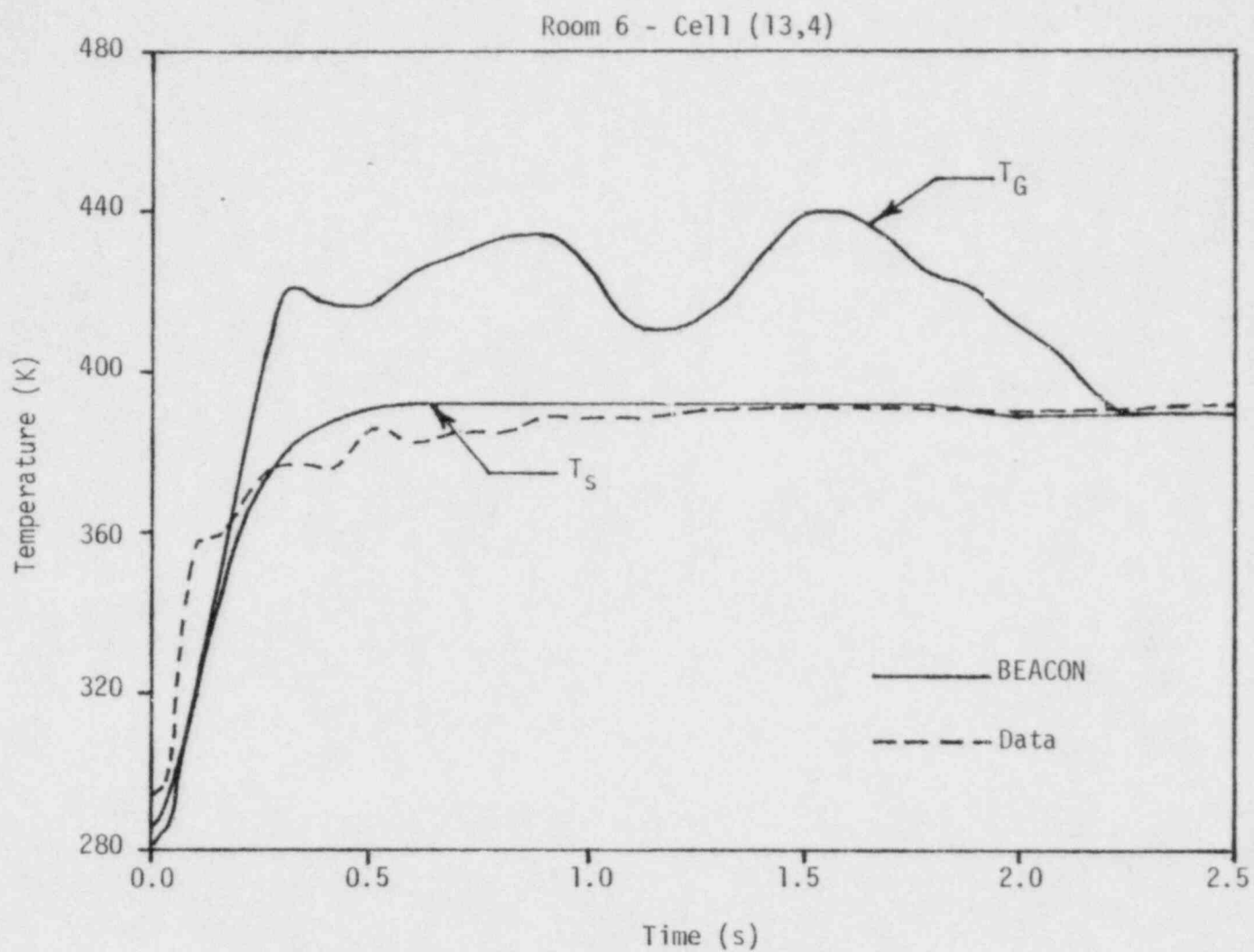


Figure E-34. Comparison between BEACON "best-estimate" temperatures and test data for Room 6 - Cell (13,4).

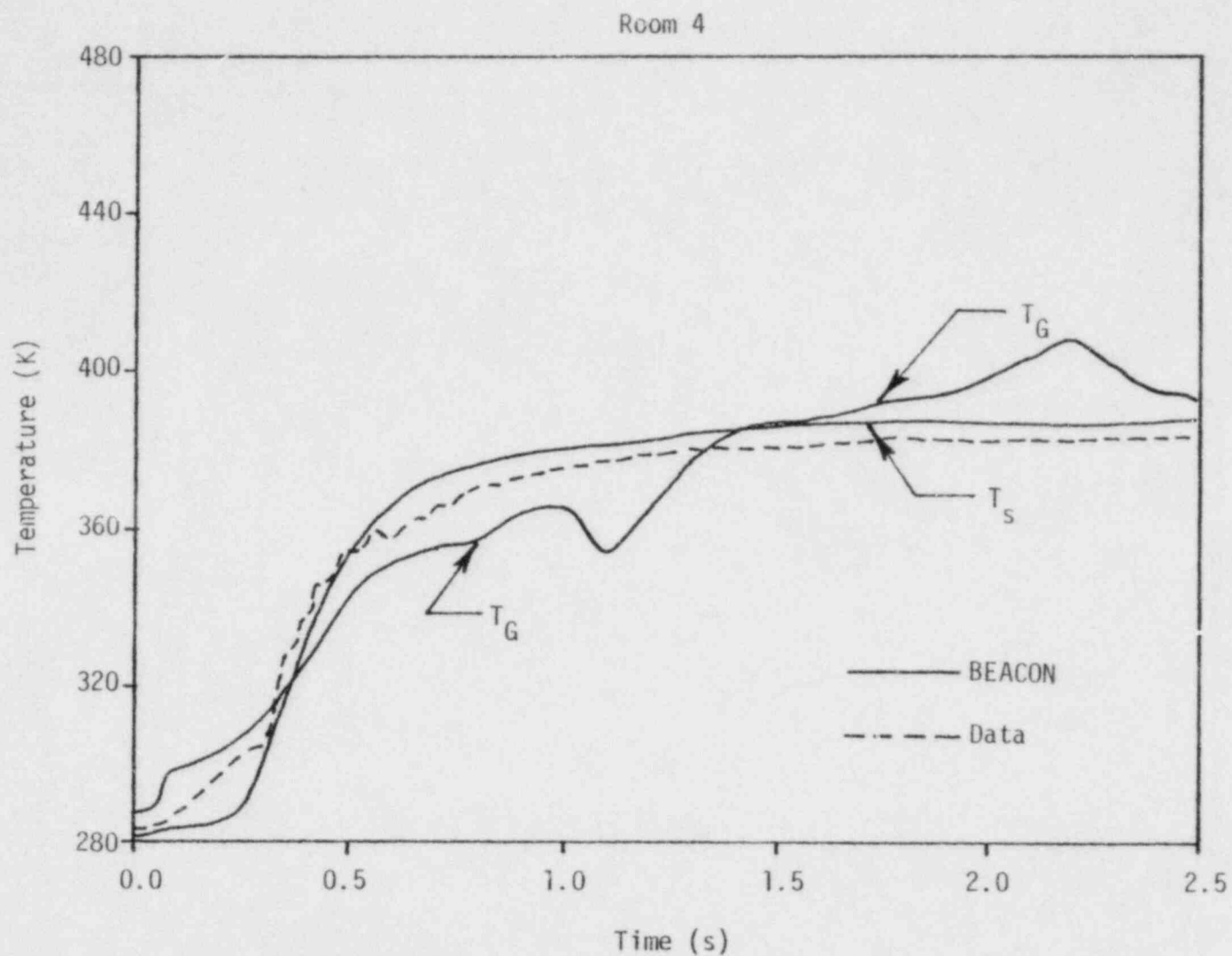


Figure E-35. Comparison between BEACON "best-est mate" temperatures and test data for Room 4.

Room 9 pressures are shown in Figure E-32 and are in close agreement with data until 1.2 seconds, when the Room 4 pressurization has become excessive and the lumped-parameter pressures respond similarly.

Temperatures in Rooms 6 and 4 are shown in Figures E-33 through E-35. Saturation temperatures in these rooms show close agreement with the thermocouple response. Generally the Room 6 temperatures are substantially above saturation until approximately 2.0 seconds, when they drop to saturation temperature quite rapidly. This occurs immediately after the two-phase portion of the blowdown begins (at 1.88 seconds). Room 4 temperatures, however, increase markedly after 1.1 seconds. This appears to be the driving force for the overpressurization discussed earlier. This, in turn, is caused by a significant decrease in the heat transfer rate in the latter part of the transient due to film formation on the heat structures.

CONCLUSIONS

With respect to the film/heat structure selection matrix, two conclusions can be drawn. First, executing problems with the film option but without heat structure modeling produces no significant benefit for a sizable computing cost increase. Second, the effect of using film on heat structures in one-dimensional regions produces questionable results. Consequently, for a "best-estimate" calculation, a user should model heat structures throughout the problem, with the film option selected only in the two-dimensional regions.

The nodalization study is inconclusive. The primary problem caused by coarse nodalization appears to be a reduction in the accuracy of losses calculated at unequal area junctions. Tentative conclusions indicate that a given volume be at least a 5×5 cell mesh region. A minimum of two cells should be used in any direction between a junction and the boundaries of the larger two-dimensional region. Lumped-parameter regions are meant to be used where only the gross average state conditions may be of interest, as illustrated by the lumped-parameter model results. Lumped-parameter region modeling was useful for Room 9, because of its large size, but was not appropriate for the other rooms.

REFERENCES

- E-1. Battelle-Institut e.V. Investigation of the Phenomena Occurring Within a Multi-Compartment Containment After Rupture of the Primary Cooling Circuit in Water-Cooled Reactors, Project RS 50, Quick Look Report Experiment D-3 (English Translation) BF RS 50-30-D3, NUREG/TR-0046, October 1978.
- E-2. Handbook of Hydraulic Resistance (English Translation) I.E. Idel'chick, 1966.
- E-3. Kondensatflächen Im Containment Bet Den Versuchen D1 Bis D15, Battelle-Institut e.V., Frankfurt Am Main, F. R. Germany, BF RS 50-31-6, July 1978.

REFERENCES

- E-1. Battelle-Institut e.V. Investigation of the Phenomena Occurring Within a Multi-Compartment Containment After Rupture of the Primary Cooling Circuit in Water-Cooled Reactors, Project RS 50, Quick Look Report Experiment D-3 (English Translation) BF RS 50-30-D3, NUREG/TR-0046, October 1978.
- E-2. Handbook of Hydraulic Resistance (English Translation) I.E. Idel'chick, 1966.
- E-3. Kondensatflächen Im Containment Bet Den Versuchen D1 Bis D15, Battelle-Institut e.V., Frankfurt Am Main, F. R. Germany, BF RS 50-31-6, July 1978.